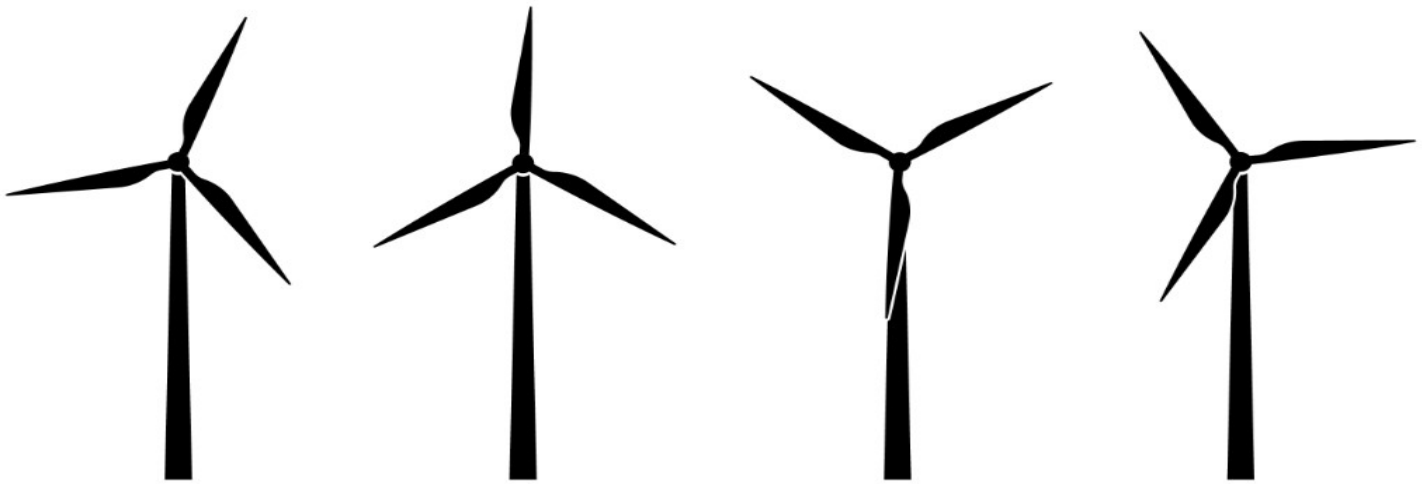

Wind Turbine Noise Simulator

An auralisation of the sound produced by a three-bladed upwind wind turbine

Gustav Juul Lind Pedersen & Jacob Alexander Rasmussen

Acoustics and Audio Technology, Group 1075, Spring 2023

Master's Thesis

Department of Electronic Systems
Aalborg University
https://www.es.aau.dk

AALBORG UNIVERSITY
STUDENT REPORT

Title:
Wind Turbine Noise Simulator

Theme:
Signal Processing and Acoustics

Project Period:
February 2023 - June 2023

Project Group:
1075

Participant(s):
Gustav Juul Lind Pedersen
Jacob Alexander Rasmussen

Supervisor(s):
Christian Sejer Pedersen

Page Numbers: 139

Date of Completion:
2nd of June 2023

Abstract:

This report investigates the noise sources for modern three-bladed wind turbines along with the pertinent parameters in outdoor sound propagation to create an auralisation of a wind turbine. Focus has been on the effect of the different propagation parameters and sound models of a wind turbine, which is reflected in the opportunity to switch between or adjust these parameters in the simulation.
In the implementation, this is carried out by various audio effects and filters, such as the chorus effect and variable filters. The simulator allows for comparison with real wind turbine recordings, which have been made as a part of the project.
From the results and informal listening observations, it is found that the simulator provides a believable sound of a wind turbine. However, further work could improve the sound experience by using models of higher complexity such as modelling turbulent wind conditions giving the sound a more natural, imperfect characteristic.

Contents

Preface

This report is written as a part of the master thesis at the MSc. in Signal Processing and Acoustics (Acoustics and audio technology).

The report is to be read chronologically and with additional explanations and measurement journals placed in the appendix.

Citation is carried out by the IEEE standard and is found in the bibliography. Furthermore, frequency plots are made as stated in IEC 20263:2020 meaning an aspect ratio of 10 dB/decade, 20 dB/decade, 25 dB/decade or 50 dB/decade.

The authors would like to thank Jesper Lumbye Andersen for contributing with both knowledge throughout the course of the project and for providing the opportunity and taking the time to do measurements on a wind turbine.

With the signatures below, all group members confirm to have written the report and cited the applied external material and sources.

Aalborg University, 2nd of June 2023

Gustav Juul Lind Pedersen
gpeder18@student.aau.dk
20182537

Jacob Alexander Rasmussen
jara17@student.aau.dk
20173509

Chapter 1

Introduction

To reduce carbon dioxide emissions and provide more green energy to the population of the world, many different technologies are used. Many power sources such as oil, coal and other fossil fuels are replaced with more green alternatives such as wind-, water or solar power.

In 2050 the EU Commission expects wind power to cover 50 % of the total power consumption within Europe [1]. This consists of both offshore and onshore wind power. However, most of the power will come from onshore wind turbines which is expected to be 75 % of new wind turbine farms [1].

Before a wind farm can be constructed, it has to comply with the regulation, for the given country. This may involve several considerations such as distance to nearest neighbours, amount of noise made by the wind turbine, surrounding nature and visual effects such as shadow cast [2], [3].

Especially the concern regarding noise pollution from wind turbines has caused scepticism from people and has led to a focus on how the noise affects people nearby [4]. This opposition can potentially delay the transition to renewable energy.

The focus of this report will be sound emissions and relevant regulation for wind turbines and how an auralisation can be produced to give a listener a plausible experience of the sound made by a wind turbine.

Initial research question for the analysis:

Which part of a wind turbine generates noise and which physical parameters affect the propagation in an outdoor environment?

Chapter 2

Analysis

2.1 Wind Turbine Noise

A wind turbine is a complex construction with many distinct moving parts. All of these parts are potentially a noise source. This section describes and investigates which part of a wind turbine produces noise and the relevance of the different sources. When looking at a wind turbine the noise can be split into mechanical noise, which is primarily coming from the generator, gearbox and other parts inside the rotor hub [5]. This type of noise can have a tonal characteristic and is often in the range 20 Hz to 500 Hz. Mechanical noise is not considered to be the most dominant factor and is in most cases only significant because of damage or wear and tear [6]. For this reason the focus will be on the other type of noise which is aerodynamic noise and is produced by the blades moving through the air.

2.1.1 Aerodynamic wind turbine noise

Modern wind turbines usually consists of three rotor blades which will be the type of turbine that is the focus of this report. Furthermore, two configurations of the three-bladed wind turbines exist, the upwind configuration and the downwind configuration. The most common configuration is the upwind turbine, with the rotor facing the wind. This means that all of the rotor is exposed to the wind at all times. However, this configuration also requires that the blades are designed to be rigid, to avoid hitting the tower [7]. For downwind turbines, the blades are on the opposite side of the tower. This means that at a certain point, the blade will be behind the tower thereby not being exposed to the wind directly. A result of this can be fluctuations in wind-power and speed [7] also leading to fluctuations in the noise characteristics because of interaction with the tower. The upwind turbine is the most common type and, for this reason, is the focus of this project [7].

A turbine starts turning, when the wind speed is high enough and this produces aerodynamic noise, which is considered the most prominent source of noise coming from a wind turbine [5]. Each of the blades will produce noise both from the leading

edge, the trailing edge and at the blade tip. These parts of the wind turbine are illustrated in fig 2.1.

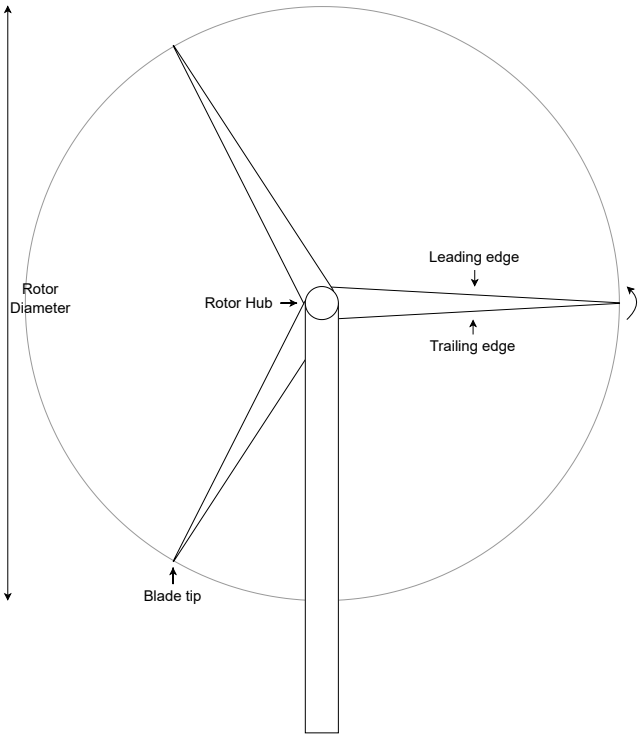

Figure 2.1: Illustration of wind turbine from the downwind position.

When rotating, the leading edge will break the wind and a flow around the blade will happen. The flow speed U is a combination of the wind speed U_w and the speed of the blade U_b. The speed of the blade varies over the length of the blade, with the speed being highest at the blade tip [5]. As the wind interacts with the blade the energy from the wind is directed away from the blade creating a force 'F' causing the rotor to spin. This is also shown in fig 2.2. Taking out the energy from the wind causes the flow to slow down and the pressure to increase, this side is known as the pressure side. The opposite side has a higher flow speed and lower pressure and is known as the suction side [5].

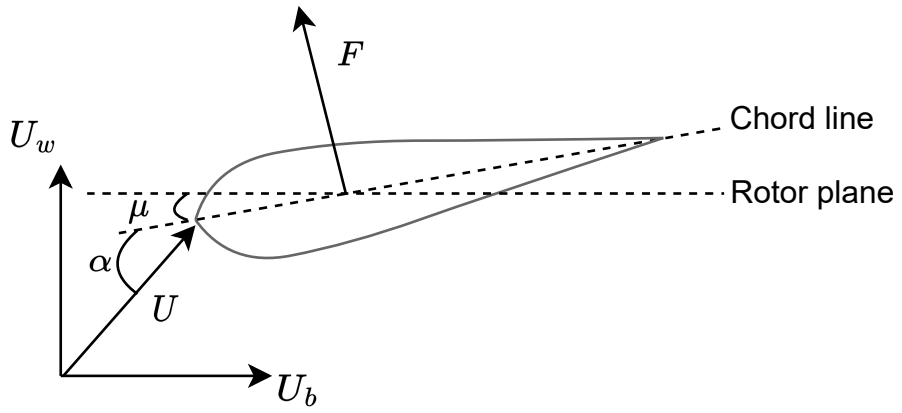

Figure 2.2: illustration of cross section of turbine blade with forces and flow directions [5].

As seen from the figure above two different angles are illustrated. α is the angle of attack and is described by the angle between the flow direction U and the chord line. The other angle μ is dependent on the pitch of the blade, which can be adjusted, to control the speed and it also has an impact on the noise characteristics [5]. The flow around the blades affects the amplitude of the noise. This flow can be described by a thin layer of air, that almost attaches to the blade and thereby, has the same speed. This is called the boundary layer. The Reynolds number is used to express flow in fluids and can give an estimate of the boundary layer. High Reynolds numbers represent a turbulent flow structure, while low Reynolds numbers represent a laminar flow [5].

$$Re = \frac{UC}{v} \tag{2.1}$$

Where:

Re	Is the Reynolds number	[-]
U	Is the flow speed	[m/s]
C	Is the chord length	[m]
v	Is the kinematic viscosity (approx 1.5E-6 in air)	$[m^2s^{-1}]$

If there is highly turbulent air in the area of a wind turbine, either caused by other turbines in the farm or caused by the weather, an additional noise called inflow turbulence noise contributes to the noise from the turbine. However, since this is difficult to predict and varies with different parameters often focus is on noise created by the blades themselves called self-noise [5]. The different types of self-noise made by the turbine blades are illustrated in fig 2.3.

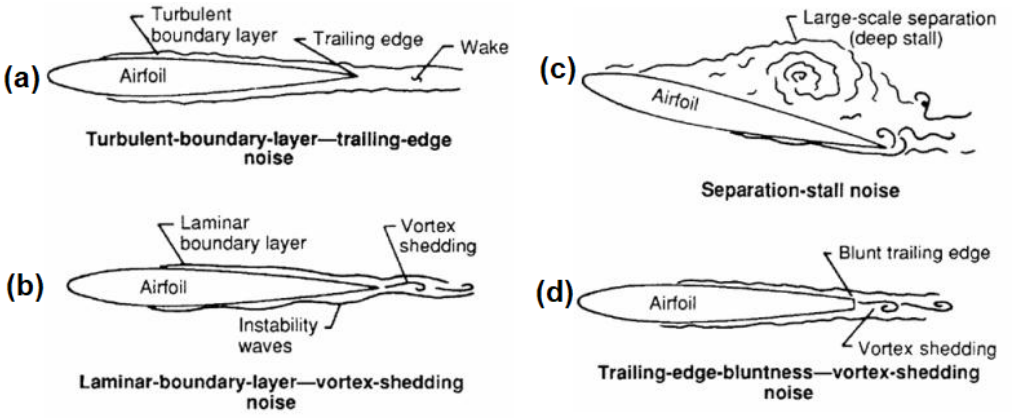

Figure 2.3: illustration of self-noise types [8].

For large wind turbine blades, with high Reynolds numbers, the boundary layer is more turbulent. This layer is close and almost sticks to the blade until it reaches the trailing edge. At the trailing edge, the sound of the turbulent air is dispersed and results in a broadband noise spectrum. This type of self-noise is called trailing edge noise and is seen as the most dominant source of noise in big wind turbines [5]. This is illustrated in fig 2.3(a).

In the case where the boundary layer has a laminar characteristic, caused by a small Reynolds number, the result at the trailing edge is an oscillating flow known as vortexes, shown in fig 2.3(b). These oscillating vortexes can create tonal components from the blades. This type of noise is mostly a problem for small wind turbines and it can be minimized by boundary layer tripping [5] (converting the boundary layer flow from laminar to turbulent).

The boundary layer thickness can be found from the Reynolds number, and is shown in eq. 2.2.

$$\delta \approx 0.05 Re^{-\frac{1}{5}} C \tag{2.2}$$

As the angle of attack gets higher it results in a bigger difference in the flow on each side of the blade and is called a stall. When this type of flow occurs it can increase the noise and is called separation-stall noise, illustrated in fig 2.3(c). For large-scale separation, the characteristics of the noise become low frequency and is emitted from the entire blade compared to the other types of self-noise. However, modern wind turbines have the ability to adjust the pitch, which reduces this type of self-noise and is therefore not seen as a major concern to the total noise spectrum [5].

The last type of self-noise is called blunt trailing edge noise, shown in fig 2.3(d). This type of noise is tonal and increases as the thickness of the trailing edge increases, thereby making the boundary layer thicker. This type is usually not problematic on modern wind turbines [5].

From these types of noise, the trailing edge noise is the most dominant. It is found that the size of swirls in turbulent inflow has an impact on the spectrum produced by the blades. If the swirls are big, compared to the blade chord, then the wavelength of those will be long and will result in an alternating force on the whole airfoil. This creates a low-frequency characteristic [5].

The broadband noise created by the trailing edge noise has a distinctive high-frequency peak created by the scattering, called edge-noise. Studying the flow using a semi-infinite flat plate approximation it is found that the acoustic power and flow speed has the relation $p^2 \sim U^5$ and the directivity $p^2 \sim sin^2(\theta/2)$ (illustrated in fig. 2.4). Thereby making the radiation biggest in the direction towards the leading edge of the rotor [5]. The peak frequency happens when the Strouhal number is approximately 0.1 [5]. The Strouhal number is dimensionless and describes the mechanisms of oscillating flow. Calculation of this number is shown in eq. 2.3.

$$St = \frac{f\delta}{U} \tag{2.3}$$

Where:

St	Is the Strouhal number	[-]
U	Is the flow speed	[m/s]
f	Is is the peak frequency of the broadband spectrum	[Hz]
δ	Is the boundary layer thickness	[m]

The sound differs with respect to the position on the blade. This has to do with parameters like flow speed, chord length, the thickness of the boundary layer and the size of the blade section of interest. This makes it relevant to divide the blade into multiple sections, each contributing to the total sound. A section of the blade along with the directivity is shown in fig. 2.4.

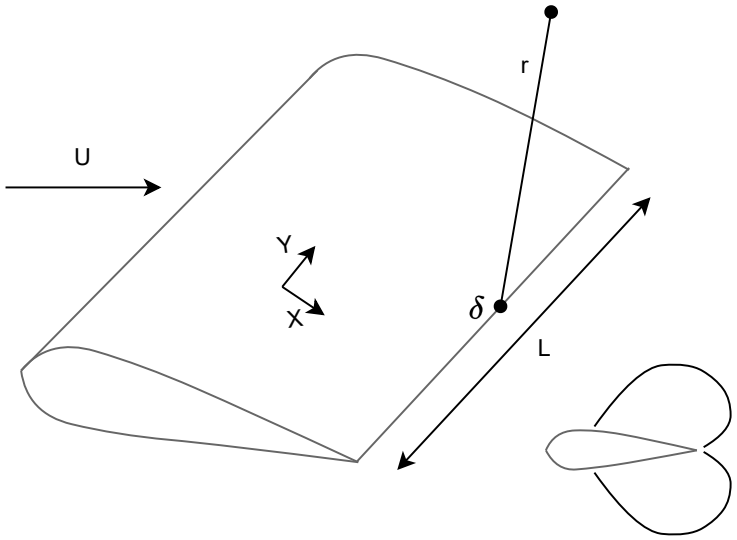

Figure 2.4: Illustration of blade section and directivity of noise [5].

This piece of a blade, with a given length L, has a certain chord length and thereby also a certain boundary layer thickness. With knowledge of these parameters, the acoustic power of this blade section can be approximated as shown in eq. 2.4 [5].

$$p^2 \sim U^5 \frac{L\delta}{r^2} cos^3(\gamma) sin^2(\frac{\theta}{2}) sin(\phi) \tag{2.4}$$

Where:

p	Is the pressure	[Pa]
U	Is the flow speed	[m/s]
L	Is length of the blade section	[m]
δ	Is the boundary layer thickness	[m]
r	Is the distance to receiver	[m]
γ	Is the angle between the x-axis and flow	[rad]
θ	Is the angle between the x-axis and receiver	[rad]
ϕ	Is the angle between the y-axis and receiver	[rad]

The sinusoidal functions describe the directivity of the trailing edge noise. $cos^3(\gamma)$ describes how the dispersion of energy is strongest when the vortexes are perpendicular to the trailing edge. $sin(\phi)$ is the directivity along the y-axis, while $sin^2(\frac{\theta}{2})$ is the directivity illustrated in fig 2.4. From this, it can be seen that a higher flow will result in higher sound pressure and since the flow speed is highest at the tips this is where the most dominant noise is produced [5].

Different companies often have a variety of wind turbine sizes and blade designs which will have an impact on the noise produced by the blades [9]. This means that

it can be difficult to give an estimate of the spectrum since this depends on the shape and size of the blade, wind speed, rotor speed in RPM and environmental variations.

2.1.2 Location of noise on rotor

The characteristics of the trailing edge state that the directivity of the noise is strongest in the direction of the leading edge. To see how that affects noise coming from the entire turbine in operation a measurement using 148 microphones arranged in an array has been carried out and is described in [10]. The microphones are placed on a platform in front of the wind turbine at an angle of 45° down from the rotor hub. The results of the noise distribution in the range 250 Hz to 800 Hz is shown in fig 2.5.

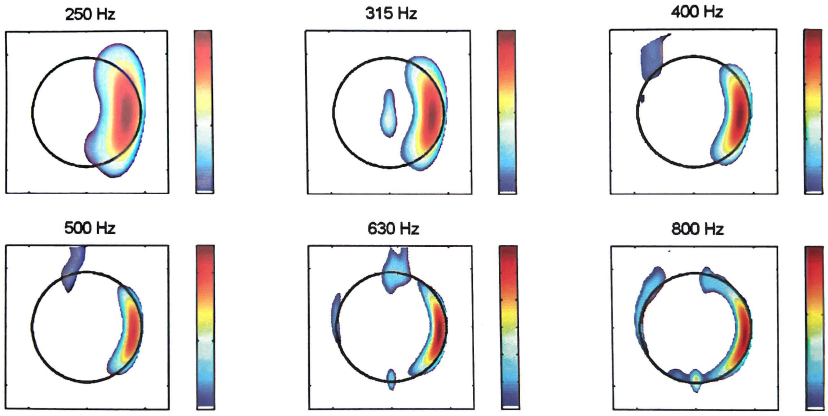

Figure 2.5: Noise distribution average of the rotor with clockwise rotation. Range is 0 dB to 12 dB [5].

There is a clear trend in the entire frequency range showing that most of the noise is generated when the blade is moving downwards (the right side of the rotor plane) and almost at the tip of the blade. This matches the link between a higher flow speed generating a higher sound pressure, since the speed of the blade is highest close to the tip. Furthermore, the noise being highest at the downwards direction matches the directivity of the trailing edge noise, which is towards the ground (and microphones) when the blade is moving downwards [5]. Another parameter is the Doppler amplification, which also contributes to a higher sound level when the blade is moving towards a listener.

Even though generator noise is not considered a major contribution, it is seen at fig 2.5 (315 Hz), that noise from the rotor hub is present. This measurement does show that some of the theoretical parameters hold but do not take into account the environmental impact. According to the author, the noise produced at approximately $\frac{\pi}{2}$ in the range 400 Hz to 630 Hz is an artefact of the microphone setup [5].

A more detailed illustration close to the blade of the noise source on the blade is illustrated in fig 2.6.

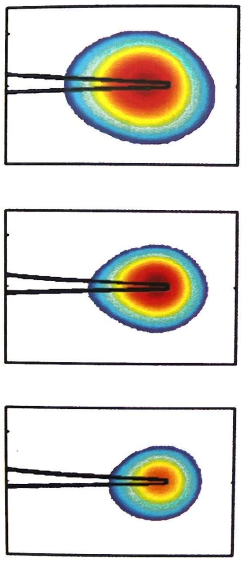

Figure 2.6: Noise source on blade for 400 Hz (at the top), 800 Hz (in the middle) and 1600 Hz (at the bottom). Range is 0 dB to 12 dB [5].

From this, it is clear that the most dominant acoustic source on the blade is located near the blade tip.

2.1.3 Amplitude Modulation

Amplitude modulation caused by the wind turbine which can be heard at short distances is often known as "swish". This characteristic sound, produced by the Doppler amplification and other factors, is heard near the turbine because of the directivity being in the direction of the leading edge [11]. The swish sound created by the blades is most dominant in the frequency range of 400 Hz to 1000 Hz. Due to the directivity the effect and other factors such as air absorption, the swish is not transmitted over longer distances [5].

Another type of amplitude modulation from a wind turbine is called "swoosh" and is an artefact of the blade and tower interaction. The tower of a wind turbine affects the flow and can be modelled as flow around a cylinder. This will typically cause a slower flow in this area. Even though this has a bigger impact on downwind turbines, the effect still applies to upwind turbines as well [12]. The change in flow speed will result in a different load on the blade when passing the tower. This creates a sound as a moving object passes a stationary object. Interaction between the tower and blades has an impact on the spectrum and this effect is characterised by the blade passing frequency and the harmonics [12]. this is shown in eq 2.5.

$$f_B = n_B \cdot f_R, \quad f_n = n \cdot f_B \tag{2.5}$$

Where:

f_B	Is the blade passing frequency	[Hz]
n_B	Is the number of blades	[-]
f_r	Is the rotor frequency	[Hz]
f_n	Is the harmonics of the blade passing frequency	[Hz]
n	Is an integer (1,2, ... , N)	[-]

For modern wind turbines, the blade passing frequency is usually in the range of 1 Hz to 3 Hz. Interaction between blades and the tower primarily adds to the lower part of the spectrum. With the harmonics of the blade passing frequency, the frequency range of this phenomenon is typically 1 Hz to 150 Hz. [12].

All of the parameters described here contribute to the noise coming from a wind turbine. The manufacturers of wind turbines have to take these parameters into account when designing a wind turbine because of noise regulations. These regulation including the method for measuring and calculating the parameters of a wind turbine will now be of focus.

2.2 Noise Regulation for wind turbines

Noise regulations regarding wind turbine noise differ all across Europe on several parameters. However, when talking about noise from wind turbines the maximum sound pressure level (SPL) in the regulation are often weighted, eg. A-weighted, the explanation of the different weighting curves and the reasoning behind it can be found in appendix A.1. In Denmark, the regulation regarding noise from wind turbines states different limits depending on the environment nearby. It is also described how to check whether these limits are complied with either by measurements or calculations. However, the regulation varies according to the type of wind turbine in question. The different types of wind turbines given in the danish regulation are as follows [2]:

- **Small wind turbines / private wind turbine:** A single wind turbine with an area of the rotor smaller than 200 m^2 and lower than 25 m.
- **Prototype wind turbines:** A new type of wind turbine that is non-mass-produced.
- **Type 0-turbines:** The first small series of a new type of mass-produced wind turbines.
- **wind farm:** A group of 3 or more wind turbines.

The noise limit for a wind turbine in Denmark is given for the worst-case point in a living area and at a maximum distance of 15 m from a residence. At this point, the SPL must not exceed these values [2]:

- General
  - 44 dB(A) at a wind speed of 8 m/s
  - 42 dB(A) at a wind speed of 6 m/s
- For noise sensitive areas:
  - 39 dB(A) at a wind speed of 8 m/s
  - 37 dB(A) at a wind speed of 6 m/s
- For low frequency noise (10 Hz to 160 Hz)
  - 20 dB(A) at a wind speed of 8 m/s and 6 m/s (Inside a residence)

All of the above limits does not hold for the residence of the owner of the wind turbine. Furthermore, all of the limits are specified for a height of 1.5 m and the wind speeds are corrected to a height of 10 m, except for the low-frequency noise, which is indoor and based on calculations. [2].

The danish regulation does not only set limits based on the noise pollution from a wind turbine. Distance to the nearest neighbour based on visual parameters states that the minimum distance between the tower and a residence is 4 times the total height of the wind turbine [13].

The procedure for measuring the noise from a wind turbine on land in Denmark is described in "bekendtgørelse om støj fra vindmøller" [2]. The apparent sound power level (L_{WA}) for a wind turbine has to be specified in 1/3- or 1/1 octave band and is measured, in different states of the turbine's power output, in the downwind position. The microphone must be positioned on a reflecting plate on the ground to avoid wind noise and a wind cap is also installed. The position of the microphone is at a distance of R from the bottom of the tower, which is R_0 $\pm 20\%$ or maximum ± 30 m. The position of the microphone and the wind turbine is shown in fig. 2.7.

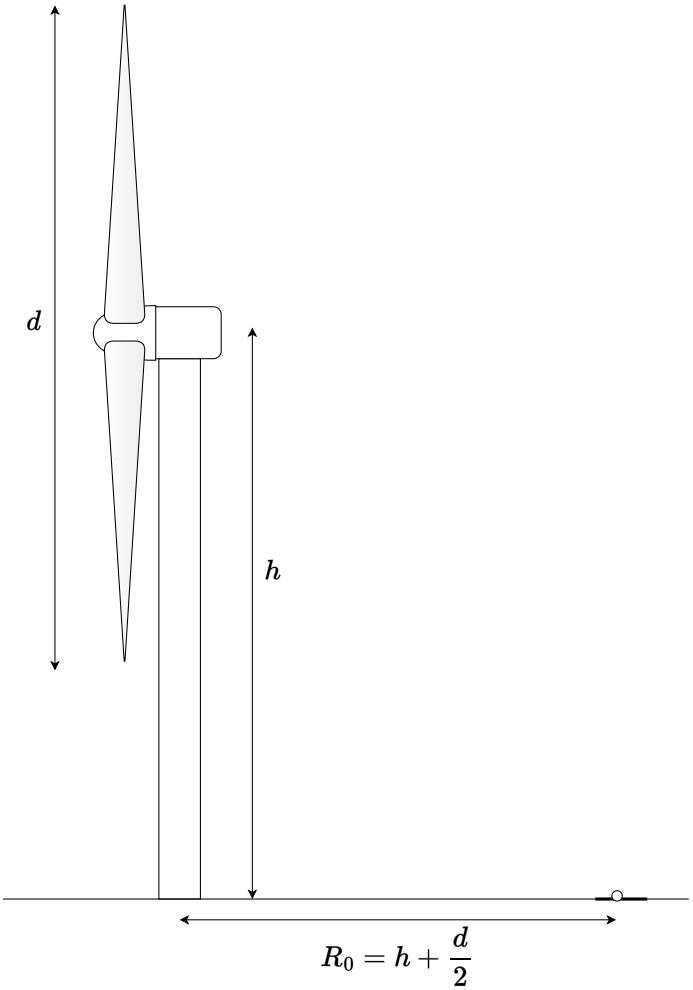

Figure 2.7: Illustration of measurement position according to [2].

If the noise from the turbine is measured in 1/3 octave bands the range is 20 Hz to 10 000 Hz. The resulting spectrum is based on 10 or 60 s, where the turbine's production of power, wind speed at the hub and wind speed at a height of 10 m is measured. The wind speed at the hub is calculated from the effect produced by the turbine. If the turbine is not spinning (when measuring background noise) or the effect curve is not known, the wind speed at the reference is calculated from eq. 2.6 [2].

$$v_{ref} = v_z \cdot \frac{ln(\frac{z_{ref}}{z_{0ref}})ln(\frac{h}{z_0})}{ln(\frac{h}{z_{0ref}})ln(\frac{z}{z_0})} \tag{2.6}$$

Where:

v_z	Is the wind speed at a height of the wind gauge (at least 10 m)	[m/s]
z	Is the height of the wind gauge	[m]
z_{ref}	Is the reference height (10 m)	[m]
z_{0ref}	Is the roughness length reference (0.05 m)	[m]
z_0	Is the roughness length of the environment	[m]
h	Is the height of the hub	[m]

The roughness length is found in a table containing a value for a number of different types of terrain [2]. The values for different types of terrain can be seen in table 2.1.

Type of terrain	**Roughness length z_0 [m]**
Water, Snow, Sand	0.0001
Open flat landscape, bare ground	0.01
Agricultural land with vegetation	0.05
Residential area, small town, area with high vegetation	0.3

Table 2.1: Roughness length for different types of terrains [2].

Measurements are carried out when the turbine is operating and for background noise without the turbine operating. The spectrum for the background noise in 1/3-octave bands is used to correct the reference spectrum for the turbine [2]. The corrected reference spectrum is calculated in eq. 2.7:

$$L_{A,ref,k} = 10 \cdot log(10^{\frac{L_{A,ref}}{10}} - 10^{\frac{L_{A,B}}{10}}) \tag{2.7}$$

Where:

$L_{A,ref,k}$	The corrected reference SPL in 1/3- octave bands	[dB re. 20 μPa]
$L_{A,ref}$	The reference SPL in 1/3- octave bands	[dB re. 20 μPa]
$L_{A,B}$	The SPL of mean background noise in 1/3 octave bands	[dB re. 20 μPa]

The SPL for the reference spectrum has to be at least 3 dB higher than the background noise spectrum, otherwise the correction is set to 3 dB. Furthermore, the total equivalent continuous A-weighted SPL L_{aeq} of the mean background noise has to be 6 dB or lower than the total level of the turbine noise. If this condition is not satisfied a new measurement with a lower background noise has to be carried out [2]. For calculating the wind turbine's apparent sound power level in 1/3-octave bands eq. 2.8 is used.

$$L_{WA,ref} = L_{A,ref,k} + 10log(4\pi(R^2 + h^2)) - 6dB \tag{2.8}$$

Where:

$L_{WA,ref}$	Is the apparent sound power level in 1/3- octave bands	[dB re 1 pW]
$6dB$	Correction for the microphone placement close to a reflecting surface	[dB]

Based on the measurements this equation gives the apparent sound power level of a point source located at the hub, having the same emission as the turbine in question [2]. The interest is often to know the SPL at a certain point. This could be the nearest neighbour or a public area. After calculating the apparent sound power level an equation for calculating the A-weighted SPL at a distance is given as shown in eq. 2.9.

$$L_{pA} = L_{WA,ref} - 10log(l^2 + h^2) - 11dB + \Delta L_g - \Delta L_a + \Delta L_m \tag{2.9}$$

Where:

l	Is the distance from tower to the point of interest	[m]
$11dB$	is a correction for the distance (10log 4π)	[dB]
ΔL_g	Correction for terrain (1.5 dB for onshore and 3 dB for offshore)	[dB]
ΔL_a	Absorption of air ($\alpha_a\sqrt{l^2 + h^2}$) with α_a being a damping coefficient	[dB]
ΔL_m	Correction for multiple reflections (0 dB for onshore turbines)	[dB]

For this equation, the height at the point of interest is always assumed to be 1.5 m. The damping coefficient is α_a is given in dB/km for 80 % humidity, 10°C and is found in a table for both 1/3- and 1/1- octave bands given in the regulation [2]. This method, described in the regulation, is similar to the standard IEC 61400-11.

The method described here assumes constant environmental parameters such as the reflections in the terrain, absorption coefficients for constant temperature and humidity along with a stationary point source located at the hub, etc. This reflects the fact that the method is primarily used in combination with measurements for checking already established turbines or for testing new prototypes.

The regulation and method described in this section is used to check whether a given wind turbine complies with the regulation. More complex methods to predict outdoor sound from eg. wind turbines exist and take into account many different parameters, some of these state of the art methods will now be explained.

2.3 Outdoor Sound Propagation & Modelling

The prediction and modelling of outdoor sound propagation is an extensive task that depend on a multitude of parameters. The geometric contours and acoustical features of a landscape, relative position of a source and receiver in said landscape, as well as meteorological and thermodynamic parameters such as wind, temperature, pressure and humidity all affect the transmission and reception of sound [6].

This section seeks to give an overview on the modelling of outdoor sound propagation, outline the parameters of relevance wrt. noise from wind turbines and elaborate on existing modelling schemes and the consequences of simplification or exclusion of details when modelling outdoor sound.

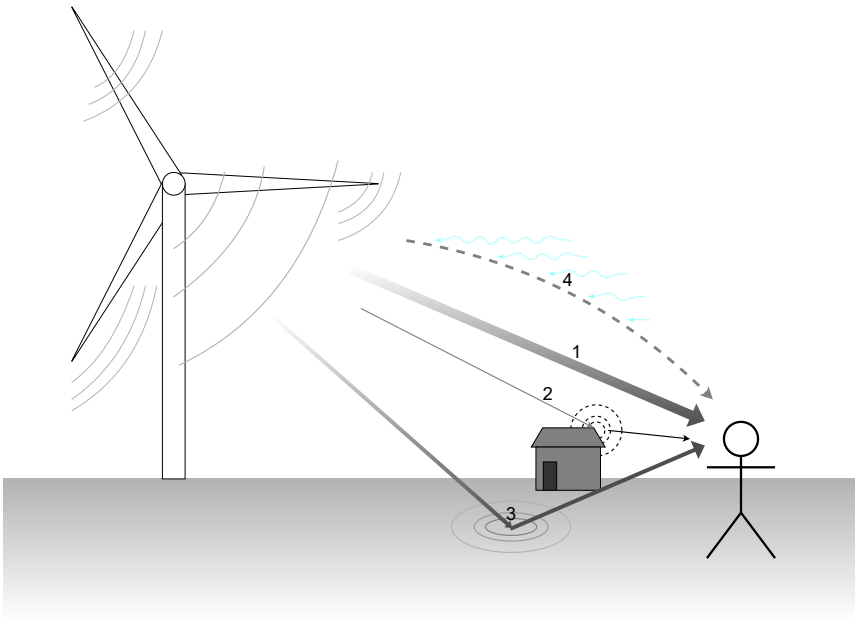

Figure 2.8: Illustration of several acoustical propagation source models.

Figure 2.8 illustrates sources of sound, caused by acoustical phenomena, which contribute to the combined sound experience.

1. Direct sound from all sound sources to the receiver.
2. Diffusion, diffraction and reflection from nearby objects.
3. Absorption and reflection from the ground.
4. Atmospheric in-homogeneity of wind speed and temperature refracting the sound paths.

It should be noted that, for the in-homogeneous medium in fig. 2.8, '4' replaces '1' as the direct path contribution, and likewise any reflected paths would similarly be curved.

There are several modelling schemes for the propagation of sound, both ray- or wave-based, with homogeneous or in-homogeneous assumptions, flat infinite plan assumption and single sound source or multiple sound source assumption. Before diving into the more complex models in sec. 2.3.6, the basic underlying principles are explained.

2.3.1 Acoustic attenuation in air

Over short distances, for small amplitudes and for certain gasses it may be valid to consider the acoustic medium, in which the wave travels, adiabatic, and hereby neglect attenuation entirely [14]. However, when the attenuation is not small enough to be neglected, it is necessary to include the thermodynamic models in order to accurately describe the resulting acoustic transmission. Generally speaking this is the case for sound carried over long distances, such as with wind turbines. It is the purpose of this section to cover the relevant elements wrt. wind turbines, however describing the collected thermodynamic intricacies of the subject is beyond the scope of this project (the reader is referred to [14] for reference).
Acoustic attenuation in a homogeneous medium may be attributed to 3 types of loss: Heat conduction loss, viscous loss and losses caused by internal molecular processes [14]. The viscous and heat conduction loss are both included in the model of the 'classical absorption coefficient' calculated as:

$$\alpha = \frac{\omega^2}{2\rho_0 c^3}\left(\frac{4}{3}\eta + \frac{(\gamma-1)\kappa}{c_{\mathscr{P}}}\right) \tag{2.10}$$

Where:

ω	is the angular frequency for a specific frequency in the medium	[rad/s]
ρ_0	is the equilibrium density	[kg/m]
η	is the coefficient of shear viscosity	[Pa · s]
γ	is the ratio of specific heats	[-]
c	is the speed of sound	[m/s]
$c_{\mathscr{P}}$	is the specific heat at constant pressure	[J/(kg · K)]
κ	is the thermal conductivity	[W/(m · K)]

The resulting absorption coefficient from eq. 2.10 is applicable to the lossy Helmholtz equation, for which the pressure at a specific time and travelled distance is calculable as:

$$\mathbf{p} = P_0 e^{-\alpha x} e^{j(\omega t - kx)} \tag{2.11}$$

Where:

P_0	is the peak difference in pressure at distance '0'	[Pa]
x	is the travelled distance	[m]
k	is the wave number	[m^{-1}]
α	is the absorption coefficient	[J/(kgK))]

In equation 2.11, the term '$e^{-\alpha x}$' defines the exponential decay that, when plottet in dB/m in relation to a logarithmic frequency axis, yields a straight line [14]. This classical modelling, however, does not account for attenuation caused by energy lost to molecular thermal relaxation and does not necessarily hold for compositions of gasses of higher molecular compositional complexity.

Molecular thermal relaxation is an attenuative effect dependent on the internal molecular structures of the specific gas, directly related to its heat capacity [14]. This capacity depend on the degrees of freedom intrinsic to the specific molecule, where a monatomic gas generally only has the 3 degrees of freedom (translational). Diatomic gasses such as the ones primarily making up earths atmosphere; dinitrogen (N_2) and dioxide (O_2), has 2 additional degrees of freedom (rotational), adding to the thermal capacity. Water vapor in air (H_2O) equates to low concentrations even at high relative humidity. However, it acts as a catalyst to excite the vibrational state of N_2 and O_2. This makes a considerable difference in the final absorption coefficient, especially in the human perceivable frequency range [14].

As the molar concentration of water vapor in air varies with pressure and temperature, empirical investigation into the resulting absorption for different humidities has been documented in e.g. ISO 9613-1 for use in the calculation of attenuation in air. The collected attenuative effect is visible in fig. 2.9.

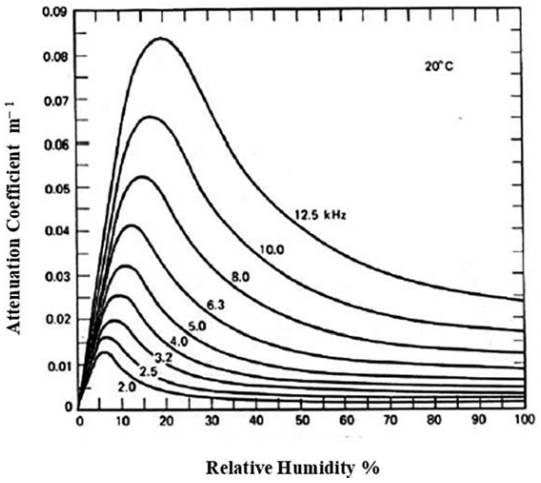

Figure 2.9: Attenuation coefficient for air at different relative humidities at 20°C [15].

The attenuation coefficients depicted in fig. 2.9, is calculated according to the ISO 9613-1 standard, also similarly depicted in ANSI S1.26-1995 [6], [16]. It is clearly visible from the figure that the effects of humidity are non-negligable when the attenuation is non-negligable.

2.3.2 Acoustical Propagation

There exists a multitude of methods for predicting or simulating the propagation of acoustic waves. The methods range in complexity from relatively simple to ones exceedingly difficult to compute. These methods may be divided into two groups: Ray-based methods, such as image-source Modelling (ISM) and ray-tracing; and wave-based methods, such as the finite element method (FEM) and the finite-difference time-domain (FDTD) method [17]. These methods attempt to model acoustical phenomena such as reflection, refraction, absorption, diffraction and diffusion, as shown in fig. 2.10:

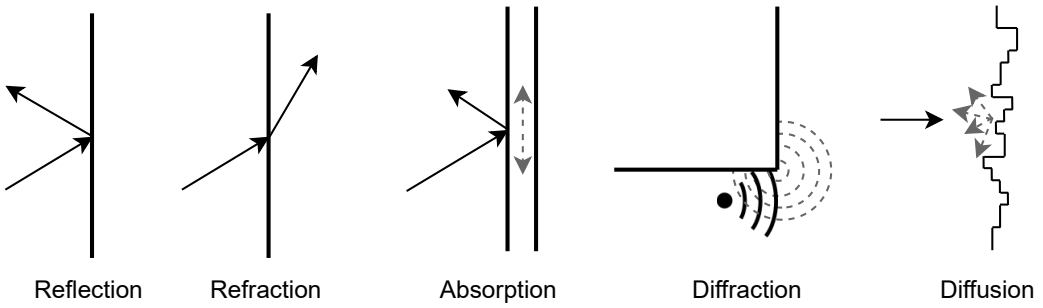

Figure 2.10: Illustration of acoustical phenomena resulting in changes in sound propagation.

Figure 2.10, illustrates the different sound phenomena, which depend on the shape

and impedance of the media, wavelength and relative direction of the acoustic wave. Some of the previously mentioned models does not consider certain phenomena. Some stochastic ray-based models does not consider acoustic scattering caused by diffraction, and the more simple ISM, additionally, does not consider diffuse scattering [17]. ISM, which is widely used in room modelling, is considered applicable for short wavelengths relative to the size of the reflecting surface. For example: for low-frequencies in small rooms, geometric models inadequately describe the propagation, as wave nature is not considered [17]. Modern large wind turbines, however, are often placed on relatively large flat surfaces (especially in Denmark), where it may be argued that wavelengths of the audible spectrum may considered small compared to the reflecting ground surface. An illustration of ISM on a flat infinite plane is illustrated in fig. 2.11:

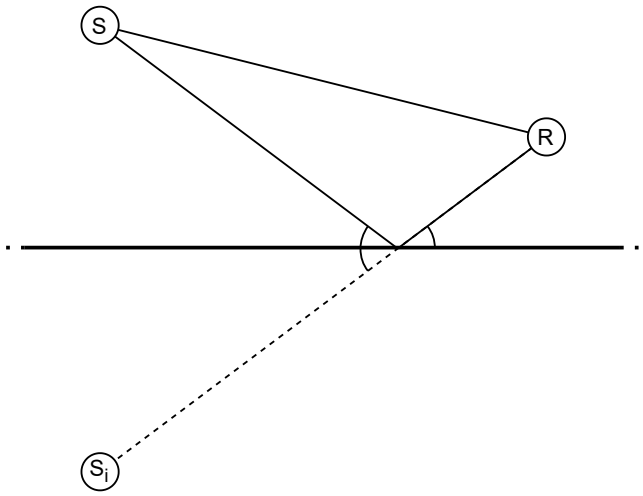

Figure 2.11: Illustration of image-source modelling of a single ground reflection

On figure 2.11, the propagation of sound from source (S) to receiver (R) is modelled as the sum of the direct path and the reflected path. The reflection may be seen as the contribution of an independent image-source 'S_i', positioned geometrically as the reflection of 'S' in the ground plane.

The summation of two identical sources at different distance from the receiver results in a frequency dependant constructive/destructive interference commonly known as comb-filtering.

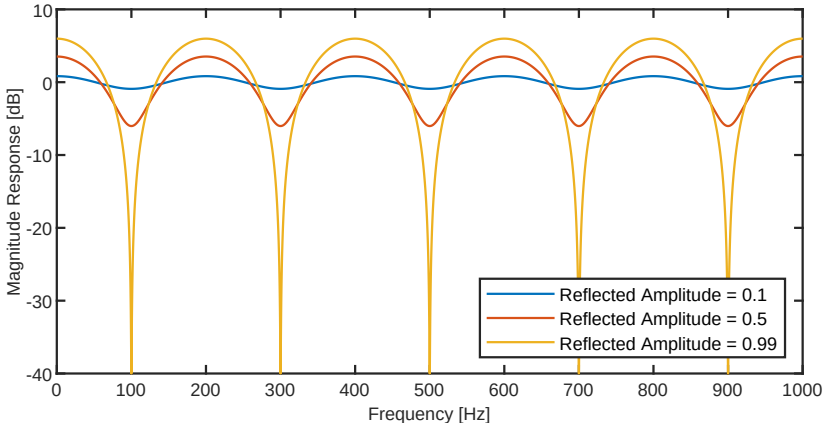

Figure 2.12: Feed-forward comb-filter effect for different reflection amplitudes.

Figure 2.12, shows the effects of comb-filtering for near-total reflection, where the acoustic delay results in an in-phase summation, resulting in $\sim +6\,\mathrm{dB}$, or near-total out-of-phase cancellation ($\approx$ -∞ dB). The cyclic nature of constructive/destructive frequencies, wrt. delay, results in the monotonically repeating patterns in the frequency domain. Most surfaces, however, does not reflect perfectly, and fig. 2.12 also illustrates how different levels of attenuation result in a decrease of the effect.

Reality, however, is complicated. A ground plane found in nature, can rarely be considered perfectly flat, and also varies in terms of hardness and vegetation. However, modelling every intricate detail of vegetation can be an arduous task, therefore standards have been created to establish general methods for calculating the most relevant effects, such as ground reflections and atmospheric absorption.

2.3.3 Ground effect

In outdoor sound modelling, the influence of ground is often spoken of as the 'Ground effect'. This effect is calculated and applied differently, for different standards and methods. While effects, such as the comb-filter effect depicted in fig. 2.12 occurs, as the result of a delayed correlated signal from an image-source; reflections are more complicated than simple magnitudal modification. For the theoretical examples of a plane wave in air hitting an infinite isotropic surface at an oblique angle, the reflection can be described using Rayleighs reflection coefficient:

$$\mathbf{R} = \frac{Z_2 \cdot cos(\theta_i) - Z_1 \cdot cos(\theta_t)}{Z_2 \cdot cos(\theta_i) + Z_1 \cdot cos(\theta_t)} \tag{2.12}$$

Where:

Z_1	is the impedance of the medium 1 (usually air)	[-]
Z_2	is the impedance of the medium 2	[-]
θ_i	is the angle of incidence	[°]
θ_t	is the angle of transmission into medium 2	[°]

For many cases, where the medium 2 is a solid (and consequently: the acoustic speed of medium 1 is far greater than medium 2) eq. 2.12 may be be approximated without the need for θ_t [14]. However, the challenging task is defining the impedance of medium 2, i.e. the ground. Ground is a complex element, and soil type, vegetation, water content etc. affects the resulting impedance. For this reason, some standards use approximate modelling of the 'ground effect'.

In ISO 9613, the effect of ground is calculated as an octave-band-wise amplification/attenuation, depending on the height of, as well as ground type at source/receiver. Other models, such as ones from NORD2000 and HARMONOISE, involve ray-based approximations with plane- or spherical-wave assumptions. All models, however necessarily involve some classification of the surface. An example of these classifications can be seen in table 2.2:

Ground surface class	**Value of ISO9613-2 parameter, G**	**Value of NMPB-2008 parameter, G**	**Representative flow resistivity R_1 ($kPa\ s/m^2$) (Harmonoise)**	**Ground surface description**
A	1	1	12.5	Very soft (snow or moss)
B	1	1	31.5	Soft forest floor
C	1	1	80	Uncompacted, loose ground
D	1	1	200	Normal uncompacted ground (pastures, forest floors)
E	0	0.7	500	Compacted fields, lawns and gravel
F	0	0.3	2000	Compacted dense ground (gravel road, parking lot)
G	0	0	20 000	Asphalt, concrete
H	0	0	200 000	Water

Table 2.2: Ground classification according to different standards, from [18].

Table 2.2, shows the different classes of ground surfaces according to some different standards. Some standards approach the surface as a wholly or partially attenuative surface by use of the parameter 'G' (ISO 9613-2 & NMPB-2008). The value of G is applied with an octave band model to calculate the band-wise attenuative effect of ground (the attenuation may be negative). Other models such as HARMONOISE use more complex methods for calculating the reflection. The ground effect can be estimated by use of the flow resistivity of the ground, but can also for some more elaborate models, contain several parameters, such as Attenboroughs four-parameter model [19]. The non-uniformity of the medium, such as increasing density with increasing depth, is also included in some model, as discrete or continuous functions. The classification of ground is a complex matter, and the models are constantly being developed and tested [20], [21]. The accuracy of these vary when compared with empirical experiments, but can be hard to cross-validate, for the same reason that e.g. "soft forest floor" is a relative term.

2.3.4 Propagation in an inhomogeneous medium

Many of the valid assumptions used in indoor acoustics such as a uniform adiabatic medium with stable temperature are not necessarily accurate for outdoor acoustics. Meteorological elements such as wind and temperature affect the propagation path of sound, and should be considered. The effect of these elements vary considerably depending on time of day, year, geographical position, and if currently in a low- or high-pressure area. Variance of atmospheric pressure wrt. height above sea level also influences propagation, but is often, for practical purposes, not considered important enough to warrant inclusion [15]. Many meteorological effects are fluctuating and may produce a reversed effect, for reversed conditions. Commonly, however, when speaking of wind turbine noise it involves windy conditions. A detail necessarily included in the directives regarding evaluation of noise, as these are usually measured downwind. A condition that worsens the effect of noise, as will be shown.

The propagation effects of shifting temperature and wind speeds directly affects

the speed of sound [5], with windspeed sometimes directly modelled as an effective change in speed of sound [22]. The propagation of sound can be described using wave or ray theory, where ray theory neglects the phenomena of diffraction. A change in sound speed in a medium, causes refraction. Commonly illustrated as going from one medium into the other, causing an abrupt angular change in direction. In the effect of a gradual change in speed, it causes gradual refraction and therefore a gradual change in direction. This changes the propagation path of direct and reflected path contributions from source to receivers, as is shown in fig. 2.13.

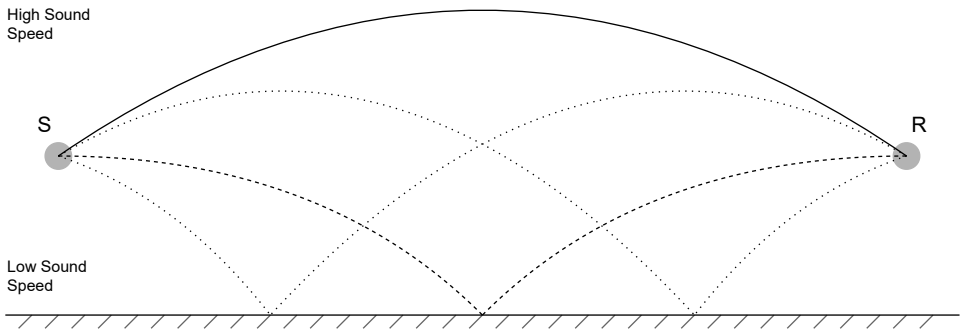

Figure 2.13: Illustration of Ray-based propagation paths between source and receiver for linearly increasing sound speed wrt. height [5].

Figure 2.13 illustrates the direct path of propagation between a source and receiver and the path of reflected contributors. This case is for a linear increase in sound speed wrt. height, which causes the path to take on a circular arc [5], [23]. Figure 2.13 only show contributions from single reflections, but in some cases propagation paths exist that is reflected multiple times. This depend on the intensity of the sound speed gradient wrt. height, as well as the height of source and receiver and distance between them [5]. For the same reason, the dotted line contributions on fig. 2.13 can only exists for an inhomogeneous atmosphere. The effects depicted on fig. 2.13 is observed in downwind conditions from a sound source (e.g. a wind turbine), where higher altitudes generally equates to higher wind speeds, which explain the empirically observed higher noise level downwind. The same effects in fig. 2.13 happens for temperature inversion, where temperature increases with height [5].

Meteorological effect cannot necessarily be modelled as linear relations wrt. height. While wind gradients at high altitudes may be approximated as linear, wrt. height; closer to the ground these effects take on a more logarithmic profile[5].

The reverse phenomena of fig. 2.13, is caused by upwind conditions, and is depicted in fig 2.14:

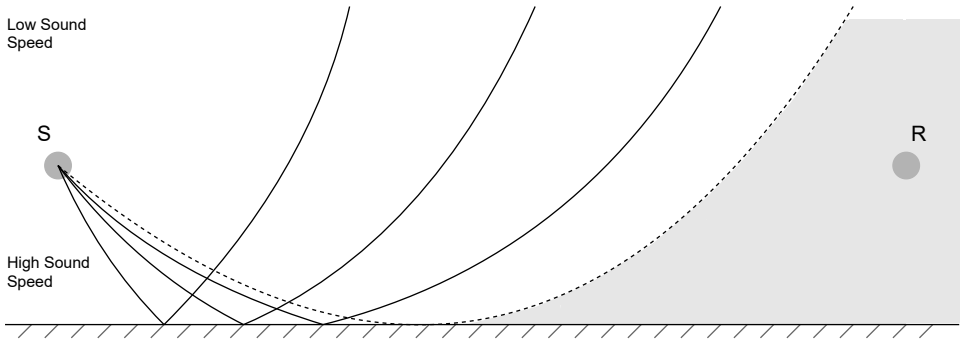

Figure 2.14: Illustration of Ray-based propagation paths between source and receiver for linearly decreasing sound speed wrt. height [5].

In the case of a decreasing sound speed with increasing altitude, the refraction causes the acoustic rays og a sound source to bend upwards, as seen in fig. 2.14. This may create a theoretical "shadow zone" (grey area in fig. 2.14), where the sounds of the source will never be introduced. This, however, is not true in practice. While this effect decreases the acoustical level experienced at the receiver, it does not completely eliminate it. This is a consequence of describing the acoustical propagation as rays, and neglecting the effect of diffraction included in wave-theory. Even though diffraction is usually described by a wave passing a barrier, is this case; diffraction causes the some part of the acoustic wave to pass into the shadow zone, with lower frequencies being diffracted greater than higher [5]. The effects depicted in fig. 2.14, moreover explain why sources that are upwind experience an increased attenuative effect wrt. acoustic propagation. Lastly, the attenuative effect of movement through the medium, as described in sec. 2.3.1, also changes as the acoustic path from source to receiver changes.

Acoustic propagation may generally be described using ray-based modelling, however state of the art propagation modelling are based on nummerical approximation of the wave equation [6]. Wave-based modelling can be exceedingly computationally complex, and usually involves quantization into discrete points or cells. The choices of the cells an approximation of the wave-equation, affect the complexity and precision of the resulting model, and is a topic of ongoing research. Some of the currently used wave models are presented in sec. 2.3.6.

2.3.5 Moving Sources

For some acoustical propagation, it is not valid to assume stationary sound sources. Since a wind turbine consists of moving parts the distance between the blades and a listener will change over time. This means the frequency of the noise will change at a listener's position. The change in frequency is a consequence of a moving source is known as the Doppler effect. In the case of a source moving towards a listener the frequency of the sound will increase. This happens as the distance between sound waves becomes smaller when the source moves in the direction of the listener. When

a source is moving away from a listener frequency of the sound will decrease instead, since the source is moving away from the listener thereby increasing the distance between sound waves [24]. The Doppler effects is illustrated in fig. 2.15.

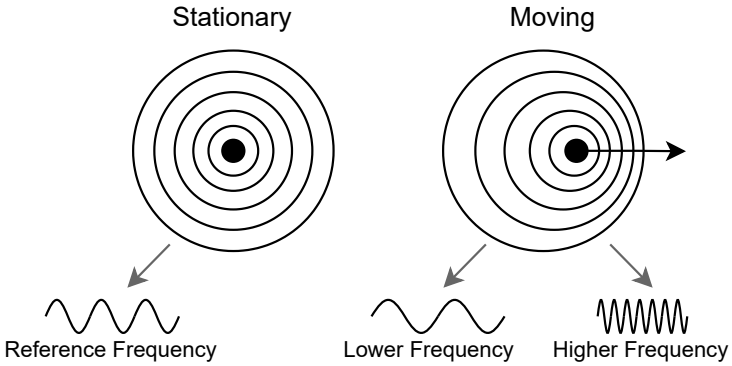

Figure 2.15: Illustration of Doppler effect [25].

The frequency shift for a moving source with a constant tone can be calculated as shown in equation 2.13. This equation is assumes the source having a constant speed.

$$f' = \frac{f}{1 - \frac{U}{c} cos(\theta)} \tag{2.13}$$

Where:

f'	Is the frequency caused by the Doppler effect	[Hz]
f	Is the original radiated frequency	[Hz]
U	Is the flow speed	[m/s]
c	Is the speed of sound	[m/s]
θ	Is the angle between source velocity and direction of listener	[rad]

Another effect caused by the movement of the noise source is the amplitude of the sound. This is known as Doppler amplification. For a source moving towards a listener the amplitude of the sound will increase, and moving away from the listener will result in a lower amplitude [5]. However, this is not a function of the speed in the same way as the frequency shift but relies on the speed compared to the medium. A factor for scaling the amplitude of the perceived sound is given by eq. 2.14.

$$g = \frac{1}{(1 - \frac{U}{c} cos(\theta))^2} \tag{2.14}$$

These are two parameters which have an impact on the sound made by moving sources which are some of the characteristics of a wind turbine.

2.3.6 Propagation models

Acoustic propagation modelling has become a valuable tool in the estimation of noise. It is used in mapping the exposure caused by existing noise sources, such as highways or wind turbines, as well as the potential consequences of additional noise sources [6]. Several models exist with varying precision and inclusion of propagation parameters, of which some of the most prevalent will be presented here.

Propagation models may be differentiated by the used scientific method:

- Engineering: Based on empirical or semi-empirical data used for practical applications.
- Analytical: Based on the full-wave equation.
- Numerical: Based on the direct- or full-wave equation.
- Hybrid: Based on any mixes of empirical, analytical, or numerical modelling.

ISO 9613

The ISO 9613 standard defines a set of methods for estimating the attenuation of outdoor sound propagation (ISO 9613-1), and physical effects caused by the ground, reflecting surfaces, and screening obstacles (ISO 9613-2) [15], [26]. It has been used extensively in noise estimation, as well as basis for further modelling.

ISO 9613-2 Takes a pragmatic empirical approach to describing the attenuative effect of ground. The standard defines 3 types of ground: Hard ground, porous ground and mixed ground. Ground type, height of receiver and source, and the distance between them is used to calculate frequency dependant attenuation/amplification in octave bands [26]. By itself, ISO 9613-2 may oversimplify the effect of ground and lead to inaccuracy in noise estimation [6]. Furthermore, the standard does not necessarily provide the most accurate basis for low frequencies. For example, for the 63 Hz octave band, the calculations always add an amplification of 4.5 dB, irregardless of the height of source/receiver, and the distance between them [6].

Sound attenuation caused by geometrical divergence, and atmospheric absorption, is described in the ISO 9613-1 and ISO 9613-2, and the scheme is adopted or adapted in newer engineering propagation modelling [6]. Geometrical divergence follows the inverse square law in sound intensity for increasing distance to the sound source [14]. The calculation of atmospheric absorption is dependent of the molecular thermal relaxation for respectively oxygen and nitrogen which is frequency dependent. This absorption depend on pressure, temperature, humidity as well as frequency [15]. The ISO 9613 follow a 'worst case' modelling scheme, where the receiver is always considered downwind from the source, which may inaccurately describe the summation of 2 independent sound sources, such as 2 wind farms, as both may not be downwind at the same time [5]. For one to be downwind ($\pm 45°$ acc. ISO9613) from 2 independent sound sources, such as 2 wind farms, they either have to be close to each other, or

be positioned approximately parallel to the wind gradient, with the receiver being downwind in the same direction.

The standard has been used widely, and even though it has faced general critique for its applicability and has been largely supplanted by newer more sophisticated engineering models, it is still used as a reference today [6].

NORD2000 & HARMONOISE

NORD2000 & HARMONOISE are similar in many regards, but with some differences. Both adopt or modify schemes from the ISO 9613 standard, and are able to incorporate geometrical ray-based modelling methods as well as numerical methods for noise propagation estimation.

The NORD2000 noise propagation modelling scheme was a joint venture of the nordic countries, used for the estimation of e.g. traffic noise in the range 25 Hz to 10 kHz. The propagation modelling does not assume straight lines from source to receiver, but incorporates refraction of propagation paths, depending on the atmospheric conditions, although this is only valid for modest refraction. NORD2000 also has more granularity in describing the effect of ground, providing 6 degrees of hardness depending on surface structure [5], [6].

HARMONOISE is a newer state-of-the-art engineering modelling scheme made as a cooperation of a number of European countries for the same frequency range as NORD2000. HARMONOISE incorporates the calculation of line-sources as well as point sources, which make it more representative of infrastructure noise sources like highways and train tracks [6]. It also features sound pressure prediction in 1/3-octave band as opposed to the octave bands in the ISO 9613 method [6].

Both HARMONOISE and NORD2000 model the phenomena similarly to the ISO 9613 standard. The modelling schemes include: Geometric divergence, Air absorption, ground, wind and temperature effects.

- Geometric divergence follow the scheme of the inverse-square law [5].
- Absorption from air is based on the ISO 9613 attenuation calculations [5].
- The ground effect is based on geometrical ray theory for the case of flat homogeneous terrain, and follows a scheme of heuristic semianalytical modifications otherwise [5].

They furthermore model the effects of wind and temperature, and allow for modelling of an in-homogeneous propagation media with methods such as ray-tracing, whereby effects of atmospheric refraction are taken into account [5], [6].

Numerical Models

Numerical methods are based on finding the direct solution to the wave equation. They are therefore approximate solutions to the full-wave equation. These methods, however, have an advantage over the full-wave solution, in that they are capable of incorporating meteorological effects such as different wind and temperature conditions. A disadvantage to this, is the need to specify substantially more variables about the scenario, which, in turn, makes the calculated solution highly specific, and therefore not necessarily applicable to other scenarios [5].

Several numerical models are based on either wide- or narrow-angle parabolic equation (PE). These equations are based on an approximate of the wave equation by direct-form partial differential equations, whereto the angle-size determine the angular elevation accuracy for the methods. Heuristically a greater angle produces more accurate results at the cost of increased computational complexity, however this is not necessarily always true [27]. Two methods commonly regarded for acoustical propagation are:

- Crank-Nicolson Parabolic Equation (CNPE).
- Green's Function Parabolic Equation (GFPE).

Generally there are some downsides to exclusively modelling acoustic propagation with parabolic equations. They are meant for evaluating the propagation at a specific frequency, and therefore take considerable computational power to evaluate for a complete spectrum. Additionally, for CNPE, the method is based on frequency dependent grid-spacing which, as the frequency increases, likewise increases in computational complexity [5]. For this reason, the frequency range for PE-based methods are primarily low frequencies. The GFPE method excels at simulating acoustic propagation at long distance, as it is capable of large horizontal range steps, although this comes with the cost of accuracy compared to the CNPE method [5], [6].

PE-methods, and other methods based on the direct-wave assumption, does not consider wind-gradient induced back-scatter back to the source. Disregarding this is still considered a good approximation, but may have to be considered for turbulent conditions [5]. Moreover; PE-methods are only considered accurate for a limited elevation angle. The span of this angle and accuracy therein is based on the angle approximations used when deriving the parabolic equations. Explanation of this relationship is beyond the scope of this project, and the reader is referred to [28] for further interest.

Other numerical methods such as ones based on the boundary element method (BEM) and the finite-difference time-domain (FDTD) method also provide prediction and simulation of sound propagation. As opposed to the PE-methods necessity for running multiple simulations for the frequency of interest, the FDTD method proves sufficient with a single [6]. For this reason, it may be computationally advantageous; although FDTD is already of considerable computational complexity, especially for

higher frequencies. This is because, similar to PE-methods, the spatial discretization of FDTD is defined by the highest frequency of interest [6].

FDTD has been adopted as a reference for other models for outdoor sound propagation modelling, but incurs a considerable computational cost, taking up to 100-1000 times longer than PE-methods [6].

BEM is used in mapping the acoustical properties of surfaces, and also for acoustic reproduction modelling of vehicles and aircraft. BEM is also favorably used to predict the effects of surfaces with different roughness [6], [29].

Many numerical methods perform well for specific conditions, and in this regard: care should be taken to select the appropriate method for the question asked, or multiple should be chosen if need be. A summary of the mentioned models can be found in table 2.3:

Characteristics	Engineering			Approximate	Analytical	Nummerical			
Model	NORD2000	HARMONOISE	ISO9613	Ray tracing	Wave	CNPE	GFPE	FDTD	BEM
Ground effect	Mean or ray (homogeneous)	Mean or ray (inhomogeneous)	Mean	Image source	Inhomogeneous	Inhomogeneous	Inhomogeneous	Inhomogeneous	Boundary
Frequency range	25Hz-10kHz	25Hz-10kHz	50Hz-10kHz	Not Bound	Not Bound	Not Bound	Not Bound	Not Bound	Not Bound
Ideal frequency range	All	All	All	High	All	low	low & mid	All	All
Source model	Point	Point/Line	Point	Point	Point	Point	Point	Point	Point
Fundamental basis	Empirical	Empirical	Empirical	Ray	Full-wave	Direct-wave	Direct-wave	Full-wave	Full-wave
Elevated sources	Yes	Yes	Yes	Yes	Yes	Yes	No	Yes	Yes
Sound speed profile	Linear or log-lin	Linear or log-lin	Mean	No	No	Linear or logarithmic	Linear or logarithmic	Linear or logarithmic	Linear or logarithmic
Meterological conditions	Yes	Yes	Yes (Mean)	No	No	Yes	Yes	Yes	Yes

Table 2.3: Overview of methods used in acoustic propagation modelling [5], [6], [29], [30].

While table 2.3 shows a concrete comparison of the methods, it should be noted that the flexibility of the methods as well as the potential overlap of some, complicates the matter of comparison. While the engineering methods are tangible and highly documented, the numerical methods are products of an approximation. They are individually modifiable in their approximation, and therefore may differ from what is presented in table 2.3. For this reason, table 2.3 is meant for advisory application only.

Hybrid Modelling

Many state-of-the-art methods use a combination of existing methods in order to construct the best prediction or simulation. This allow for the precision of one highly specialised model in one area, whilst maybe having the generality of another. Especially the empirically based engineering methods, such as HARMONOISE, allow for, and even suggest using other methods, such as the PE-based methods, for the prediction [6]. In this sense it is possible to more accurately model the propagation, as the effect of an in-homogeneous atmosphere can be considered. Other recommended hybrid modelling schemes include FDTD and PE or BEM and ray tracing. It should be noted that increased complexity, as will always be the case with using multiple models, may not always lead to better modelling. In one cases ([22]), simulations using CNPE along with ISO 9613-1 observed lower sound pressure levels downwind than upwind for the same distances from a windmill; an observation which contradicts general empirical observations.

Currently, no one-fits-all model exist, and in order to obtain the best predictions or simulations, the appropriate modelling scheme should be chosen according to the conditions. Many of the current modelling methods are not meant for illustrative noise simulation purposes, but are intended as methods for noise mapping, where computation time of minutes or hours are acceptable; which is not the case for a illustrative noise simulator.

The analysis has shown that the most common type of wind turbine today is the upwind wind turbine with three blades. These vary in size and have to comply with different types of rules such as distance to the nearest neighbour and how much noise they produce near those neighbours. The most dominant noise source is the aeroacoustic noise called trailing edge noise, caused by the blades cutting through the air. Different parameters affect this sound when propagating in an outdoor environment e.g. atmospheric attenuation, geometrical attenuation, reflections etc. Modelling the propagation can be more or less complex according to the model and can take up to many processor hours for the most complex models.

These observations will be used in the implementation of a wind turbine noise simulator.

Chapter 3

Simulator overview

The analysis of wind turbines and sound propagation shows that a lot of different parameters can influence how the sound propagates in an outdoor environment. Looking at the wind turbine; the size, rotational speed and design all form the characteristics of the noise. This noise then travels through the air where parameters like wind, humidity, temperature, ground surface and distance all play a role in how the noise is shaped.

To illustrate how some of these parameters affect the noise of a wind turbine the following problem formulation is:

How can a near real-time simulation of wind turbine blade noise be implemented to give a plausible experience of the sound at an arbitrarily chosen position, including the possibility to add/remove effects representing the sound's propagation and physical interaction with different media?

The focus of this project is to construct a real-time simulator that may enable a user to experience the effect of different parameters and compare different scenarios and positions. Furthermore, it is chosen to focus on the wind turbine blade noise, since it is found in the analysis that this is the primary noise source from modern wind turbines.

Based on the problem formulation and analysis some focus points for the implementation of the simulator is.

- The simulator must be possible to adjust the desired position in the "sound environment" relative to the wind turbine.
- There must be an opportunity to choose which parameters to include/exclude in the simulation.
- The focus is on fast computation, enabling a sound to be produced shortly after choosing positions and effects.
- The focus of the simulator will be on a specific type of wind turbine.

A simplification of the simulator is illustrated in fig 3.1. It consists of a blade noise model, which matches a given wind turbine which is used to create the noise of the 3 blades thereby constructing a complete source model.

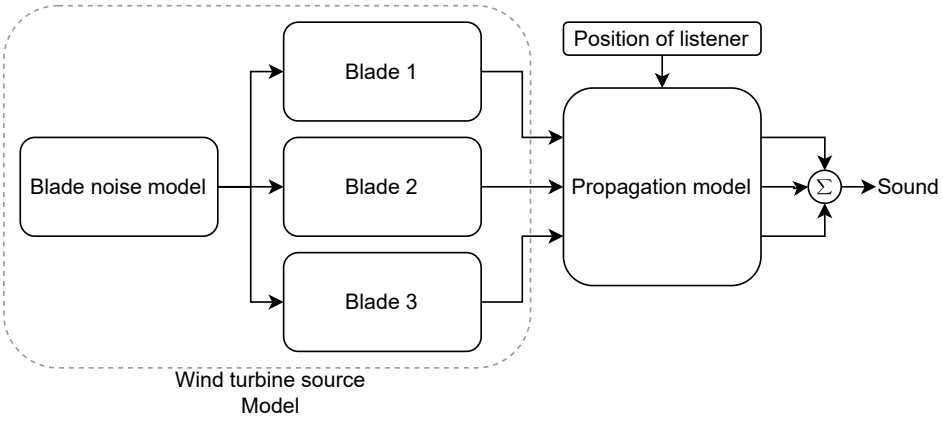

Figure 3.1: Simplification of the elements in the blade noise simulator.

Regarding the wind turbine source model, different approaches can be taken. Some methods assume a point source at the rotor hub [2], [23]. However, in the analysis, it has been shown that the biggest contribution is a point source near the blade tip on each blade, illustrated in fig 2.6 in sec 2.1. Both of these approaches will be investigated and available in the simulator to demonstrate the difference in sound.

The propagation model contains different environmental parameters and can be adjusted to different scenarios. The propagation model shown in fig 3.1 contains different parameters that affect the sound in an outdoor environment. For the simulator, the parameters chosen are based on the analysis of outdoor sound propagation, and the parameters used in various methods/standards as in [26], [2], [23]. The foundation for the propagation model will be a ray-based method, based on the fact that fast computation is the focus, so the output can be produced in a short amount of time.

The widely used Nord 2000, sums up the parameters used to calculate a sound pressure level at a point, based on a point source with a known sound power level. These parameters are seen in eq. 3.1.

$$L_R = L_W + \Delta L_d + \Delta L_a + \Delta L_t + \Delta L_s + \Delta L_r \tag{3.1}$$

Where:

L_R	Is the sound pressure level at the receiver for each frequency band.	[dB]
L_W	Is the sound power level within the considered frequency band.	[dB]
ΔL_d	Is the propagation effect of spherical divergence of the sound energy.	[dB]
ΔL_a	Is the propagation effect of atmospheric absorption.	[dB]
ΔL_t	Is the propagation effect of terrain. (ground and barriers)	[dB]
ΔL_s	Is the propagation effect of scattering zones.	[dB]
ΔL_r	Is the propagation effect of obstacle dimensions and surface properties when calculating a contribution from sound reflected by an obstacle.	[dB]

These parameters will be the main focus to include in the propagation model of the simulator. Each parameter is implemented with the possibility to adjust sub-parameters that will change the way it affects the sound. Furthermore, all of the parameters should be possible to switch on and off, thereby making the contribution of each parameter more noticeable.

Another parameter, not described in eq. 3 but possible to include in the Nord 2000 model is refraction caused by eg. different wind speeds creating an inhomogeneous medium. This requires a more complex model to calculate the curved path of the sound. Furthermore, earlier studies find that including a variation in wind speed in the range of 5 m/s to 12 m/s only caused a difference in the calculated sound pressure level of 1 dB(A) for a distance of 530 m in the downwind direction [31]. Based on this the refraction effect will not be of focus. An alternative solution would be to consider the medium as homogenous and with a constant wind speed for the entire atmosphere. However, a constant wind speed does generally not have a significant impact on sound transmission [32].

Wind turbine coordinate system and measurements

If the position of a receiver changes some of the parameters in the propagation model will also change. A position in the 3-dimensional space of a receiver will be in relation to a reference point. The reference point is chosen to be at the centre of the wind turbine tower at a height of 0 m. The three axes in fig. 3.2 define the directions relative to the reference point.

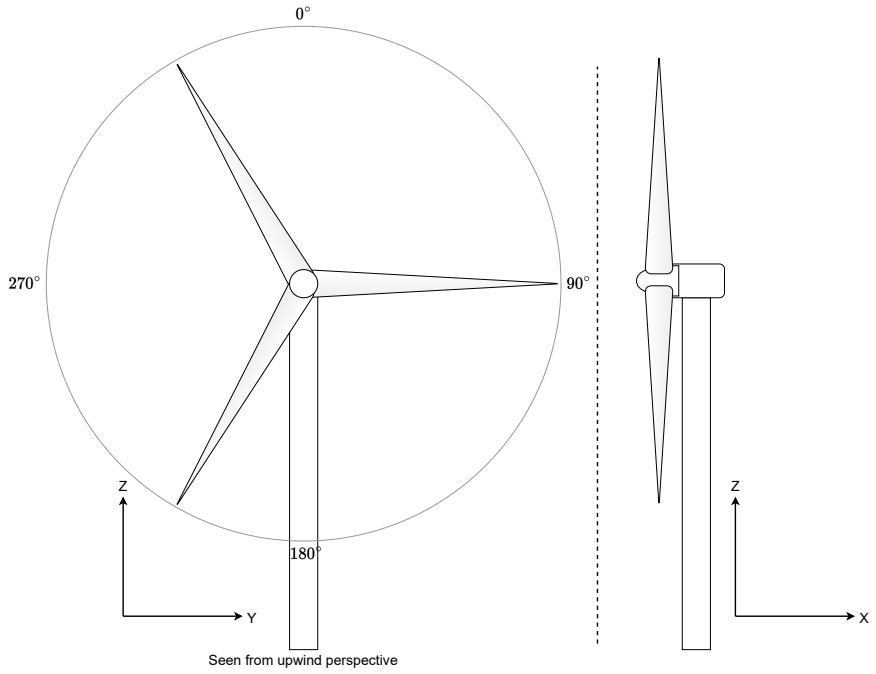

Figure 3.2: Illustration of a wind turbine and the axes defining the positions in a 3-dimensional plan.

The directions are defined as the X-direction being in the upwind/downwind direction, with the downwind direction representing the positive direction. The positive Y-direction is the side of the downstroke e.g. to the right when looking at the turbine from the front as in fig 3.2. The Z-direction defines the height where the positive direction is upwards.

In collaboration with Jesper Lumbye Andersen from Siemens Gamesa, measurements on a wind turbine have been made. These measurements will act as both a reference point to compare the output of the simulator with a real life recording, but also as a tool to build models and extract turbine parameters. The journal describing the setup and additional info is provided in appendix A.4.

In agreement with Siemens, the wind turbine is kept anonymous due to company development discretion. For this reason, the recordings, photos or turbine parameters can not be shared in this report. Spectrograms, spectrums and octave-band analyses are however allowed to be presented in the report and will be used throughout the report for various purposes.

A sketch giving an overview of the different microphone positions used during the measurements is to be seen in fig 3.3.

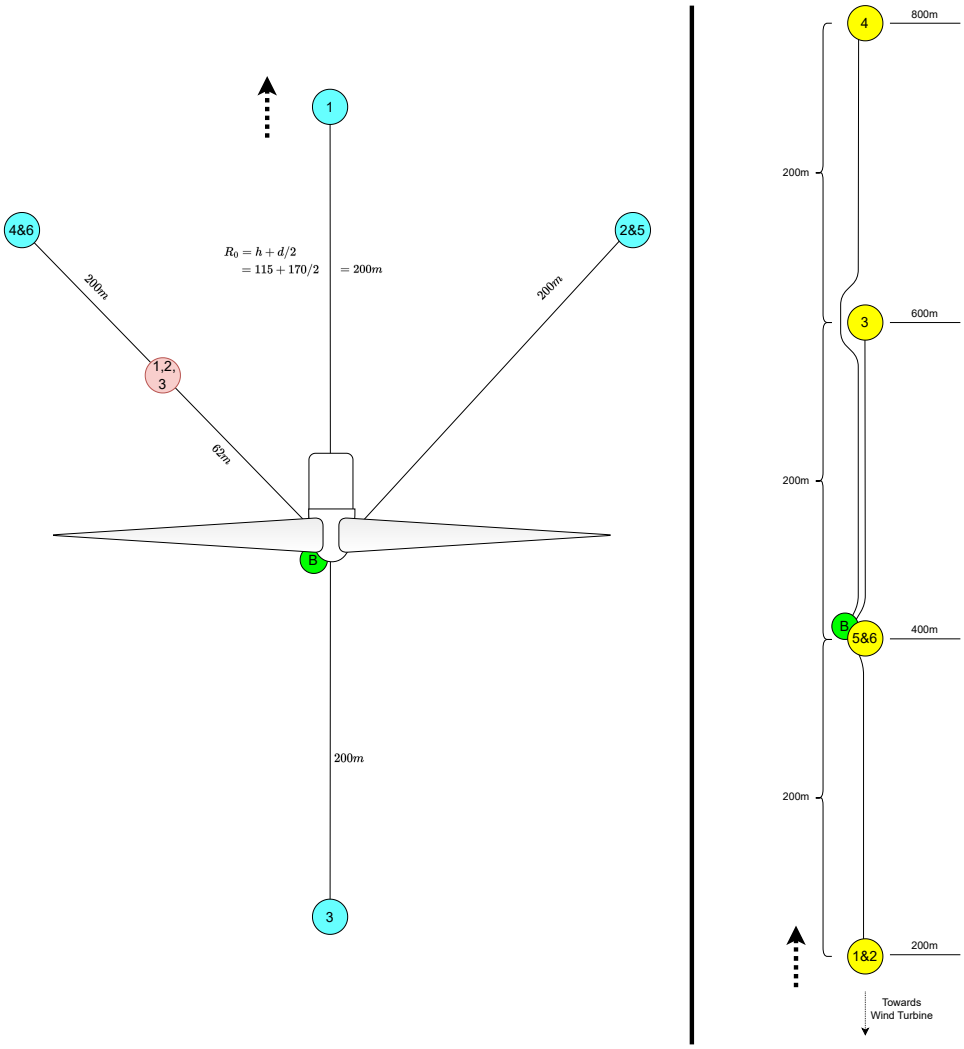

Figure 3.3: Different measurement microphone setups. The 'B' indicates the base station where the microphones are connected. Numbers are microphones. More numbers in same place indicates different heights.

The positions are chosen to represent the turbine at numerous angles and at various distances to have multiple scenarios of the sound from the turbine. Furthermore, microphones have been placed at different heights in the range 0 m to 1.5 m to capture effects caused by reflections. The measurements are divided into three groups: red categorized as near field, blue as short range and yellow as long range. These names will be used to categorize the setup throughout the report.

The large range of distances from the turbine to a receiver measured at different times of the day means that the environment changes. Some measurements contain mechanical noise from the turbine turning towards the wind as the wind direction changes, while some measurements are contaminated by bird song. To avoid large

variance in the measurement it is chosen to use the material with the least of these sources of error.

Simulator concept for implementation

To give an overview of the simulator a more detailed version of the simulator is shown in fig 3.4. Here the different parameters of focus in the propagation model are specified. Compared to eq. 3.1 the two parameters ΔL_s and ΔL_r are not included, since the characteristics of the environment were reasonably flat and no major objects/obstacles were present. While the recordings act as a reference for the simulator, placing obstacles and scattering zones in the simulator would not be representative of the environment of the recordings.

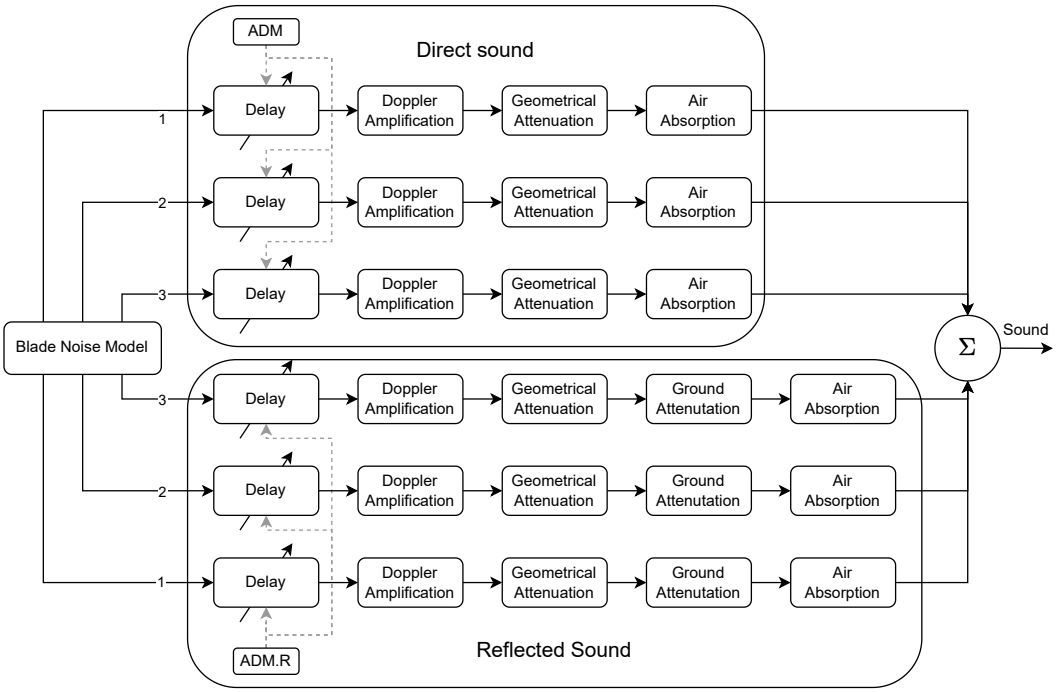

Figure 3.4: Overview of the simulator flow and parameters to be included.

The figure illustrates how the simulator is split into three major parts a blade noise model and a propagation model for the direct sound and the reflected sound. The blade noise model will act as an input to the propagation model and does not change as the propagation model does. This enables the blade noise model to be produced before the start of the simulation begins. This allows for more complex computations and gives more computational time to the propagation model.

Based on these choices the focus will now be on the implementation of the blade noise model and all of the parameters in the propagation model.

Chapter 4

Development

This chapter describes the methods and implementation of the sound model and the different parameters in the propagation model. All of the implementations are made in Matlab and the results will be extracted and presented as plots or tables.

4.1 Wind turbine noise model

This section elaborates on the methods and implementation of the model that represents the wind turbine noise. This model will be the first step in recreating a plausible experience of the sound from a wind turbine. The sound model is a constant noise signal, which can then be modified by effects representing physical parameters such as moving sources, reflections etc.

There exist different approaches for creating a sound model of a wind turbine, these approaches vary in complexity and input parameters. For some models, it is necessary to know the exact geometry and dimensions of the blades, whereas other approaches rely on recordings or wind tunnel tests.

As explained in sec 3, and the additional info in appendix A.4, measurements on a wind turbine have been made. The recordings made on the turbine will in this section be used to create one sound model and another model will be based on theoretical models.

During the measurements, one of the positions for the microphone were close to the blades of the wind turbine. This position is illustrated in fig. 4.1 with the microphone being located at the ground on a plate and shielded with two hemispherical windscreens (further description of measurements found in appendix A.4).

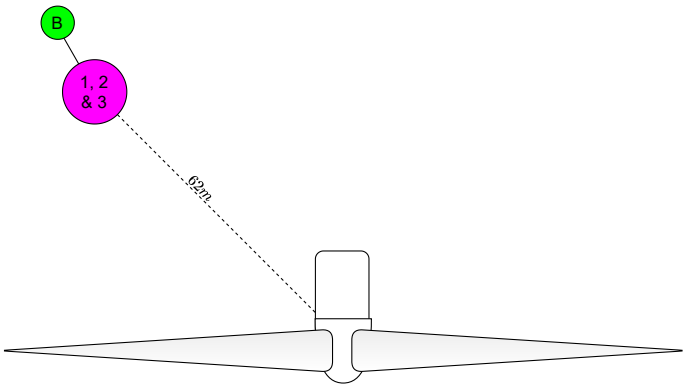

Figure 4.1: Illustration of near field microphone setup.

With this position being close to the blades and minimizing wind-induced noise by windshields, the wind turbine noise can be recorded while maximizing the snr. Since the recording changes over time as the blades pass by the characteristics of the sound also change. This is shown in the spectrogram in fig 4.2.

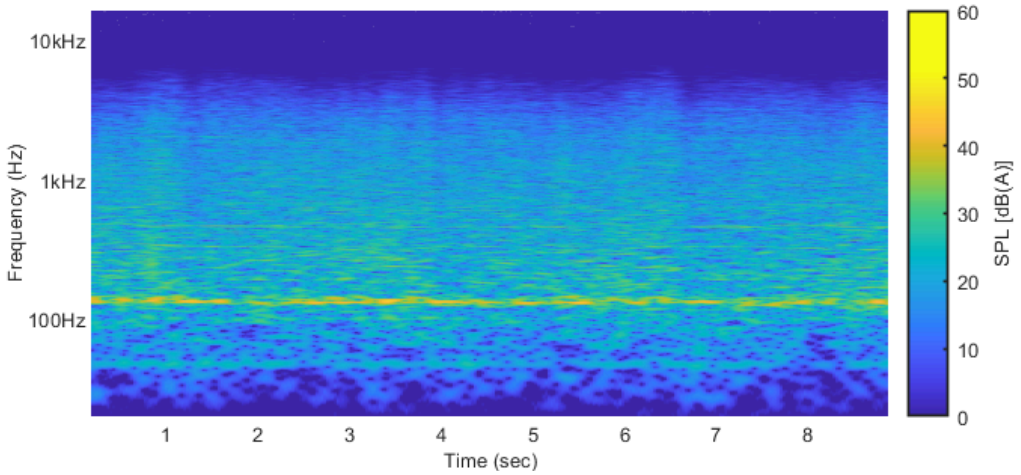

Figure 4.2: Spectrogram of measurement at the near field measurement position plotted in SPL dB(A).

The spectrogram shows that the signal is not constant and that various elements affect the sound. Especially the tonal component at around 140 Hz is clear. The triangular variation in the high frequent energy shows how the strength of the sound changes over time, possibly caused by the combination of changing distances between the sources and microphone. Another interesting thing is seen at approx 1.4 s and 6.8 s, where the energy suddenly drops for a short time (in the high frequency area). This is suspected to be caused by the blade-tower interaction as the microphone is placed on the shadow side of the tower at this point.

Since the spectrum is periodic and the turbines rotational speed was logged to be approximately 9 rpm, the time for a particular blade to complete a cycle is approx. 6.5 s. Looking at the recording over a longer period the frequency content would converge towards a steady state, under the assumption that the signal is periodic. Based on this it is chosen to look at a signal length of 2 full rotations (13 s). The frequency content of this is shown in the spectrum in fig 4.3.

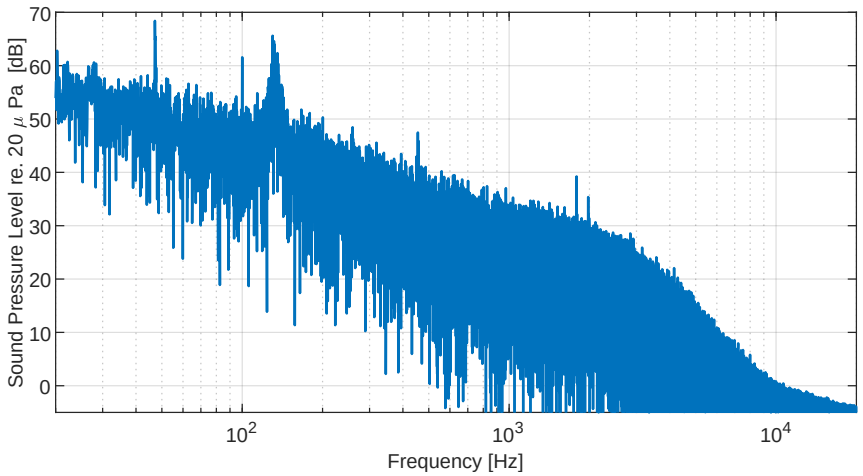

Figure 4.3: Spectrum for 2 full rotations of the wind turbine.

From the spectrum, it is clear that the sound has a pink noise characteristic. Several tonal components are also seen in the spectrum eg. at 47 Hz, 100 Hz and a wider band containing energy around 140 Hz. As earlier described these tonal components can be caused by different parameters such as wear and tear on the blades or different kinds of dirt stuck on the blades. It is also possible that the tonal components can be caused by the mechanical noise from the generator, which is often considered to be more tonal than blade noise [5]. It should be noted that the spectrum is specific to this wind turbine and is not necessarily representative of other wind turbines.

Sound model for a specific wind turbine

To simulate this specific wind turbine with this spectrum, a method called the frequency sampling method is applied. The method makes it possible to design FIR-filters based on a known frequency spectrum [33].

The objective is to find the impulse response (IR) of the desired filter that can be convolved with a signal, having a flat frequency response, to simulate the sound from the turbine. To find the IR the frequency response of the recording is uniformly sampled. For this, the number of frequency samples 'N' should be chosen, preferably N is a power of 2 to exploit the properties of the inverse fast Fourier transform (iFFT). The equation for this is shown in eq. 4.1.

$$h(n) = \frac{1}{N} \sum_{k=0}^{N-1} H(k) e^{j(\frac{2\pi}{N})nk} \tag{4.1}$$

Where:

$h(n)$	Is the IR of the filter	[-]
N	Is the chosen number of samples	[-]
$H(k)$	Is the N-1 samples of the frequency spectrum	[-]

As seen from the equation the resulting filter order will equal the number of chosen samples. This also means that the number of samples must be chosen sufficiently high to represent the desired frequency response [33]. Sampling uniformly in the frequency domain corresponds to sampling 'N' equally spaced samples of the FIR-filters z-transform at the unit circle [33] shown in eq. 4.2

$$H(k) = H(z), \quad for \quad z = e^{\frac{j2\pi}{N}k} \tag{4.2}$$

The link between the specific frequency used for the calculations and the number of samples is shown in eq. 4.3.

$$f = \frac{k}{N} fs \tag{4.3}$$

Where:

f	Is sampled the frequency	[Hz]
N	Is the chosen number of samples	[-]
k	Is an integer k = 0,1, ... ,N-1	[-]

The entire spectrum in the range as in eq [0, fs[is used, which provides a symmetric response, and thereby obtaining a real-valued IR. To ensure a linear phase after taking the iFFT, the IR is shifted to be symmetric by performing a circular shift by N/2 [34].

Sampling the spectrum from fig. 4.3 with 2^{17} equally spaced samples and obtaining the IR by the frequency sampling method is calculated in Matlab. The resulting IR is plotted in fig. 4.4.

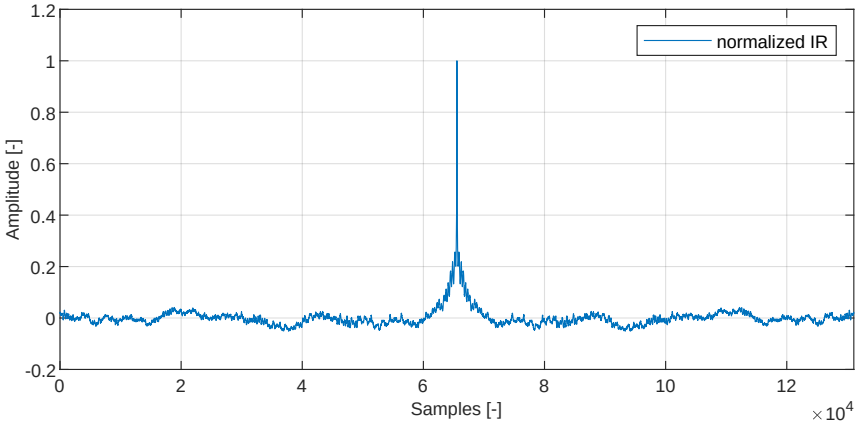

Figure 4.4: Impulse response for filter with order 2^{17}, based on recording of wind turbine.

The corresponding frequency response of the filter is shown in fig. 4.5. The flow of the implementation is described later in fig.4.8.

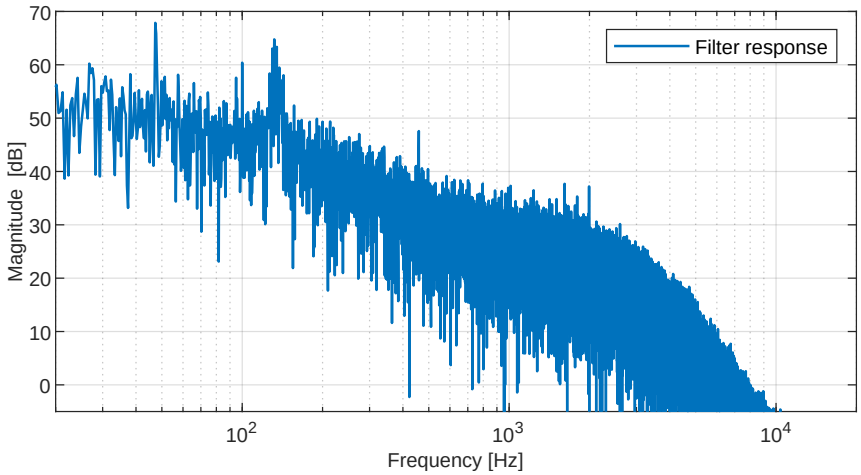

Figure 4.5: Frequency response for filter with order 2^{17}, based on recording of wind turbine.

The results shows a symmetric IR and spectrum with the same characteristics as the spectrum of the recording. The length of the filter is chosen sufficiently high, and a power of 2 for performance reasons, to represent the entire frequency range. This has the consequence that calculations take longer time compared with a more simple filter. However, the sound model is made before the simulator is started and computational complexity does not have a high priority at this point. To compare the filter response and the spectrum of the recording both are shown in fig. 4.6.

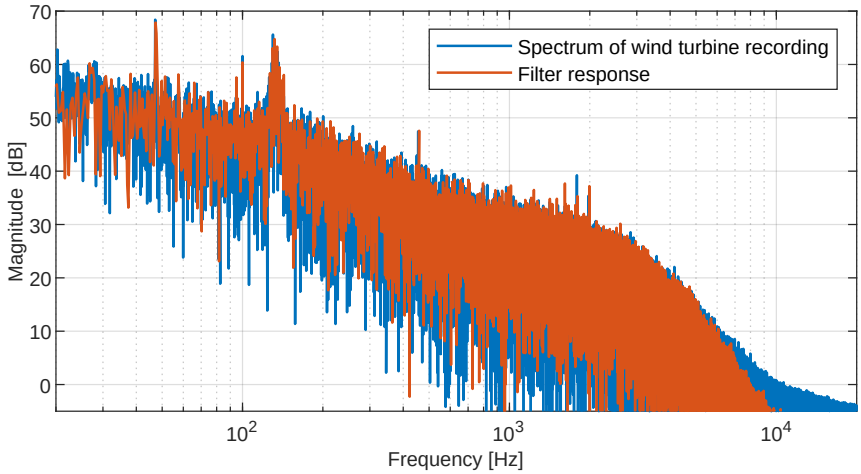

Figure 4.6: Filter response and spectrum of wind turbine recording.

The overall characteristics of the two spectrums are similar. Both have the boosted band around 140 Hz and the attenuation above 2 kHz are recreated in the filter response. However, the filter response deviate approx 4.5 kHz. This is, however, representative of the position for the microphone. To estimate the sound source the method from "Bekendtgørelse om støj fra vindmøller" to find the apparent sound power level of the wind turbine can be applied. The parameters that influence the sound from the source and to this position have to be accounted for.

The method for estimating the apparent sound power level of the source is described in IEC 61400-11 and "Bekendtgørelse om støj fra vindmøller" [2]. The formula was presented in eq. 2.8 in sec 2.2, but is presented again here in eq. 4.4.

$$L_{WA,ref} = L_{A,ref,k} + 10log(4\pi(R^2 + h^2)) - 6dB \tag{4.4}$$

Where:

$L_{WA,ref}$	Is the apparent sound power level in 1/3- octave bands	[dB re 1 pW]
$6dB$	Correction for the mic. placement close to a reflecting surface	[dB]
$L_{A,ref,k}$	Corrected reference SPL in 1/3- octave bands (from eq. 2.7)	[dB re. 20 μPa]
R	Is the distance from the tower to microphone	[m]
h	Is the hub height	[m]

This is based on the parameters of geometrical attenuation and the reflections on the plate. However, the atmospheric attenuation is not considered in this case and can be included to expand the model, when going back to the source. The effect of the atmospheric attenuation, how this is calculated and implemented is explained in sec 4.4. Using the eq. 4.4 to calculate the apparent sound power level in 1/3-octave bands, based on the recording, both with inverse atmospheric attenuation and without, as shown in the equation, is illustrated in fig 4.7.

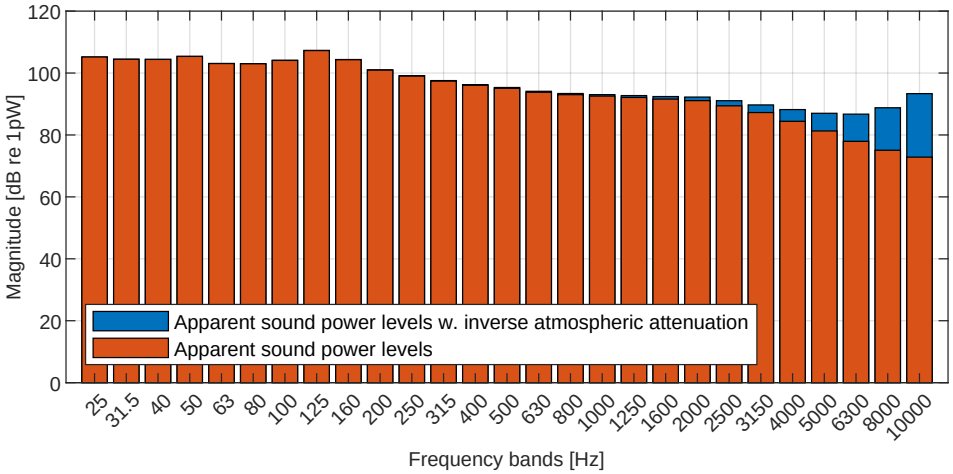

Figure 4.7: Apparent sound power levels in 1/3-octave bands with inverse atmospheric attenuation and no atmospheric attenuation.

This method assumes that the source is located at the rotor hub. For this reason the parameter 'h' (hub height) has value 115 m and 'R' (distance to the tower) is 62 m. The calculated distance for the air attenuation is based on the length $\sqrt{R^2 + h^2}$. Calculating the A-weighted apparent sound power level without atmospheric attenuation results in 103.0 dB(A) re. 1 pW and with atmospheric attenuation results in 104.3 dB(A) re. 1 pW (Note that fig. 4.7 is not A-weighted). This value corresponds with other measurements made on wind turbines [5]. The flow of the algorithm for calculating the output based on the apparent sound power level of the wind turbine is illustrated in fig 4.8.

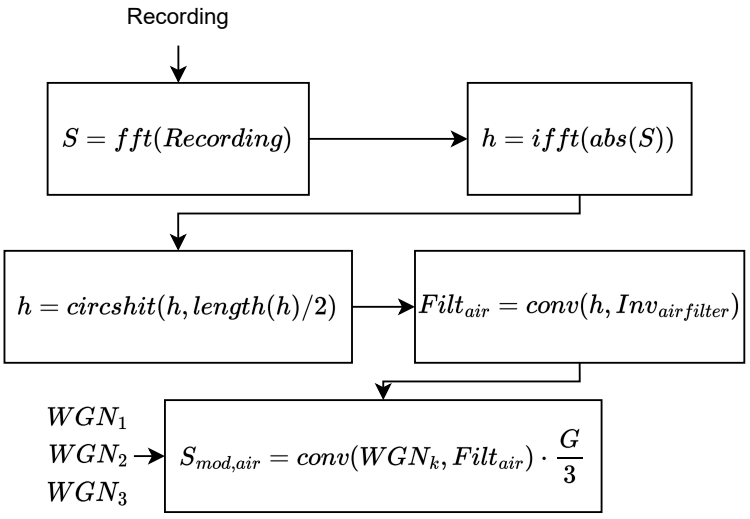

Figure 4.8: Flow of the calculation for the sound model of a single blade.

The flow illustrates that the filter is calculated by taking the fast fourier transform (FFT) of the recording of the wind turbine. Then the absolute values of the bins in the spectrum is found and the iFFT is carried out, after which the IR is shifted into the middle to be symmetric resulting in a linear phase. Taking the absolute value neglects the phase information in the original signal, but this is chosen for the reason that the recording includes time information such as the Doppler effect the, which is unwanted in the source model. These types of effects is added afterwards in the simulator. The resulting filter is shifted to have a linear phase. The impulse response is then filtered with an inverse atmospheric attenuation filter (explained in sec 4.4). The last part of the calculations is that white Gaussian noise (WGN) is convolved with the filter. The output of the algorithm is a sound signal with the spectrum of the source. At the bottom of the flow, three signals of white Gaussian noise are used as input. These three different signals are uncorrelated and represent each blade of the turbine. The sources are uncorrelated because of the small differences in the blades due to wear and tear and the difference in load on the blade due to variations in environmental parameters among other factors. The factor "G" is a gain to ensure that the apparent sound power is gained to have a value of 104.3 dBre 1pW to match the strength of the source. This is for a single source at the rotor hub and since a point source near the blade tip is assumed, the gain is divided by a factor of three to split the total strength of the source into three sources. The filter response and effect of the inverse atmospheric attenuation can be seen in fig 4.9. The blue response corresponds to "$Filt_{air}$" in the flow diagram and the red corresponds to "h" in the diagram.

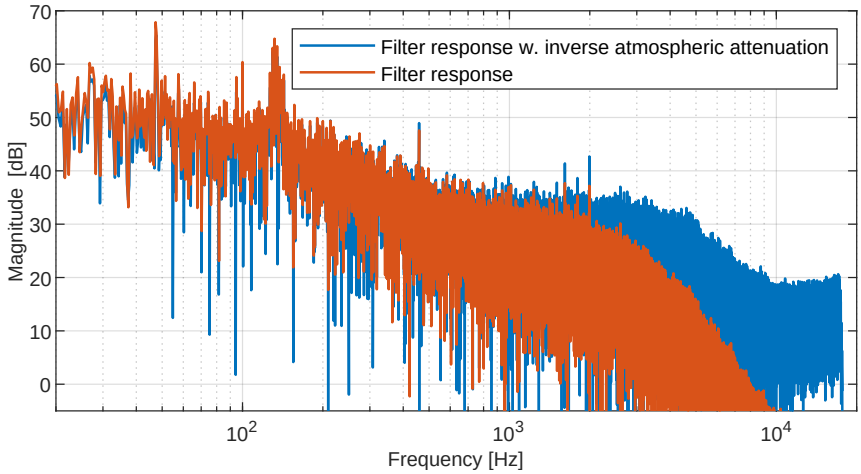

Figure 4.9: Comparison of filter response with inverse atmospheric attenuation and no atmospheric attenuation.

Since this model is made to simulate this specific wind turbine, a comparison with other wind turbines would probably not be representative. For this reason,

other sound models will be available in the final simulator.

General sound model for trailing edge noise

A more general sound model, which can be adapted to suit other wind turbines is relevant since a lot of parameters differ from one wind turbine to the other. A sound model like this is based on the most dominant noise factor found in the analysis, the trailing edge noise. For this, the generator- and mechanical noise are not considered. Most models with a focus on aerodynamic noise are either heavy simulation programs or semi-empirical models. The noise produced by the blades differs according to the turbine's physical parameters and environmental parameters [18].

A semi-empirical model can be sorted into the following steps [18].

1. Establish wind turbine parameters and relevant environmental parameters.
2. Split the blade into a number of segments.
3. Calculate aerodynamic parameters for the chosen noise type. (Trailing edge noise)
4. Use semi-empirical noise prediction model to every segment of the blade.
5. Take the sum of all the segments to get the total apparent sound power level of the blade.

To obtain the aerodynamic parameters from the blade it is required to know the exact dimensions of the blade, especially both the length and width of the entire blade. However, this is not often available because of company interests. For this reason, it will be difficult to accurately reproduce the turbine in the recordings, but an approximation will be used.

A model for calculating the apparent sound power level for a blade segment of the trailing edge noise is shown in eq. 4.5.

$$L_{TE} = 10log_{10}(4\pi\delta^* M^5 s) + A \tag{4.5}$$

Where:

L_{TE}	Is the apparent sound power level for a blade segment	[dB re 1 pW]
δ^*	Is the boundary layer displacement thickness	[m]
M	Is the Mach number	[-]
s	Is the length of the blade segment	[m]
A	Is a spectral shape and amplitude function, which depend on the semi-empirical model	[-]

With the model for a blade segment presented the calculation of aerodynamic parameters will now be of focus. An illustration of the division into blade segments are shown in fig. 4.10.

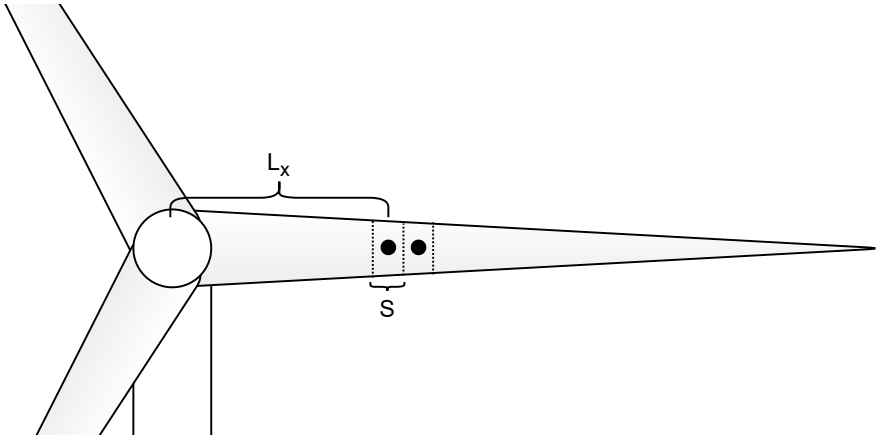

Figure 4.10: Illustration of division into blade segments.

In the figure, the length of each segment 's' is illustrated along with the distance, L_x, from the rotor hub to the centre of the segment of interest.

It is clear that the flow speed 'U' which is calculated as the sum of the vectors for the wind speed 'U_w' and blade speed 'U_b' (earlier shown in fig 2.2) will vary for each blade segment. For the calculations, a constant wind speed will however be assumed. The flow speed is used to calculate the mach number for each segment and this is calculated as shown in eq. 4.6.

$$M_x = \frac{|U_w + U_b| \cdot L_x}{c} \tag{4.6}$$

Where:

M_x	Is the Mach number for blade segment x	[-]
U_w	Is the wind vector	[-]
U_b	Is blade vector for rotational speed	[-]
L_x	Is the distance from hub to center of segment x	[m]
c	Is the speed of sound	[m/s]

Furthermore it is neccesary to calculate the dimensionless constant (the Reynolds number), often used in fluid dynamics, in eq.4.7:

$$Re_x = \frac{|U_w + U_b| \cdot L_x C_x}{v} \tag{4.7}$$

Where:

Re	Is the Reynolds number for segment x	[-]
C_x	Is the chord length for segment x	[m]
v	Is the kinematic viscosity (approx 1.5E-6 in air)	$[m^2 s^{-1}]$

The Reynolds number is used to calculate the boundary layer thickness and the boundary layer displacement thickness [18].

$$\delta = C_x 0.05 Re_x^{-0.2}, \qquad \delta^* = \frac{\delta}{8} \tag{4.8}$$

Where:

δ	Is the boundary layer thickness	[m]
δ^*	Is the boundary layer displacement thickness	[m]

Now the parameters can go into the apparent sound power model. However, the parameters are also used in the spectral shape and amplitude function A. The function is shown in eq. 4.9.

$$A(f) = 10log_{10}\left(\frac{4\left(\frac{f}{f_p}\right)^{2.5}}{\left(1+\left(\frac{f}{f_p}\right)^{2.5}\right)^2}\right) + 128.5 \tag{4.9}$$

Where:

f	Is the frequency	[Hz]
f_p	Is the peak frequency $\left(\frac{0.02UM^{-0.6}}{\delta^*}\right)$	[Hz]

With all the parameters for the apparent sound power model in place calculations for a blade can be made using equation 4.5. With approximations of the blades of the Siemens turbine divided into 10 segments and a constant wind speed of 10 m/s and a rotational speed of 10 RPM the contribution of each blade can be seen in fig 4.11.

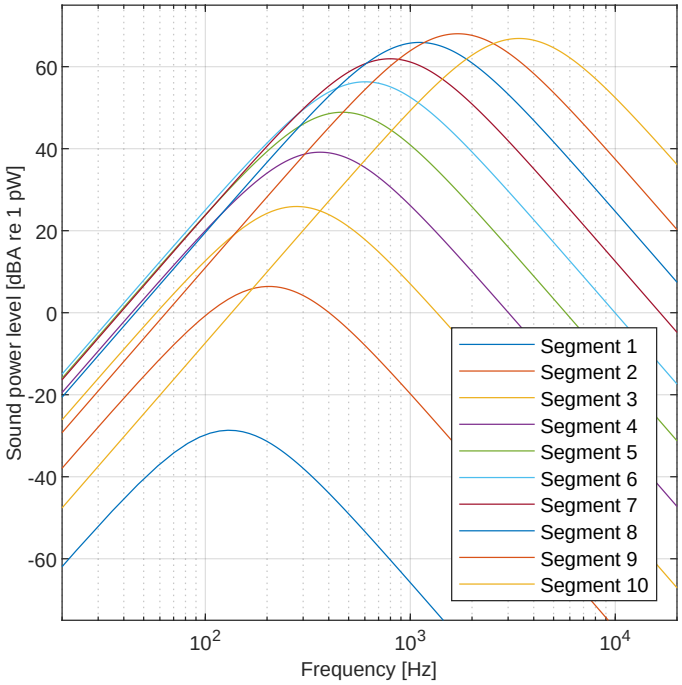

Figure 4.11: The sound power level dB(A) re. 1 pW for 10 blade segments with segment 1 closest to the hub.

Summing all of the blade segments thereby representing the total power of one blade results in the spectrum seen in fig 4.12.

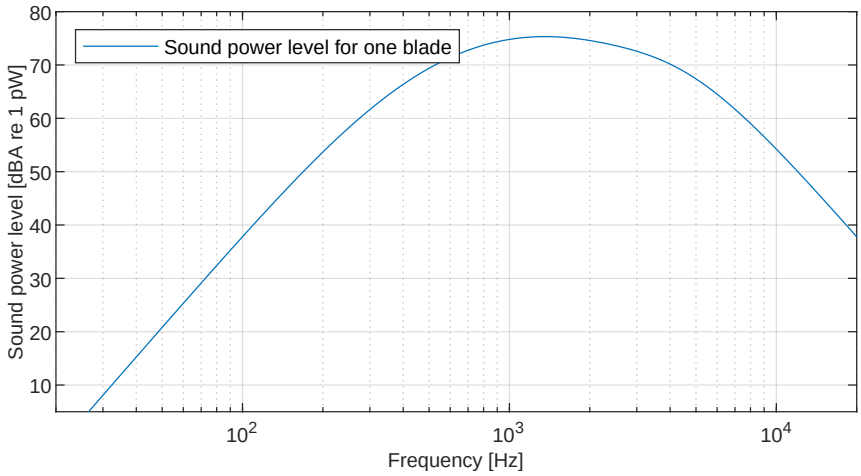

Figure 4.12: The sound power level dB(A) re. 1 pW for the entire blade

The total apparent sound power level for the trailing edge noise has similar char-

acteristics of other results also using semi-empirical methods [35]. However, it should be noted that the power spectrum depends on both environmental and turbine parameters.

This sound model will be an available option to chose in the final simulator representing the trailing edge noise.

Other studies have obtained results with pink noise [31], which will also be included in the simulator for comparison. The options for the sound models in the simulator will be.

- Sound model based on frequency sample method including inverse atmospheric attenuation.
- Sound model based on frequency sample method without inverse atmospheric attenuation.
- Sound model based on blade segments for trailing edge noise.
- Pink noise
- White noise

4.2 Moving sources

In this section, the theory behind the implementation of the three moving sources, the blades, is explained as basis for the acoustic distance model.

As the turbine rotates the distance from each blade to an observer placed on the ground will change over time resulting in the Doppler effect and etc, as explained in sec 2.3. A single moving sound source, such as an ambulance passing by, can be approximated by the basic flanger effect, which is based on a modulated delay line. For simulating multiple sources a chorus effect can be applied. The main difference between the two effects is the delay times used in each effect and that the flanger usually consists of only the direct and a delayed version of the sound, whereas the chorus has multiple versions of the same signal with different delays [24]. An illustration of the turbine mapped to the chorus effect is illustrated in fig 4.13.

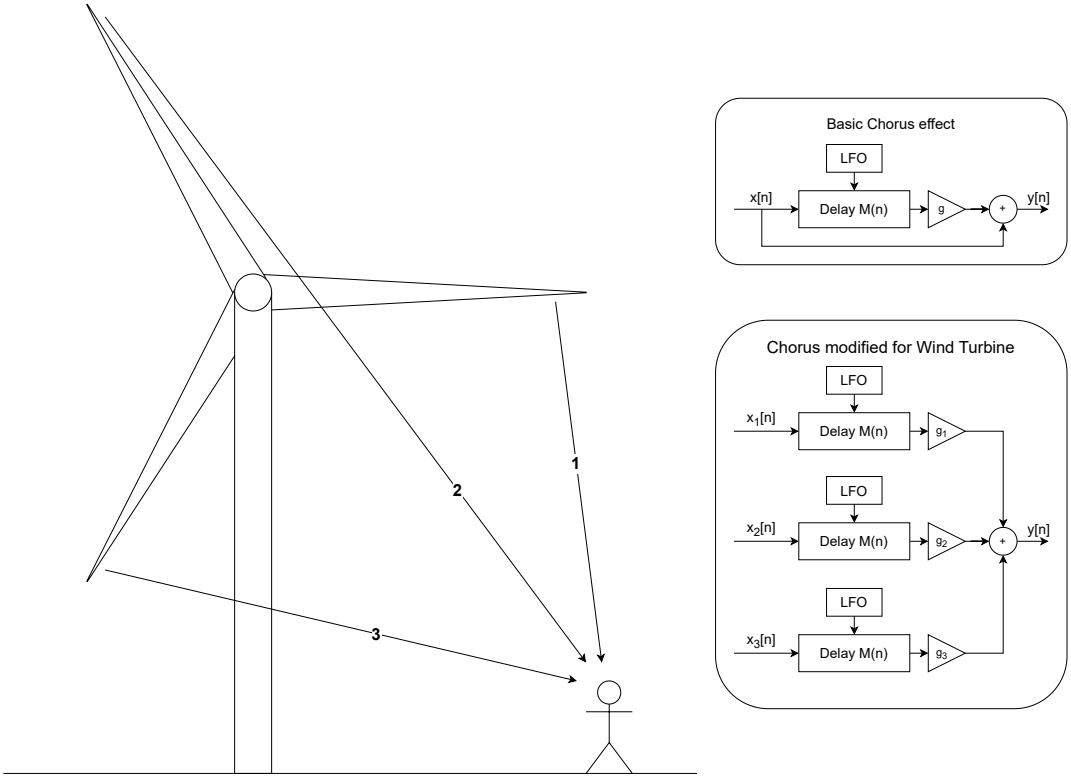

Figure 4.13: Illustration of wind turbine and chorus effect.

The basic chorus (seen in top right) effect consists of a continuously variable delay, a gain factor, addition with the direct signal and an low frequency oscillator (LFO). Comb-filter effects will happen as a consequence of the signal being added with a delayed version of itself. This effect will also produce the Doppler effect since the delay of the input signal varies over time thereby simulating a source moving closer

or further away [24]. The delay is chosen to be in a certain range and is controlled by the LFO. Different types of signals can be chosen for the LFO such as a triangle, square or a sinusoidal function, which is the most common. The frequency of LFO determines the rate at which the delay changes and thereby "the speed" of the moving source [24]. The basic chorus effect is described by eq. 4.10.

$$y[n] = x[n] + gx[n - M[n]] \tag{4.10}$$

Where:

$y[n]$	Is the output at sample n	[-]
n	Is the sample number	[-]
$x[n]$	Is the input at sample n	[-]
$M[n]$	Is the delay length	[-]
g	Is a gain factor	[-]

Since all of the blades move the basic chorus has to be modified, so there won't be a direct sound from input to output without a continuously modified delay. Furthermore, an expansion of the basic chorus is made to include three different sources, i.e. each blade of the wind turbine. The chorus effect modified to suit the characteristics of a wind turbine is shown in fig 4.13.

The modified chorus effect can be described by eq. 4.11.

$$y[n] = g_1x_1[n - M[n]] + g_2x_2[n - M[n]] + g_3x_3[n - M[n]] \tag{4.11}$$

The equation of the modified chorus is based on the assumption that each of the blades is independent, thereby making the delay and LFO take different values for each blade at a time instance 'n'. The gain block for each blade can not be considered constant either, as in the basic chorus effect, and could represent variable gain as a function of distance, Doppler amplification etc. The implementation of the Doppler amplification is based on the acoustic distance model (ADM) and will be explained in sec 4.3.

The LFO on the other hand can not be a sine function as in the simple chorus, because the LFO controls the rate of change in the delay, which maps to the blade's movement w.r.t. an observer in the physical world. This means that both the size of the delay, the range of the delay and the rate of change are different from one observer position to another. Thus it is important to look at the change in acoustic distance from the noise source to the observer.

4.3 Acoustic Distance & Velocity Model

To calculate the delay in time samples and the rate of the delay change the distance over time needs to be calculated. For this, an acoustic distance model describing the distance between each blade tip (sound source) and an observer over time is formed. This will replace the LFO in the original chorus effect.

4.3.1 Acoustic Distance Model (direct)

The acoustic distance model is the length from the noise source on the blade and to the observer. This distance varies with the rotation of the turbine, but different approaches to how sound travels through the medium can differ. A ray-based method would result in a straight line as the ADM, under the assumption that temperature, difference in wind speeds, humidity etc have no impact on the path between source and observer. More complex methods that take into account that the environmental parameters change with position would result in the path taking different shapes eg. a curve. This is also explained in sec 2.3.

In three-dimensional space, the distance from the position of a stationary observer to a rotating blade can be found. This requires knowledge of the hub height, rotational speed, and rotor diameter. Knowing these parameters the location of a desired point on a blade e.g. the tip can be found by eq. 4.12.

$$\mathbf{p}(\theta) = \begin{bmatrix} 0 \\ 0 \\ hub_{height} \end{bmatrix} + \frac{r_d}{2} \cdot \begin{bmatrix} 0 \\ sin(\theta) \\ cos(\theta) \end{bmatrix} \tag{4.12}$$

Where:

p	Is the position of the blade tip	[m]
hub_{height}	Is the height of the turbine hub	[m]
r_d	Is the rotor diameter	[m]
θ	Is the angle relative to 12 o clock position	[°]

This function describes the path of the tip on the wind turbine blade. From this, it is possible to relate the position, and thereby also the change of position, of the blade to an observer. An example of eq. 4.12 is given in fig. 4.14, where the distance from blade tip position to the origin (base of tower) is plotted for the 3 blades. The turbine having a hub height of 80 m and a rotor diameter of 120 m.

Figure 4.14: Illustration of ADM, based on straight line distance at observer position [0, 0, 0]

The figure illustrates three blades, where each blade is offset by 120° compared to the previous one. It can be seen how, for this case, the position changes in the range hub height ± rotor diameter/2. Converting the distance from the blade tip to the observer of the ADM to a time delay in samples enable the modified chorus to simulate the Doppler effect of the blades moving. A resulting chorus effect can be seen in fig 4.15.

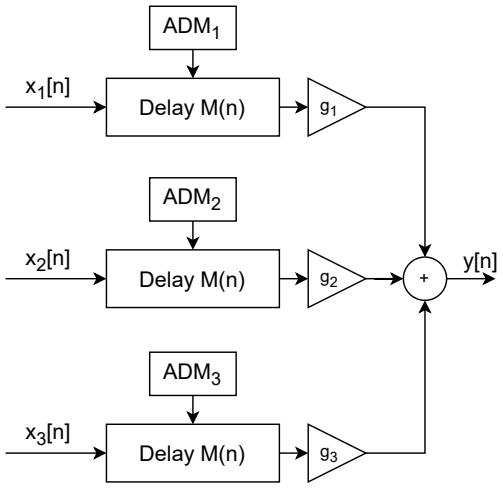

Figure 4.15: Illustration of the modified chorus effect with ADM as delay input.

In order to map the input samples $x[n]$ to the correct ADM value, the ADM value needs to be either calculated for each sample for the entirety of the signal, or alternatively calculated as a circular periodic constellation, where the rotor frequency fits an integer amount of samples. For the latter, periodicity can be exploited, and the

calculated distances re-used, and therefore only a single rotation need be calculated.

The modified chorus effect has to take some inputs, such as the observer position and the sound model of the wind turbine blade noise. Furthermore, a maximum source distance (MaxSD) and minimum source distance (MinSD) are necessary to optimize the output of the chorus effect. These values are found as the maximum and minimum of the ADM. An illustration explaining the optimization is shown in fig 4.16.

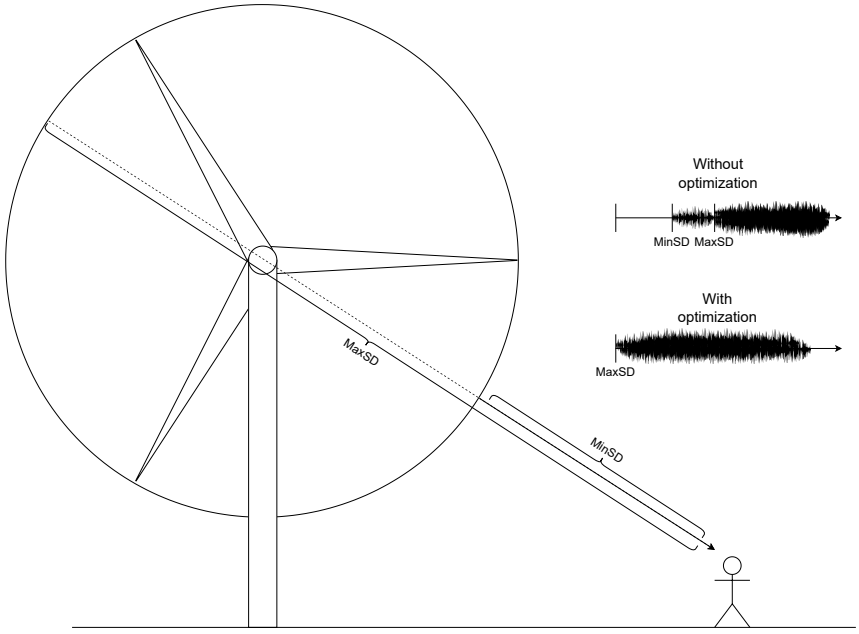

Figure 4.16: Illustration of MaxSD and MinSD and the output of the chorus with/without optimization.

Illustrated in the figure is that MinSD is the shortest distance from the blade tip to the observer and the MaxSD is the maximum distance from the observer to the point where the blade tip is furthest away (in this case MinSD + rotor diameter). As seen in figure 4.16 the top right without any optimization the output of the modified chorus would be starting with a silence period corresponding to the inverse of the speed of sound multiplied by the distance in meters, whereafter the contribution from the source at the MinSD will arrive. From a listening perspective, the consequence of this will be a period of silence followed by a "startup period" before the sound of the turbine is complete. An example would be if a listener is placed in a position with a MinSD of 343 m. Then the silence period would be 1 s followed by a short startup period before the sound reaches a steady state.

Shown in fig 4.16 to the right with optimization the output is sliced to start at the time corresponding to the arrival of the sound from MaxSD. This means that the sound will begin in a steady state. The output of the optimized version of the chorus is shown in fig 4.17.

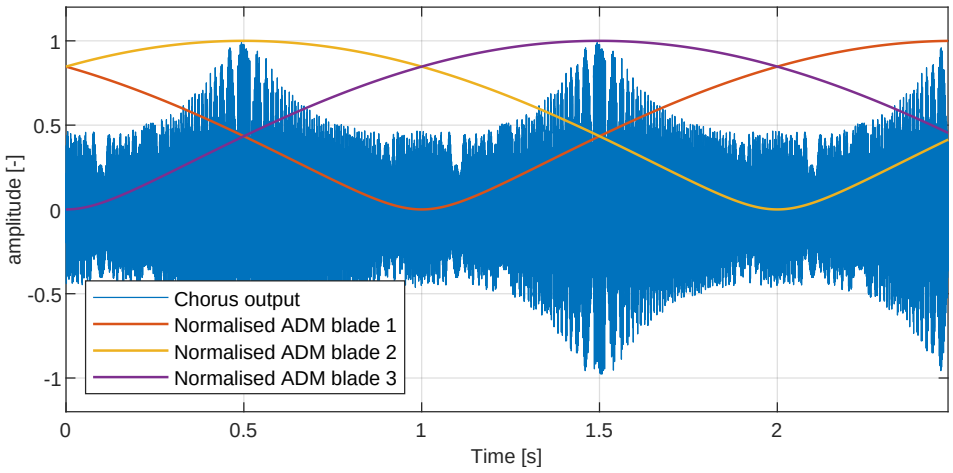

Figure 4.17: Output of chorus with 1500 Hz sine wave as input and the ADM for each blade with an observer position at [0,0,0].

The input is three 1500 Hz sine waves whose combined output amplitude has been rescaled to be between -1 and 1. The output signal is periodic with the periodicity of the three ADM combined, which is directly proportional to three times the rotor speed. For this scenario 20 rpms (0.33 Hz), times three resulting in 60 rpm or 1 Hz.

The normalised ADM in the plot will result in the maximum delay at value 1 and the minimum delay at 0. This result also contains the effect of Doppler amplification.

4.3.2 Acoustic Velocity Model (direct)

When regarding the wind turbine blade tips as 3 moving sound sources, the velocity of these sources are simply the derivative of their position. From the position (given in eq. 4.12) the derivative wrt. time can be calculated as:

$$\mathbf{V}(t) = \frac{r_d \cdot 2\pi f_{rot}}{2} \cdot \begin{bmatrix} 0 \\ cos(2\pi f_{rot} t) \\ -sin(2\pi f_{rot} t) \end{bmatrix} \tag{4.13}$$

Where:

V	Is the velocity vector of the blade tip	[m/s]
hub_{height}	Is the height of the turbine hub	[m]
r_d	Is the rotor diameter	[m]
f_{rot}	Is the rotation frequency of the turbine	$[s^{-1}]$
t	Is the time	$[s]$

The velocity model in eq. 4.13, however, describes the velocity in 3 dimensions, and not the velocity towards the receiver. In order to know the velocity towards a

receiver, the velocity vector is projected onto the direct (line-of-sight) vector. An example of this is given in fig. 4.18.

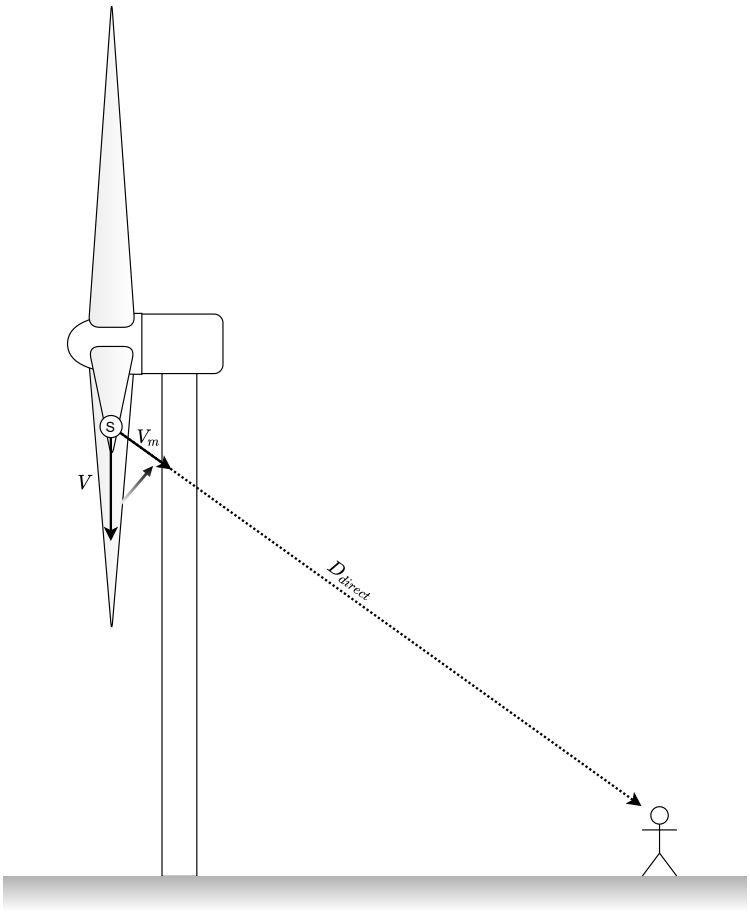

Figure 4.18: Illustration of the projection of velocity vector V onto the direct vector.

Figure 4.18, illustrates the scenario of a single source 'S', in a down-stroke movement. Velocity vector 'V', is the velocity vector of the source, as given by eq. 4.13. This vector i mapped onto the direct-path vector (D_{direct}), by projection, as shown in eq. 4.14:

$$V_m(t) = \frac{V(t) \bullet D_{direct}(t)}{||D_{direct}(t)||^2} \cdot D_{direct}(t) \tag{4.14}$$

Where:

V_m	Is the velocity vector from source to receiver	[m]
V	Is the velocity vector of the blade tip	[m/s]
D_{direct}	Is the direct vector from source to receiver	[m]
'$\bullet$'	Denotes the dot product operator	[-]

The one-dimensional velocity from source to receiver is found by scaling with the norm of D_{direct}:

$$V_{toward}(t) = \frac{V(t) \bullet D_{direct}(t)}{||D_{direct}(t)||^2} \cdot ||D_{direct}(t)|| \tag{4.15}$$

This V_{toward} is used for calculating the effect of Doppler amplification at different times.

4.3.3 Doppler Amplification

The Doppler amplification described in sec 2.3 is a function of the constant Mach number and the angle between the moving source and the observer. The eq. (2.14) can be rewritten by using the position of the blade and the observer to be the function shown in eq 4.16.

$$g(t) = \frac{1}{(1 - \frac{V_{toward}(t)}{c})^2} \tag{4.16}$$

Where:

g	Is the gain factor	[-]
t	Is the time	[s]
c	Is the speed of sound	[m/s]
V_{toward}	Is speed towards the observer (the eq. 4.15)	[m/s]

The result of the Doppler amplification for a turbine with a fixed rotor speed of 16 rpm and the observer placed at a point 0.5 m from the tip is plotted in fig 4.19.

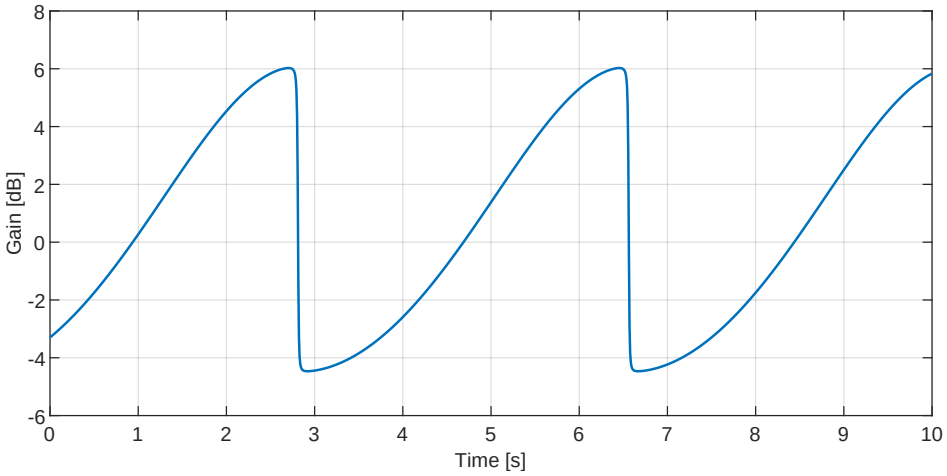

Figure 4.19: Doppler amplification with a rotor speed of 16 rpm and a fixed observer position at distance of 0.5 m from the blade tip path.

The amount of gain will vary with the rotor speed since the speed of the moving source dictates the gain [5]. For this particulate example, the gain is approximately in the range [-4.5 : 6] dB.

A simplified flow diagram of the Matlab implementation for only one blade is shown in fig 4.20. The procedure is the same for all three blades, but each ADM is shifted 120° compared to the previous blade.

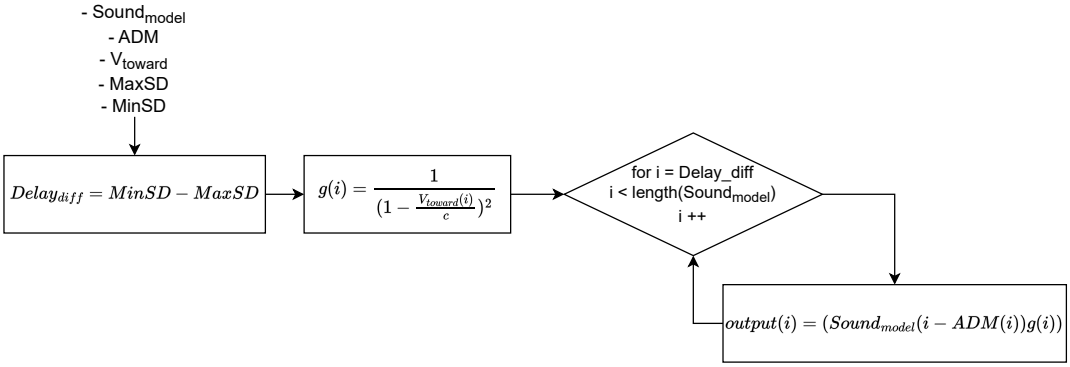

Figure 4.20: Illustration of the flow in the modified chorus effect with Doppler amplification

The flow of the modified chorus indicates that the earlier calculated parameters control the effect. The output of this illustration is only for one blade of the wind turbine and needs to be added to the other two blades after the propagation model.

4.3.4 Acoustic Distance & Velocity Model (reflected)

The distance and velocity explained in sec. 4.3.1 & 4.3.2 only apply to the direct contribution of the sound source. The reflected sound source (also referred to as the image-source) will always travel a longer distance, but the difference wrt. the direct distance will vary with position. To model the distance of the reflected contribution, some simple geometry calculations are needed. An illustration of this is shown in fig 4.21:

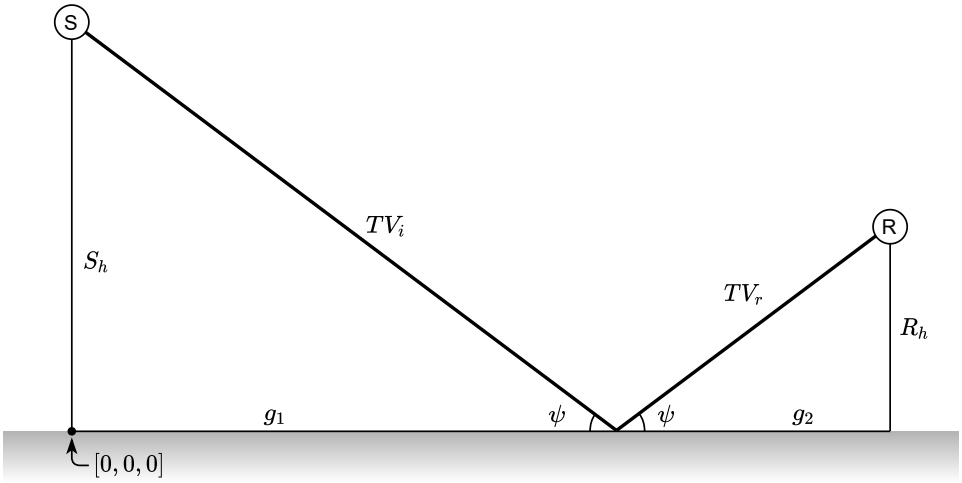

Figure 4.21: Illustration of the reflection path.

Figure 4.21 illustrates the propagation path of the reflected contributions from source to receiver on an infinite plane. Since angle of incidence equals angle of reflection ($90° - \psi$), two right-angled triangles can be formed at the point of reflection. Given the height of source (S_h), height of receiver(R_h), as well as the combined vector of $g_1 + g_2$ is known, it is possible to calculate the point of reflection (g_1), by manipulation of the trigonometric formulas. The ratio of g_1/S_h must equate to g_2/R_h, which reduces to the following expression of g_1:

$$g_1 = \frac{S_h}{S_h + R_h} \cdot (g_1 + g_2) \tag{4.17}$$

With g_1 it is possible to calculate the angle of incidence; moreover the incident toward-vector (TV_i) and reflected toward-vector (TV_r), are calculable with g_1 by simple vector subtraction. The combined length of TV_i and TV_r equates to the total acoustic distance of the reflected contribution. The reflected contribution will always be the last to arrive at a listener, compared to the direct path. This means that the output of the simulator has not reached the steady state before the last reflection of the reflected path has arrived. For this reason the output is further sliced, so the sound starts when the last reflected contribution arrives.

The velocity of the reflected contributions toward the receiver is calculated by the same method as the direct velocity (eq. 4.15), however, with the velocity vector (V) projected onto the incident toward-vector (TV_i), instead of the direct vector (D_{direct}). This may yield a considerably different Doppler effect. For scenarios where the receiver is far from the wind turbine, the direct velocity toward, and the reflected velocity toward approaches the same value. When closer toward the turbine, however, the difference may be non-negligible.

For the specific, although highly unlikely scenario, that the receiver find themselves in hub height, a little more than the rotor radius to the side of the wind turbine: the blade tip would, at 90° clockwise position, have no direct velocity toward

the receiver. However, the reflections velocity toward would approach the actual tip velocity. This merely highlights the potential difference in velocity of the two contributions. For this example, however, it could be reasonably argued that the reflected contribution is imperceptible, when the direct contribution is directly next to the receiver.

The ADM provides a basis for calculating the Doppler effect, but is also used as part of the Geometric attenuation.

4.3.5 Geometric attenuation

Although not necessarily complicated, the geometric attenuation is very important to scale the SPL to the correct value for a given distance. This value is calculated wrt. the assumption of point sources with a spherical radiation pattern. For this case, the geometric attenuation can be calculated by the relations of the inverse-square law. For the sound pressure at a given point, this means halving the sound pressure for every doubling of distance. This is evident from eq. 4.18 [14].

$$p = \frac{A}{D} e^{j(\omega t - kD)} \tag{4.18}$$

Where:

p	Is the pressure	[Pa]
D	Is the distance	[m]
A	Is the amplitude of the acoustic wave at distance 'D'	[-]
ω	Is the angular velocity	$[rad/s]$
t	Is the time	$[s^{-1}]$
k	Is the wavenumber	$[m^{-1}]$

The implementation of geometric attenuation uses the first term 'A/D' to calculate the attenuation, where 'A' is the numerical value that corresponds to 104.1 dB, and 'D' is the distance, provided by the ADM. This is adjusted sample-wise, using the ADM according to the specific sample.

While this is applicable as a sample-wise adjustment by multiplication, other filters, such as the implementation of atmospheric absorption require further consideration, which will now be explained.

4.4 Atmospheric absorption

At longer distances, the absorption in the air is an important parameter to take into account. The absorption coefficient is frequency dependent and varies with temperature and humidity. In ISO 9613-1, a method for calculating the absorption coefficient is given, similarly used in the NORD2000 and HARMONOISE models [5]. The standard also provides tables with coefficients for different temperatures and humidities [15].

For calculating the atmospheric absorption at a certain humidity and pressure (dependent on altitude and weather) the relaxation frequency for both oxygen and nitrogen has to be calculated [15]. The relaxation frequency for oxygen is calculated as shown in eq. 4.19.

$$f_{rO} = \frac{p_a}{p_r}\left(24 + 4.04 \cdot 10^4 h \frac{0.02 + h}{0.391 + h}\right) \tag{4.19}$$

Where:

f_{rO}	Is the relaxation frequency for oxygen	[Hz]
p_a	Is the ambient atmospheric pressure	[kPa]
p_r	Is the reference ambient atmospheric pressure (101.325)	[kPa]
h	Is the molar concentration of water	[%]

Often the amount of water in the air is provided by metrological institutes in relative humidity. To calculate the exact attenuation coefficient a conversion can be calculated [15]. This shown in eq. 4.20.

$$h = h_r\left(\frac{10^{-6.8346(\frac{T_{01}}{T})^{1.261}+4.6151}}{\frac{p_a}{p_r}}\right) \tag{4.20}$$

Where:

T_{01}	Is the triple-point isotherm temperature (273.16)	[K]
h_r	Is the relative humidity	[%]

The relaxation frequency for nitrogen is also a function of the ambient temperature and is calculated as shown in eq. 4.21.

$$f_{rN} = \frac{p_a}{p_r}\left(\frac{T}{T_0}\right)^{-\frac{1}{2}}\left(9 + 280h \cdot e^{-4.170\left[(\frac{T}{T_0})^{-\frac{1}{3}}-1\right]}\right) \tag{4.21}$$

Where:

f_{rN}	Is the relaxation frequency for oxygen	[Hz]
T	Is the ambient atmospheric temperature	[K]
T_0	Is the reference air temperature (293.15)	[K]

The two relaxation frequencies for oxygen and nitrogen are included in the calculation of the attenuation coefficient [15]. The formula for calculating the atmospheric attenuation coefficient is shown in eq. 4.22.

$$\alpha = 8.686 f^2 \left(\left[1.84 \cdot 10^{-11} \left(\frac{p_a}{p_r} \right)^{-1} \left(\frac{T}{T_0} \right)^{\frac{1}{2}} \right] + \left(\frac{T}{T_0} \right)^{-\frac{5}{2}} \right. \\ \left. \left(0.01275 e^{\frac{-2239.1}{T}} \left[f_{rO} + \left(\frac{f^2}{f_{rO}} \right) \right]^{-1} + 0.1068 e^{\frac{-3352}{T}} \left[f_{rN} + \left(\frac{f^2}{f_{r_N}} \right) \right]^{-1} \right) \right) \tag{4.22}$$

Where:

α	Is the attenuation coefficient	[dB/m]
f	Is the frequency of interest	[Hz]

The attenuation coefficient is given in dB/m and to get the correct attenuation the distance between the observer and source (in meters) has to be multiplied by the coefficient [15]. The attenuation coefficient is given for pure tones, and to get a wide-band estimate of a given scenario the complexity of this calculation relies on the frequency resolution.

Filter design

To implement atmospheric absorption based on the calculation of the attenuation coefficient the frequency sampling method is used. The frequency sampling method makes it possible to design FIR-filters based on a known frequency spectrum [33]. The method is earlier described in sec 4.1. The objective is to find the IR 'h[n]' of the desired filter that can be convolved with the sound to simulate atmospheric attenuation.

The steps of the algorithm are illustrated in a flow diagram in fig. 4.22.

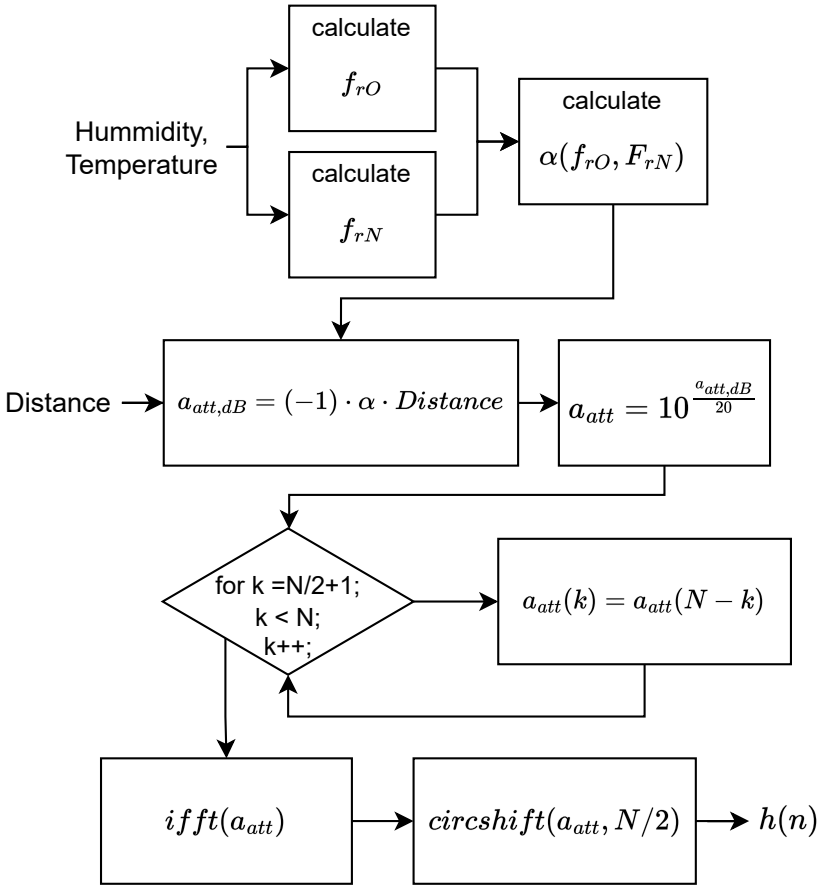

Figure 4.22: Illustration of the frequency sampling method for creating a FIR filter to simulate atmospheric attenuation. N in the figure is the number of frequency samples.

The first step is to calculate the relaxation frequencies of nitrogen and oxygen, with temperature and humidity as inputs. For the implementation the atmospheric pressure is always assumed to be 1, i.e at ground level. From this the attenuation coefficient, alpha, can be calculated. The attenuation coefficient is calculated for the frequency range [0 , fs/2]. This vector is multiplied by the distance and multiplied with a factor of -1 to ensure the resulting filter is attenuating and not amplifying (since the attenuation coefficient is positive). Next step is converting the response to magnitude from dB. To avoid the resulting IR being complex, the spectrum needs to be symmetric around fs/2 [36] which is implemented as a for-loop that mirrors the samples around the fs/2 point. Now the iFFT can be calculated and the IR is shifted to be symmetric, which is a property of the FIR filter with linear phase [36].

The frequency- and impulse response of a filter implemented in Matlab based on the flow diagram illustrated in fig 4.22 for a distance of 250 m, a temperature of 20 °C and a relative humidity of 20 % is illustrated in fig 4.23.

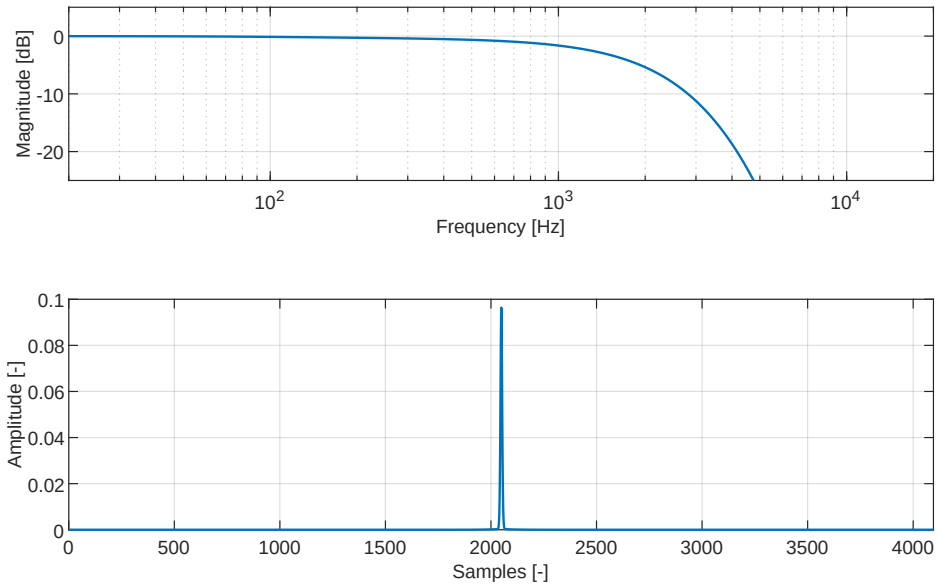

Figure 4.23: Atmospheric attenuation with temperature at 20 °C, relative humidity of 20 % at 250 m and 1 atm pressure, with the resulting IR.

From the figure, it can be seen that the filter has an order of 4096 and is symmetric. The resulting frequency response has a low pass characteristic, which is expected. Different distances is plotted in fig. 4.24 for a temperature of 20 °C, relative humidity of 20 % and at 1 atm pressure, to show the attenuation as a function of distance.

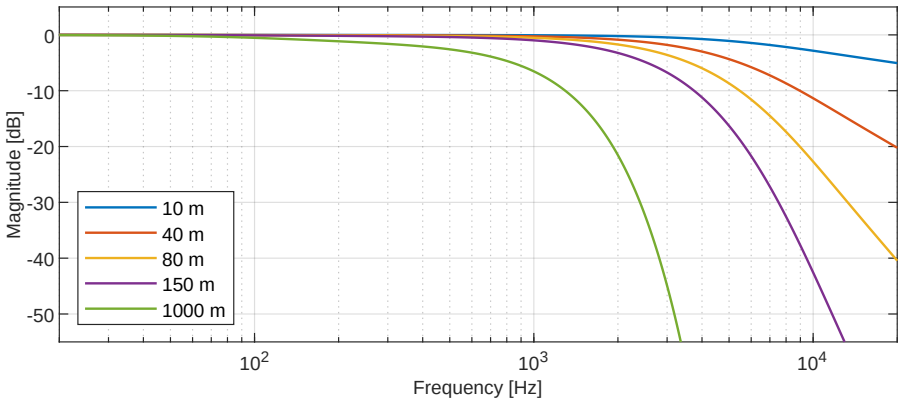

Figure 4.24: Atmospheric attenuation with temperature at 20 °C, relative humidity of 20 % and 1 atm pressure, at different distances from the source.

Calculating the atmospheric attenuation and converting the spectrum to a filter has the consequence that the filter coefficients change every time the distance changes. A constant distance for this filter type is assumed and has the rotor hub as the reference point. To verify the resulting filter a comparison with the table values in ISO 9613-1 has been made for some selected frequencies. This is based on the same environmental conditions as figure 4.23.

Attenuation in dB/km at 10°C and relative humidity 20 %			
Frequency [Hz]	Filter value [dB]	Table value [dB]	Difference [dB]
50	0.19	0.19	0
100	0.46	0.46	0
250	1.19	1.20	0.01
500	3.26	3.27	0.01
1000	10.98	11.00	0.02
2000	36.31	36.20	0.11
4000	91.90	91.50	0.40
10000	171.61	172.00	0.39

Table 4.1: Atmospheric attenuation as a function of frequency compared to the table values in ISO 9613-1 [15].

Small differences are observed when comparing with the table values from ISO 9613-1. These deviations can possibly be caused by the use of rounding errors when using the e-value, as seen in eq. 4.22. The table values of ISO 9613-1 might have been rounded, which may be the source of the calculated discrepancies, but this is not stated in the standard.

Variable air attenuation

At large distances, the relative difference between the point sources will be small and the higher frequencies will be attenuated to be very low (illustrated in fig 4.24 at 1000 m). Standing close to the turbine, and with the big rotor diameter that wind turbines have today, variable air attenuation becomes relevant when assuming point sources at the blade tip. It is not uncommon for wind turbines to have rotor diameters of 150 m, which corresponds to an atmospheric attenuation at 10 dB at 3 kHz (fig 4.24).

A variable filter can cause artefacts such as clicking when the parameters of the filter are changed [37]. Furthermore changing all the filter coefficients of the implemented filter for every step the blade moves will be resource intensive. The low-pass characteristic of atmospheric attenuation can be approximated by a low-pass filter at short distances.

The state variable filter is a second-order filter that allows a change in the cutoff frequency. An illustration of the state variable filter is shown in fig 4.25.

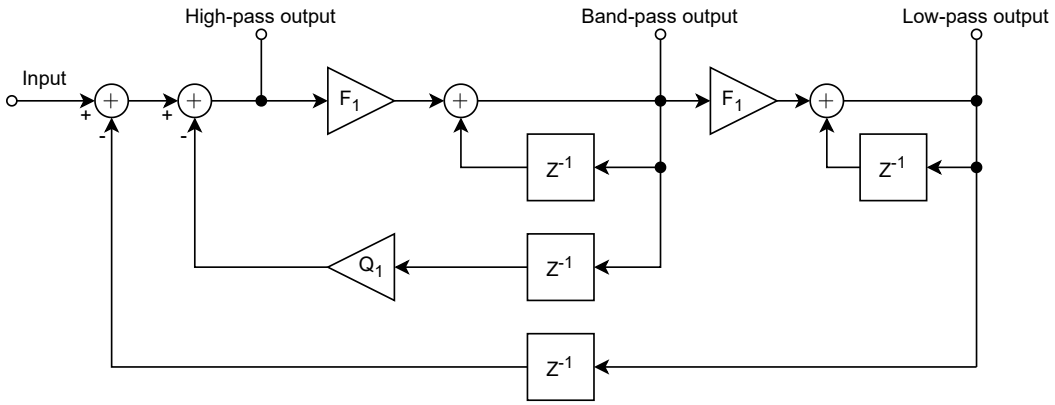

Figure 4.25: Illustration of state variable filter [37].

From the illustration, it can be seen that the filter structure provides both a low-pass, band-pass and high-pass output. For the atmospheric attenuation, the low-pass output will be used. This type of filter is commonly used in different audio effects because of the ability to change parameters with a small number of artefacts and for that reason, this filter is chosen [37]. The coefficients in the filter structure is given as stated in eq. 4.23.

$$F_1 = 2 \cdot sin(\frac{\pi \cdot f_c}{f_s}) \quad \text{and} \quad Q_1 = \frac{1}{Q} \tag{4.23}$$

Where:

f_c	Is the cutoff frequency for the filter.	[Hz]
f_s	Is the sample frequency.	[Hz]
Q	Is the desired Q-value for the filter.	[−]

The parameter Q determines the height of the resonance in the filter. When $Q = \frac{1}{\sqrt{2}}$ it ensures the response is flat up until the chosen cutoff frequency [37]. The transfer function for the low-pass output is given as shown in eq. 4.24.

$$H(z) = \frac{F_1^2}{1 + (F_1^2 - q - 1)z^{-1} + qz^{-2}} \tag{4.24}$$

Where:

q	Is defined as: $1 - F_1 Q_1$	[-]

The difference equation is found by the inverse z-transform and solving for $y[n]$. The result is shown eq. 4.25.

$$y[n] = F_1^2 x[n] - (F_1 - q - 1)y[n-1] - qy[n-2] \tag{4.25}$$

The difference equation shows that this is a recursive Infinite impulse response (IIR) filter. To approximate the atmospheric attenuation, the distance from the source to the receiver is mapped to a cutoff frequency. It is shown earlier that at large distances the low frequency area is attenuated more than at a short distance, but the low-pass characteristics remain. This corresponds to moving the cutoff frequency of the variable filter down in frequency.

The mapping function is found by doing a regression of the -3 dB cutoff frequency at different distances calculated from the actual atmospheric attenuation. For this, the atmospheric parameters 10°C and 80 % relative humidity are chosen, since this is comparable with the conditions of the measurements on the reference recordings. The mapping has the best fit with an exponential function with $R^2 = 0.97$ and is is found to be.

$$G(x) = 6055.27e^{-0.0032x} \tag{4.26}$$

Where:

$G(x)$	Is the cutoff frequency	[Hz]
x	Is the distance form source to receiver	[m]

Since not all IIR filters are stable, a stability requirement for the filter is given as $F_1 < 2 - Q1$ [37]. This means that to ensure stability a trade between the peak of the resonance and the desired maximum cutoff frequency has to be found. From fig. 4.24 it can be seen the atmospheric attenuation has little impact at 10 m. Using the function in eq. 4.26 this corresponds to a cutoff frequency of 5865 Hz and thereby $F_1 = 0.749$. This means that Q-value has to be bigger than 0.79 to fulfill the requirements. A Q-value of 0.8 is chosen, since this is closest to the value that assures a flat response until the cut off frequency.

To show the approximation of the atmospheric attenuation two results with different atmospheric parameters at the same distance are shown in fig 4.26.

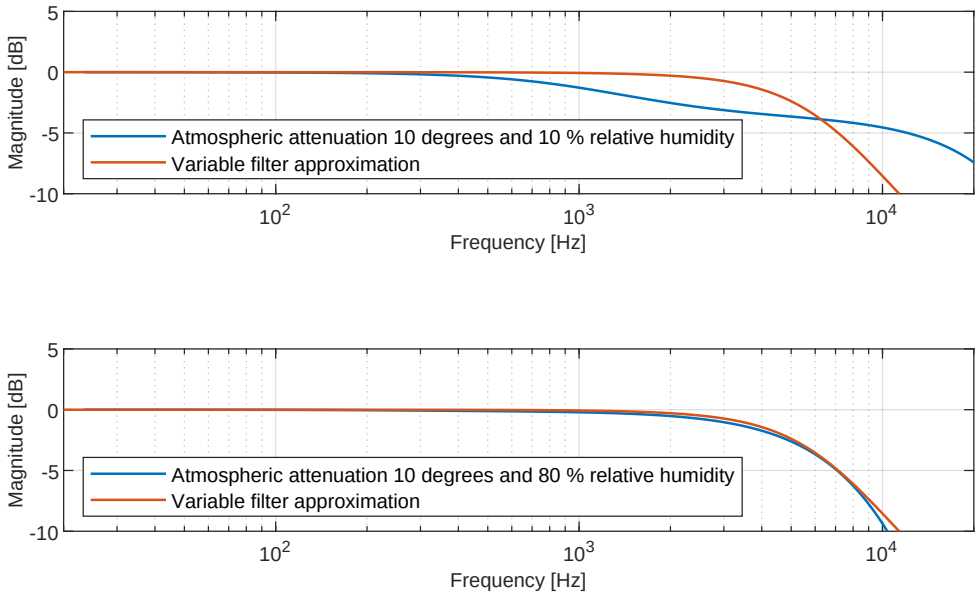

Figure 4.26: Frequency response of the variable filter compared with the actual atmospheric attenuation at 60 m with different atmospheric parameters.

The results show that the variable low-pass filter can be a good approximation in some cases, but not as good an approximation in other cases as a change in the atmospheric parameters can cause a more complex function than a simple low-pass filter. However, this variable filter allows for effective computation of the atmospheric attenuation of the moving sources on the blade tips. The implementation illustrated in fig. 4.27 shows that the ADM, which is the distance between source and receiver, can be used as a direct input to calculate the desired cutoff frequency.

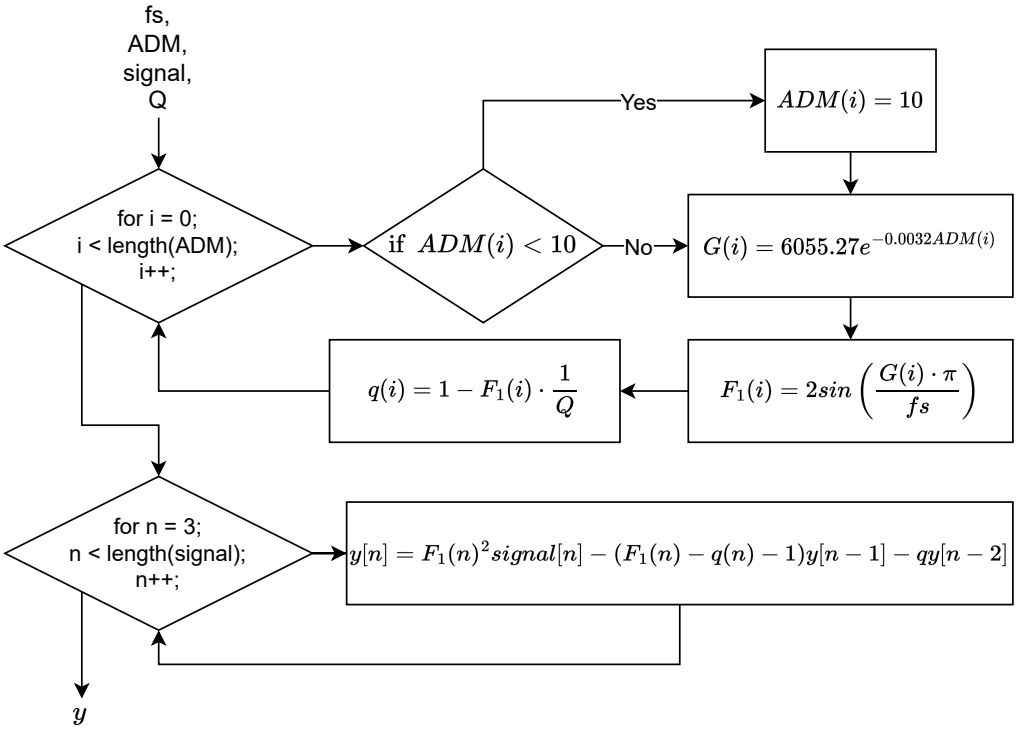

Figure 4.27: Flow of the variable filter implementation.

From the figure, it can be seen that the filter is implemented as the difference equation, where the cutoff frequency is updated for every sample. It should be noted that the output vector is initialized with zeros. This is necessary for the first two iterations of the loop at the bottom of the figure since the filter relies on past values. The implementation also shows that the limit of the ADM is restricted to be no smaller than 10 m to ensure the stability of the filter.

A result of the time varying filter for a receiver located beneath the rotor at [0,0,0] and with turbine parameters of hub height 115 m and rotor diameter 170 m is shown in fig 4.28.

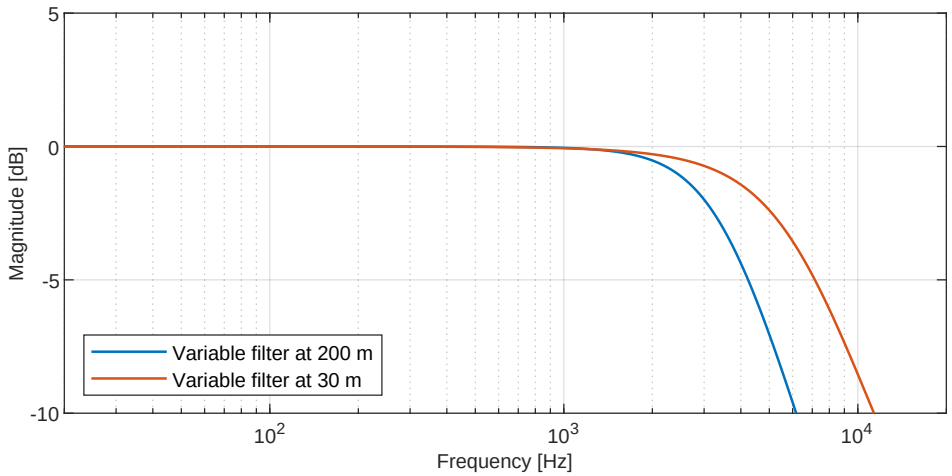

Figure 4.28: Result of the two extremes for the variable atmospheric attenuation for a receiver in [0,0,0] with a rotor hub of 115 m and a 170 m in rotor diameter.

The result shows that the sources of this wind turbine will be in the range of 30 m to 200 m. A significant change in the high-frequency content is visible in the figure and will have an impact on the sound.

The two different implementations of atmospheric attenuation will both be an option to choose in the simulator.

Focus will now be on the simulation of the ground effect.

4.5 Ground effect

As described in sec 2.3.3, the effect of ground can be calculated octave-band-wise in ISO 9613-2. This makes sense in a noise analysis perspective, but is not directly applicable for synthesis. For this reason, an approach to model the altering effect depending on ground will be based on calculating the reflection coefficient by using the flow resistivity of the ground. The surface provides a complex reflection coefficient, where both phase and magnitude are changed depending on frequency. As the wind turbine noise model is also based on three moving sources the angle of incidence is also a time-varying element. This complicates the creation of a filter because the characteristics need to change over time, as will be shown.

For estimating the impedance of ground, the one-parameter method presented in [18] (by use of flow resistivity), is used. The impedance is calculated as:

$$Z_m = \rho c \sqrt{\rho_m(f)\kappa(f)} \tag{4.27}$$

Where:

ρ	is the density of air	[kg/m^3]
f	is the frequency	[Hz]
c	is the speed of sound in air	[m/s]
ρ_m	is the normalized complex density of the ground	[kg/m^3]
κ	is the normalized complex compressibility of the ground	

The calculations of the normalised complex density and compressibility are both dependant on flow resistivity of the ground, the ratio of specific heats for air, and the frequency. The calculation of these have been allocated to appendix A.2, for the sake of brevity.

The impedance is then used to estimate the reflection coefficient. For a plane-wave the reflection coefficient (R_p), this is calculated as:

$$R_p = \frac{Z_m \cdot cos(\theta_i) - \rho c \cdot cos(\theta_t)}{Z_m \cdot cos(\theta_i) + \rho c \cdot cos(\theta_t)} \tag{4.28}$$

Where:

θ_i	is the angle of incidence	[°]
θ_t	is the angle of transmission into the material	[°]

$cos(\theta_t)$ may be calculated, according to [38], as:

$$cos(\theta_t) = \sqrt{1 - (\frac{k}{k_m})^2 sin^2(\theta_i)} \tag{4.29}$$

with k being the wave-number and

$$k_m = \frac{2\pi f}{c} \cdot \sqrt{\frac{\rho_m}{\kappa}} \tag{4.30}$$

As mentioned in sec. 2.3.3, the effect of ground can be estimated by its flow resistivity, i.e. R_1, by using it to estimate the impedance of the ground. This flow resistivity takes different values for different ground types. The following examples will be based on a flow resistivity of 80, corresponding to "uncompacted loose ground".

Using equation 4.27-4.30 (as well as the supporting equations in appendix A.2) the following frequency reflection coefficients are obtained, as shown in fig. 4.29:

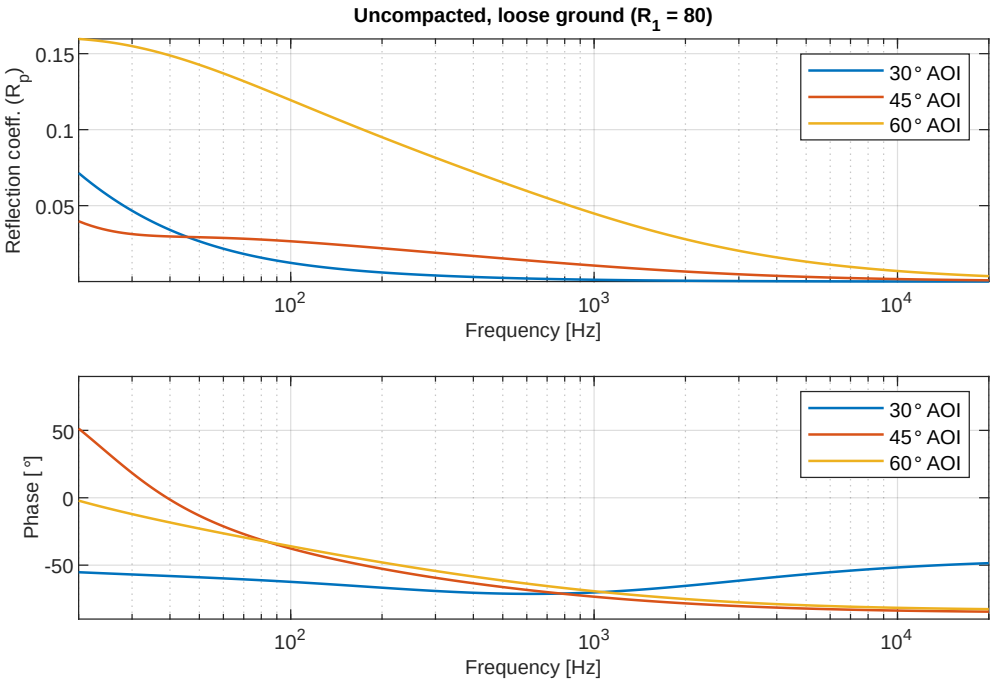

Figure 4.29: Reflection coefficient for loose ground from 20 Hz to 20 kHz.

Figure 4.29 show the frequency dependant reflection coefficient for 3 different angles of incidence (AOI), for loose ground, using the one-parameter (flow resistivity) model. Clearly evident is a non-linear behavior of reflection magnitude wrt. AOI. Moreover the magnitude does not necessarily have a continuous rising, or contiuous falling characteristic, for increasing/decresing AOI. A clear example of this can be seen for the magnitude at frequencies below ∼45 Hz, where the 45° AOI is both lower than 60° and 30° AOI. This highlights a problem wrt. implementation, as the source change AOI over time (as the blades are moving), and change magnitude and phase response, in a more complex manner. The filter characteristic therefore cannot be approximated by a low-pass filter, as in sec. 4.4, and moreover does

not necessarily follow similar characteristic for different flow resistivity values. The frequency sampling method is an evident choice for designing an appropriate filter, since arbitrary reflection coefficients can be drawn from eq. 4.28 for any frequency. Although it should be noted that eq. 4.28 is based on a plane-wave assumption, and is only valid for AOI's up to 85° [18], which can become an issue for low source/receiver height and for long distances. For a wind turbine such as the one in the measurements with a hub height of 115 m and a rotor diameter of 170 m the angle would approach the limit for the plane wave assumption at approximately 300 m. Calculations are shown in eq. 4.31

$$AOI = atan\left(\frac{D_{tower}}{h_{min}}\right)\frac{180}{\pi} \tag{4.31}$$

Where:

AOI	Is the angle of incidence	[°]
D_{tower}	Is the distance from reflection point to tower	[m]
h_{min}	Is minimum height from the ground that the blade tip is at	[m]

For a distance of 300 m and a h_{min} at 30 m using eq. 4.31 the AOI will be 82.2 °, which is close the limit. The effects of exceeding this limit, however, has not been investigated.

The necessity for a constantly changing filter for different samples may prove strenuous in terms of necessary processing power, as a cascade of different filters would be needed for new samples. For this reason, inspiration is drawn from a method used for the implementation of head-related transfer functions, specifically estimation by adjacent linear interpolation [17].

4.5.1 Filter Interpolator

The basic principle of adjacent linear interpolation is to estimate the unknown filter characteristic by use of two adjacent known filters. The signal is fed through both filters, and weights are applied to shift emphasis on one filter to the other as needed. The simple example of this, using 2 filters is shown in fig. 4.30

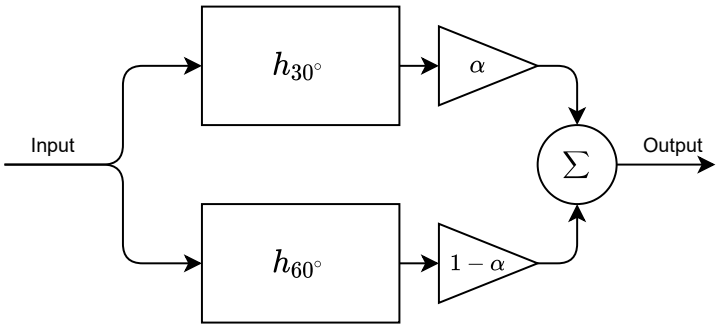

Figure 4.30: Illustration of linear adjacent filter interpolation, using 2 FIR filters.

Figure. 4.30 shows the input being fed into 2 FIR filter constructions (30° and 60° AOI), whereafter multiplication by parameter α or $1-\alpha$ ($0 \leq \alpha \leq 1$) dictates the linear interpolation factor. For $\alpha = 0.5$, angle 45° is estimated; for $\alpha = \frac{1}{3}$, angle 40 is estimated, et cetera. The advantage is that α can be changed sample-wise for different AOI's. However, filter accuracy is sacrificed, in the sense that the estimated filter does not exactly represent the actual filter.

An example of a 45° response estimation comparison can be seen on fig. 4.31

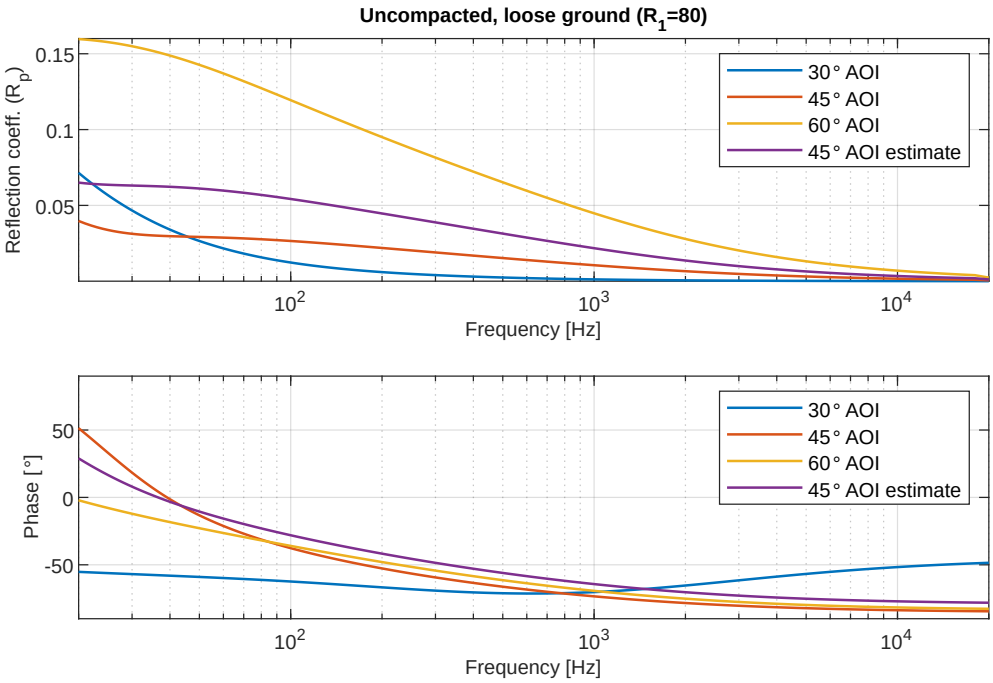

Figure 4.31: Reflection coefficient estimation comparison at 45°

Figure 4.31, presents the estimate 45° AOI response, based on the adjacent linear interpolation between the frequency response at 30° AOI and 60° AOI. It is moreover the response of the system depicted in fig. 4.30 for $\alpha = 0.5$. The actual filter at 45° AOI is also plotted for comparison. It is clear that the estimate does not exactly reflect the correct filter response, and improvements can be made by having the adjacent filters closer to the actual filter. The necessary amount of filters is, however, dependant on the situation.

Relating the previous interpolation examples to a wind turbine modelled as a moving source: the AOI's of the sound sources are not known beforehand, but may be calculated from the incident vectors on the ground after a position is chosen, as described in sec. 4.3.4. From this, it is possible to find the maximum and minimum AOI. A position example with max/min angles is illustrated in fig 4.32. The extended response is then inverse Fourier transformed, to obtain the impulse response.

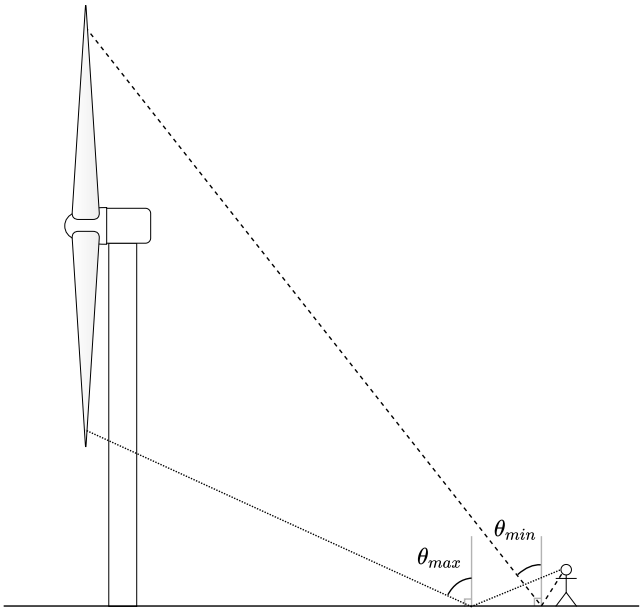

Figure 4.32: Illustration of the two source position that gives the maximum AOI and the minimum AOI.

Figure 4.32 illustrates a simple example for a minimum/maximum AOI (denoted θ_{max} / θ_{min}), when the person is located on the x-axis. The difference in min/max AOI, is positionally dependant, however when a position is selected, only filter values within this range make sense to calculate, as no source move beyond these values. This is used as basis for creating filters to interpolate between. To make a qualified estimate of the necessary filter subsets to interpolate between, it is necessary to know, not only the magnitudal and phase error for interpolation at different AOI's, for different ground types, but also the audible consequences of these errors. This is an extensive task, that will not be covered in this report, but may be a point of further research. The implementation is based on calculating 3 filters, that will be interpolated between. An illustration of this is seen on fig. 4.33

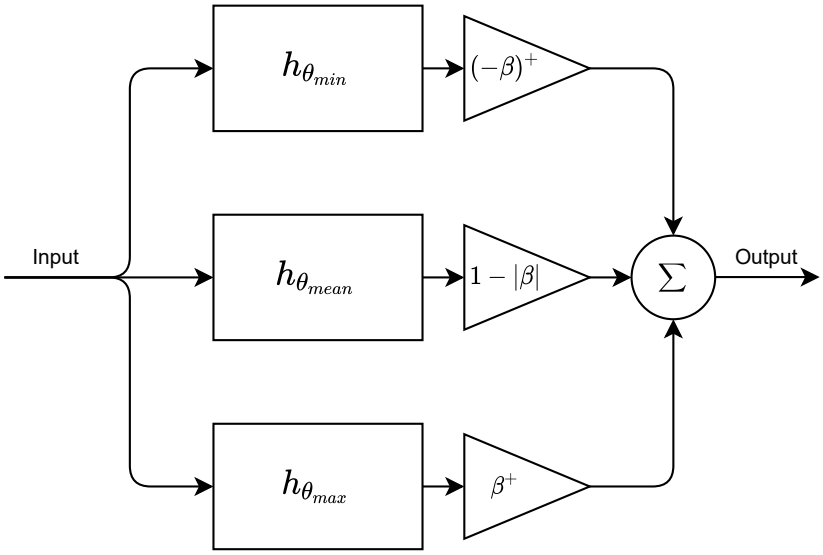

Figure 4.33: Illustration of linear adjacent filter interpolation, using 3 FIR filters.

The filter structure depicted on fig. 4.33 uses 3 filters: One at each extremity (θ_{max} & θ_{min}), as well as one at the angle in between ($\theta_{mean} = (\theta_{max} + \theta_{min})/2$). The variable '$\beta$' represents the normalized calculated AOI's from the ADM. β is normalized to take values from -1 to 1, where -1 corresponds to θ_{min}, 0 corresponds to θ_{mean} and 1 corresponds to θ_{max}. It should furthermore be noted that the '$^+$' in the multiplication segments of fig 4.33 denotes the relu/rectifier operator. i.e. any negative values are set to '0'. With this, it can be seen that two filters are active at a time. This filter topology can be expanded to use more than 3 filters for interpolation, should this be deemed necessary.

4.5.2 Filter computation

The filters $h_{\theta min}$, $h_{\theta mean}$ and $h_{\theta max}$ depicted in fig. 4.33 are FIR filter constructions using the coefficients from an impulse response. This impulse response is derived by the inverse Fourier transform of the collected ground reflection coefficients from eq. 4.28. Implicitly: the number of filter coefficients depend on how many frequency bins are drawn. An initial nr. of coefficients is chosen to be 4800, amounting to 1/10'th the sample rate ($f_s = 48kHz$), and therefore one frequency bin every 10 Hz, in order to faithfully represent the frequency spectrum. The amount of coefficients can be increased, but large coefficient FIR filter implementations are, however, computationally expensive because of the inherent convolution.

While time domain FIR filter implementation may be advantageous for a real-time implementation, where computational resources are plenty and the real-time requirement strict; converting this computation to the frequency domain makes more sense for this implementation, where real-time requirements are more loose. Since a convolution in the time domain equates to a multiplication in the frequency domain, the

input data (the sound signal) can be Fourier transformed, and element-wise multiplied with the frequency response, for the same result. This, however, necessitates that the vectors are the same length. While a frequency domain resolution of same length as the input may be drawn from eq. 4.28, the calculation involved in calculating eq. 4.28 for each bin may become taxing for long vectors. Moreover, such a fine filter resolution is not deemed necessary, considering the relatively smooth characteristics illustrated in fig. 4.31 as well as the potential accuracy lost in estimation.

Although the calculation times for the algorithms in the simulator are very hardware dependant, a preliminary test has been made, to compare calculation times. Even though the simulator does not have strict real-time requirements, a sensible decision is that the solution should not take minutes or even many seconds to complete, as previously discussed in sec. 2.3.6 (i.e. disregarding wave-based solutions because of high computational complexity).

Three filter methods are proposed for individual computation and response comparison.
The filter method setups are as follows:

1. Convolution in Matlab, with 4800 coefficient FIR filters, obtained with the inverse FFT from the frequency sampling method.

2. Multiplication in the frequency domain, by using the FFT of the zero-padded impulse response. The impulse response is obtained similarly as in scenario 1, windowed, then padded to the same length as the input signal.

3. Multiplication in the frequency domain with the frequency sampled response of same length.

Method 1, 2 & 3 can also be seen in fig. 4.34:

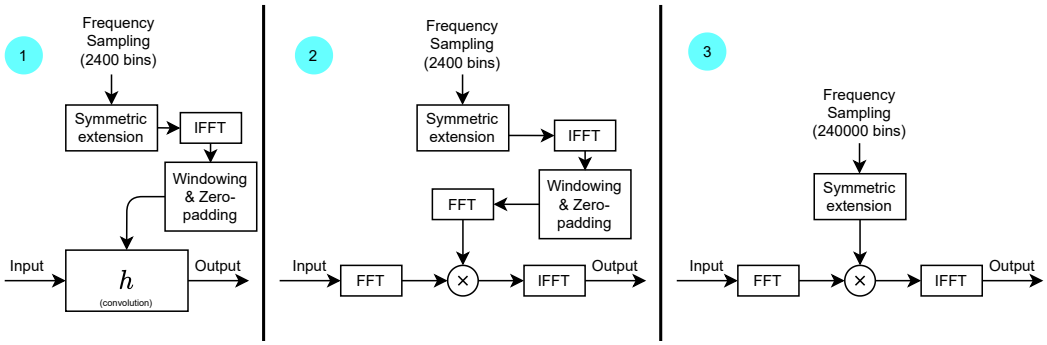

Figure 4.34: Illustration of 3 different methods for filtering.

The symmetric extension in fig 4.34 simply involve extending the frequency response to include the negative frequency contribution by mirroring and conjugating.

In order to measure the time it takes to apply the filter a test has been conducted with the methods depicted in fig. 4.34 where it is measured for 4 scenarios in Matlab.

The two first scenarios using the matlab functions 'conv' and 'fftfilt' for doing the convolution (method 1), and the other two (method 2 & 3) as depicted in fig. 4.34. The filter methods are consecutively applied on a 10 second noise signal 9 times (3 filters, as in fig. 4.33, for the 3 independent blade sources). Averaged over 5 runs, the following computation times are obtained:

Calculation time	Method 1 (conv)	Method 1 (fftfilt)	Method 2	Method 3
Average [s]:	1.724	0.2497	0.2931	1.262

Table 4.2: Average time for completion from the 3 calculation methods.

Based on this rudimentary experiment, the calculations of the ground effect in the simulator is implemented with the fftfilt function. It should, however, be emphasised that this is based on the application of processing a 10 second chunk input signal in Matlab, and another method may be preferable, should the scenario change. The function fftfilt, if preferable for larger blocks of data, and uses an overlap-add scheme, reducing the amount of floating point operations needed, by selecting an appropriate datablock size. It is also able to use the GPU, should this be enabled, but consequently this becomes highly hardware dependant, and has not been enabled in the test.

4.5.3 Filter Response

The filter characteristics shown earlier, drawn from eq. 4.28 (p. 73) are the desired response for the filters. For implementation, however, the length and consequences of the length needs to be considered. Some preconditioning of the signal also needs to be conducted to avoid artefacts. While the filter response will vary according to the flow resistivity of the ground and AOI, the example given here will be on the basis of a flow resistivity of 80 (i.e. uncompacted, loose ground) and for an AOI of 60°. An example of this can be found in fig. 4.35

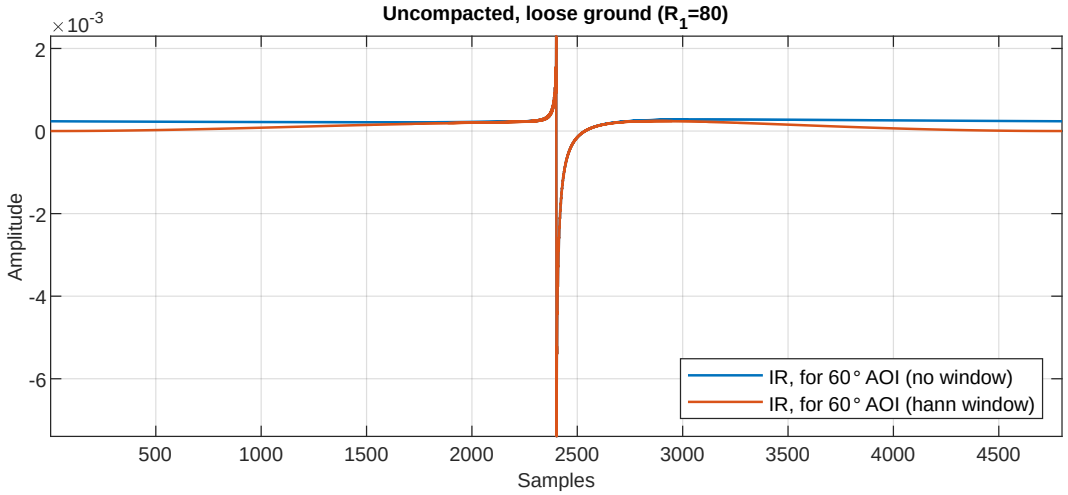

Figure 4.35: Impulse response of length 4800, derived from the 60° AOI, before and after windowing.

Figure 4.35, depicts the derived impulse response, as well as, after a hann window has been applied to it. The hann window has been applied to reduce artefacts in the frequency domain, caused by the abrupt change to '0', when such an impulse is zero-padded. Examples of these artefacts can be seen in fig. 4.36

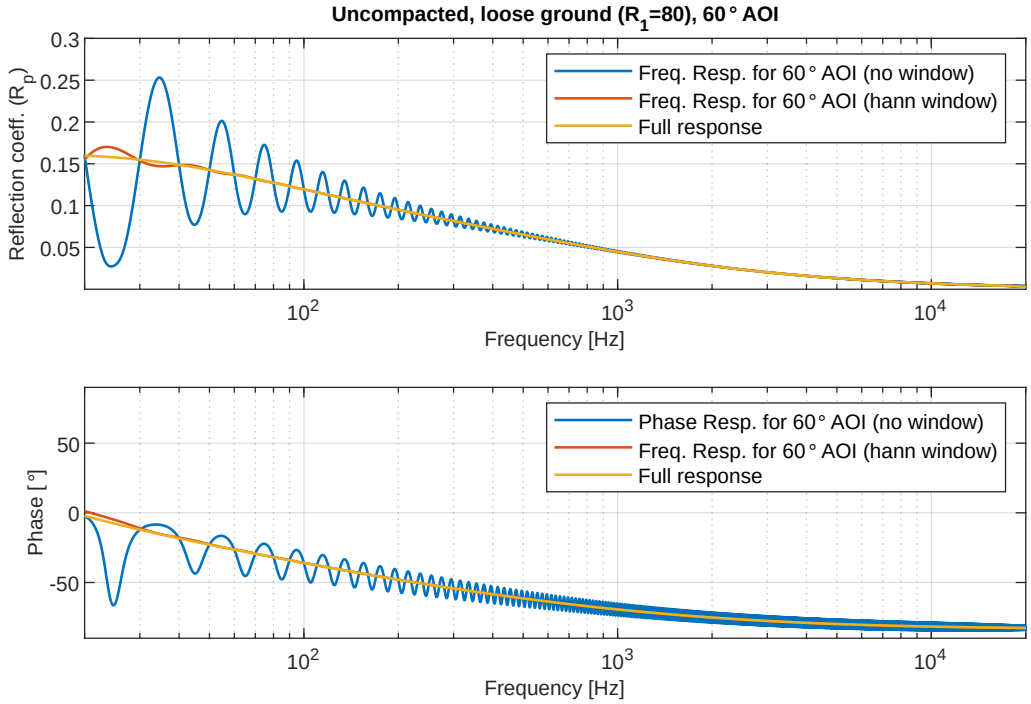

Figure 4.36: Frequency/phase response for the 60° AOI.

Figure 4.36 shows the frequency and phase response of the impulse response depicted in fig. 4.35. Clearly visible is the artefacts introduced by using a rectangular window, i.e. no window. While the hann-windowed filter characteristics may seem sufficiently acurate, another problem arises from filtering.

All the filters introduce a time delay, as can be seen in the corresponding impulse response. Compensating for this delay is highly important in this scenario. While the delay introduced by the atmospheric absorption filters delay the whole system equally, the ground effect is only affecting the reflected contribution. Without correction, this delay would shift the potential comb-filter effects caused by the reflection. A solution to this, is to either shift the impulse response to the beginning, or introduce a similar delay to all the direct sound lines (upper part of 3.4, page 38). In the attempt to avoid non-causal artefacts, such as the reflected contribution arriving before the minimum delay difference of reflected/direct energy, it is chosen to avoid delaying the direct sound, and shift the ground filter instead.

The obtained impulse response impulse response depicted in fig. 4.35, spikes near 2401 samples, but has an initial build up to the spike. The response is shifted 2390 samples to the left, so the signal starts 10 samples before the main spike. An example of this can be seen in fig. 4.37:

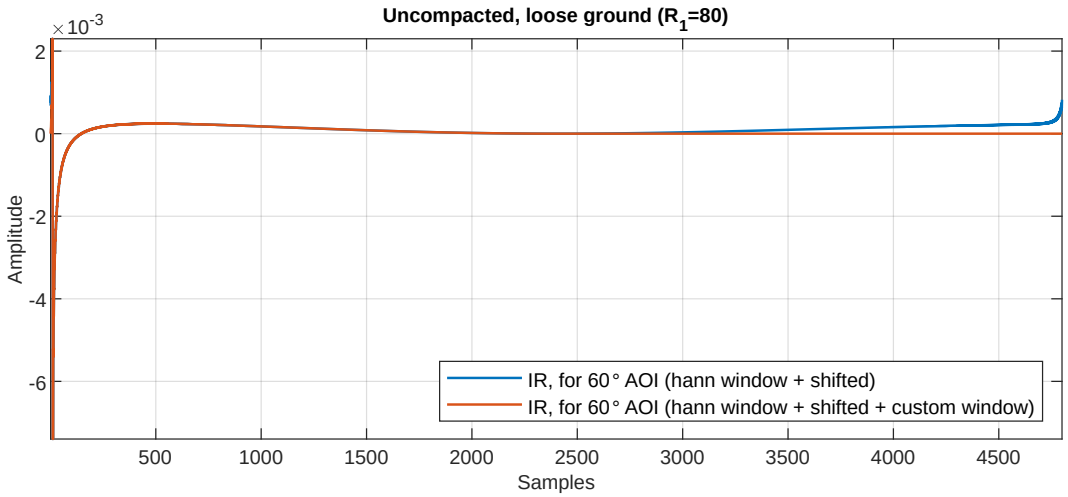

Figure 4.37: The shifted impulse response, derived from the 60° AOI, before/after custom windowing.

Figure 4.37 shows the previously hann-windowed, and now shifted, impulse response. A custom window function is also applied to the impulse response after shifting. This window eases into the impulse response, by multiplying the first 10 samples with a vector that linearly increases from 0 to 1. The custom filter also sets any values after 2410 to '0' (2400+10 i.e. '10' being the number of included samples before the spike), to avoid the artefact caused by the circular-shifted remnants from the beginning, similarly to the motivation for the hann-window application. The resulting frequency response can be seen on fig. 4.38

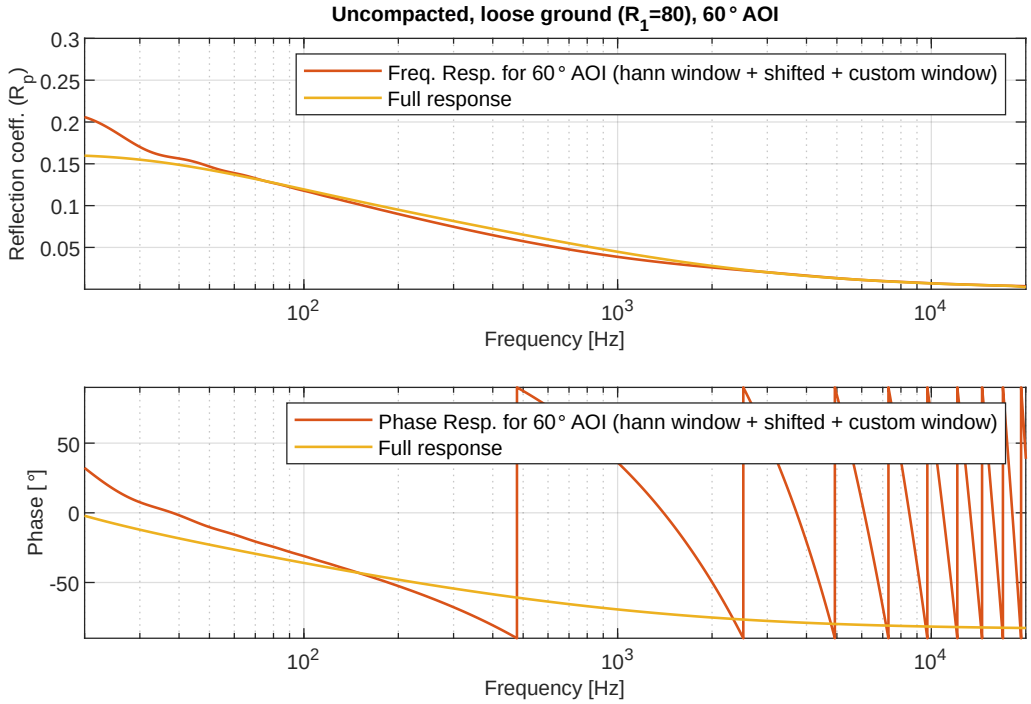

Figure 4.38: Frequency/phase response for the 60° AOI, after custom windowing of the impulse response.

Figure 4.38 show the frequency and phase response of the designed filter, after hann-windowing, shifting and applying the custom window. There are slight deviations from the full response, i.e. the desired response. The phase response consequently has considerable deviations that exacerbates as the frequency rises. This is, however, just a consequence of the intentionally time-shifted signal. While this can be remedied by shifting the impulse closer to the beginning, it is not necessarily in the interest to remove the information herein (as a consequence of the custom filter). To summarize, it is a balance to strike: Whether to shift the filter less, gaining more accurate filter characteristic but introducing unintended delay to the reflected contribution; or shift the filter more, and gain more accurate relative time response, but potentially introducing artefacts. However, this method of shifting the impulse to the start (-10 samples) is applied to all filters. Again, it should be said that this is very case specific, i.e. dependant on AOI, as well as the flow resistivity of the ground.

The current simulator implementation is based on the 10 second chunk-wise data processing method using fftfilt. In the simulator, the ground effect can be calculated for different ground types (based on flow-resistivity), and the current implementation give a user 6 presets to chose from:

- Snow or moss ($R_1 = 12.5$)
- Uncompacted, loose ground ($R_1 = 80$)

- Normal uncompacted ground (pastures, forest floors) ($R_1 = 200$)
- Compacted fields, lawns and gravel ($R_1 = 500$)
- Compacted dense ground (gravel road, parking lot) ($R_1 = 2000$)
- Water ($R_1 = 200\ 000$)

For the sake of brevity, the responses at different flow-resistivities can be found in appendix A.3.

In order to convert the numerical representation of the input signal to an actual representative sound level, it is necessary to map this accordingly, which will be covered in the following section.

4.6 Sound levels & Data representation

To ensure the output of the simulator can be compared with the recordings from the measurements and that the calculations in the simulator are comparable with a physical value a data representation is chosen. All of the measurements have a calibration section with a reference of 94 dB at 1 kHz. All measurements are scaled with this reference so a sound pressure level can be calculated, meaning that all samples directly represent the pressure in Pascal eg. the value of 1 in samples corresponds to 1 Pa. The approach is taken for the signal generated by the simulator. From earlier calculations in sec. 4.1 it is found that the apparent sound power level of the wind turbine is 104.3 dB(A) re. 1 pW. (or 115 dB re. 1 pW.). To make the data representation match, all the sound models, before the different effects of the simulator affect the signal, the models are scaled to have the sound power level corresponding to 1 m from the source. The SPL is found as shown in eq. 4.32.

$$L_p = L_{WA} - |10log_{10}\left(\frac{Q}{4\pi r^2}\right)| \tag{4.32}$$

Where:

L_p	Is the SPL	[dB re. 20 μPa]
L_{WA}	Is the apparent sound power level	[dB re 1 pW]
Q	Is the directivity factor (chosen to be 1)	[-]
r	Is the distance to the chosen point (chosen to be 1)	[m]

This corresponds to a SPL of 93.3 dB(A) at a distance of 1 m from the source. All the sound models will be scaled to represent this SPL, which corresponds to the RMS value of the signal being 0.89. It is chosen to scale the sound model based on an A-weighted level since this matches the human perception of sound better, thereby making the different models appear to have the same sound level despite their different spectrums. It should be noted that the signal that goes into the simulator

is not A-weighted, because this would make the output signal A-weighted. Without the A-weighting, the SPL at 1 m is 104.1 dB, which corresponds to a numeric value of 3.28. This is assumed to be the worst case or highest possible SPL and will be the reference for mapping. This is illustrated in fig 4.39.

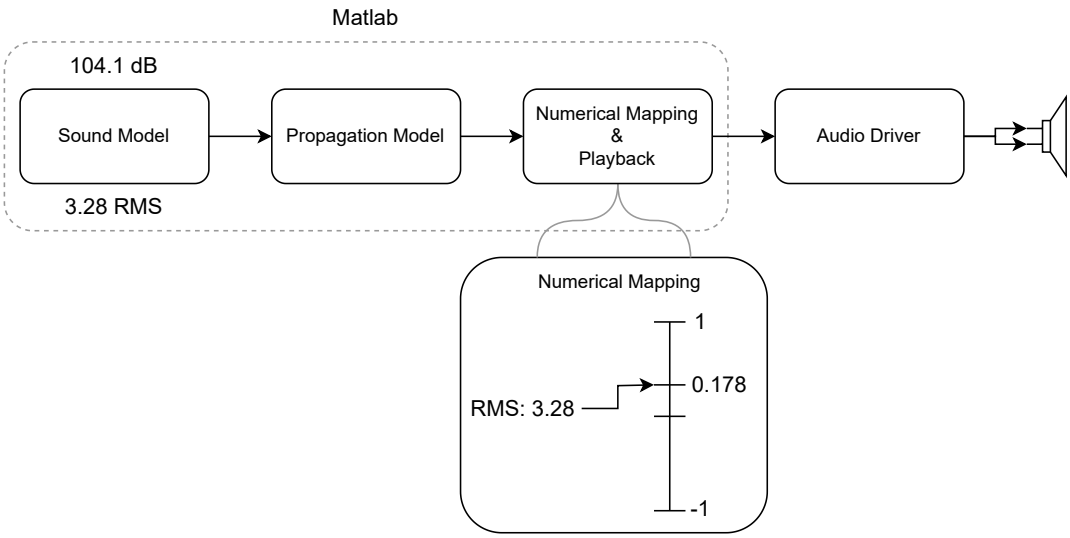

Figure 4.39: Illustration of numerical mapping in the simulator.

The data is kept in the format of being directly proportional to pressure until the playback occurs. For the playback Matlabs audioplayer object is applied. For single and double precision the sample value has to be in the range of -1 to 1 in the audio player and for this reason a numerical mapping is needed to avoid clipping. Since the crest factor of the white Gaussian noise in Matlab is found to be 13.5 dB a headroom of 15 dB (factor of 5.62) is chosen. For the worst case, this means mapping the value of 3.28 to a value of 0.178 (e.g. $1/5.62$) as shown in the figure. Getting the correct sound pressure level at the speaker or headphones requires that the hardware and software outside the Matlab box are known. One fixed gain at the audio driver would produce the correct level in one case, but changing the headphones or speaker will create a different result.

A setup with a pair of Sennheiser HD650 headphones connected through an RME Fireface UFX+ soundcard is set up, and measurements with a headphone coupler are carried out to calibrate the system. This setup is visible in fig. 4.40

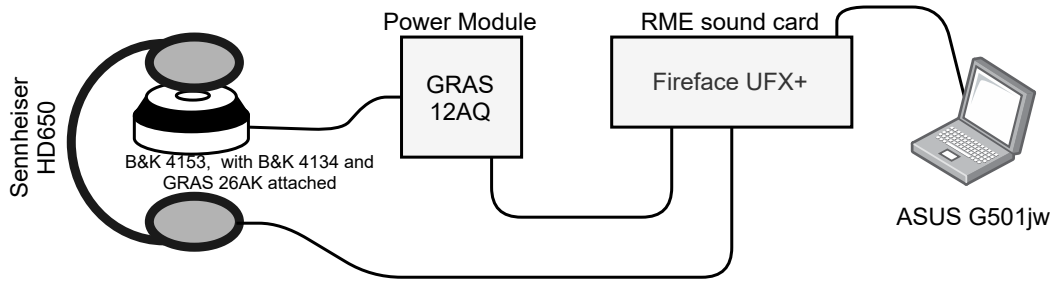

Figure 4.40: Setup for measuring the sound pressure level output of a pair of headphones.

Using the setup in fig. 4.40, calibration of the sound card and headphones is carried out by using the matlab script "calibrate.m". This script is executed separate from the simulator script, and is performed using the procedure stated in appendix A.5. This script first calibrates a microphone using a calibrator, then takes two inputs: The desired output level, and the desired numerical value. These two values are the previously mentioned 104.1 dB SPL and 0.178 numerical. The script then may ask that the output level on the sound card be turned up, or or that a reducing factor be adjusted in the script. If the output is within ± 0.5 dB of the goal, a scaling factor is output, which is implemented in the simulator output. This scaling factor is, importantly, only applicable using this sound card and headphone setup. Lastly it has been chosen to use a pair of open-back Sennheiser HD650 headphones because of the inherent diffuse field equalized characteristics, in order to compensate for the effects of the ear when listening with these headphones. The imperfect characteristics of the headset (i.e. deviations from the listeners diffuse field characteristic) as well as the sound card output (i.e. deviations from a flat response), will affect the final playback. Although the current setup is not a perfect solution, it still provides some compensation. This, however, has not been deemed an important focus for the project.

4.7 Simulator presentation

This section gives a short introduction to the layout of the implemented simulator. The different parameters and how they are changed will be presented along with the plots and other opportunities. The layout for the wind turbine simulator is presented in fig 4.41.

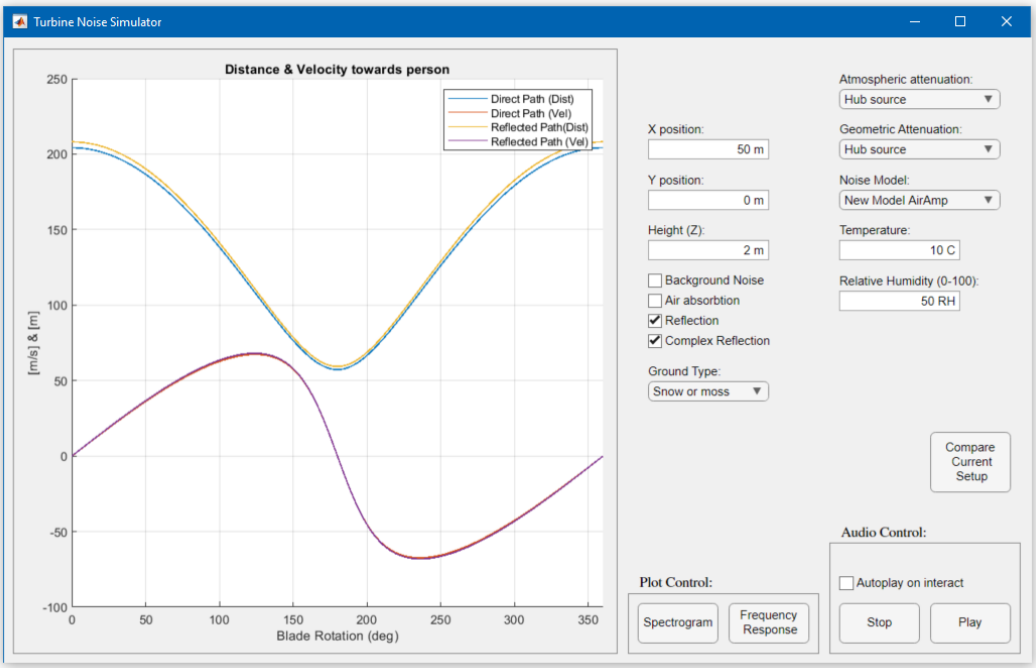

Figure 4.41: Layout for the wind turbine simulator.

The simulator layout is divided into two main sections. On the left is a window with a plot showing the currently calculated acoustic distance model (blue) and the acoustic velocity model (red). These are the function that is used as input to the different parameters and change if a new position is selected. Furthermore the distance- and velocity model for the reflecting sound will also appear in the plot if reflection is selected.

The right side of the layout is where the selection and adjustment of different parameters are placed. The parameters correspond to the sections earlier described in the report. Some parameters can be included or disregarded in the simulator by a checkbox, if not checked this removes the effect from the calculation and the pertaining thereto adjustment will not change the resulting sound.

The adjustments possible are are:

- Position: Given as an input (decimal or integer) in three different boxes (x,y,z).
- Atmospheric attenuation: Drop-down menu with hub/blade source. (takes input for temperature and relative humidity for hub source.)
- Geometric attenuation: Drop-down menu with hub/blade source.
- Noise model: Drop-down menu with the different noise models.
- Reflection: If reflection is selected a slider appears to chose the reflection coefficient, or if complex reflection is chosen a drop-down menu with different ground surfaces appear.

The audio control section in the bottom right makes it possible to play the sound or stop the sound. If the checkbox "autoplay on interact" is checked, the sound will start playing as soon as a parameter is changed. The sound generated is approx 10 s.

Compare current setup can be clicked and a new window will open. The new windows is shown in fig 4.42.

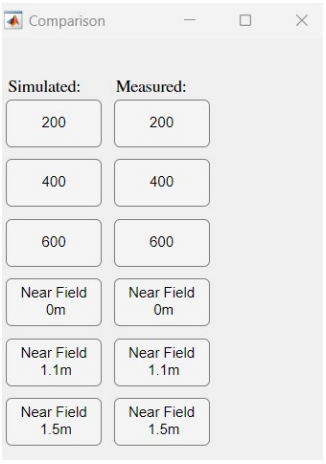

Figure 4.42: Compare current setup button opens a new window.

The push of the button generates 6 different sound files ready for playback. This takes your current setup (all the chosen parameters) and generates sound corresponding to six of the measurement positions at a height of 0 m except two near field positions at a height of 1.1 m and 1.5 m. The left column in the new window is the simulations at those positions and the right column is the recording in the same positions. The simulations or recordings will start playing after a push of a button.

Plot control opens a new window with the current setup parameters and generates a spectrogram if the spectrogram button is pushed. The frequency response buttons opens up two frequency responses, one with the current setup and another with the past setup for the user to compare the past setup.

With the layout of the simulator explained, results generated by the simulator will be presented.

Chapter 5

Verification & Results

This chapter presents the results of the simulator with different parameters and compares them with the measurements from the wind turbine. It also includes a section with informal listening observations, which seek to describe how the different models and parameters change the perception of the sound from the simulator.

With adjustable parameters, many different combinations for the output of the simulator exist. To compare the ability of the simulator to reproduce the correct SPL at a given position the following parameters are chosen, which represent the conditions of the time the measurements were made.

- Ground: Complex ground reflection with "compacted fields"
- Atmospheric attenuation: Blade source (temperature 10 °C and humidity 80 %)
- Geometric attenuation: Blade source

The sound pressure level at the position of the near field measurements [44, -44, 0] is simulated with three different sound models. The resulting sound pressure level along with the result from the measurement is shown in fig 5.1.

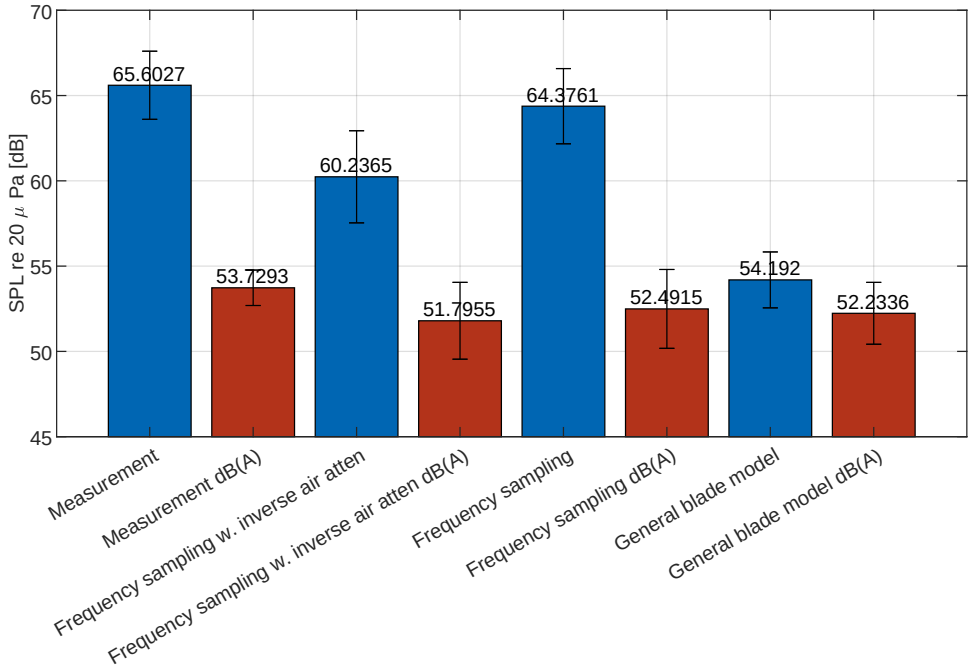

Figure 5.1: Sound pressure level for a measurement and simulations with different models at the position of the near field measurement [44, -44, 0].

The figure shows both the A-weighted SPL and non-weighted SPL at the position. The numbers represent the calculated SPL and the lines represent the variance based on a 10 s signal for each simulation and a 60 s for the measurements. It is clear from the results that the non-weighted sound pressure levels differ, especially the general blade model is approximately 13 dB lower than the measurement, where both of the frequency sampled models are within approx 5 dB. The A-weighted results for this position show that all of the simulations are within approximately 2 dB. It should be noted that these simulations do not include background noise which is a part of the measurement. The SPL produced by the simulator and the recorded levels for the measurements at the long range position 1 [200, 0, 0] are also compared. The results are shown in fig 5.2.

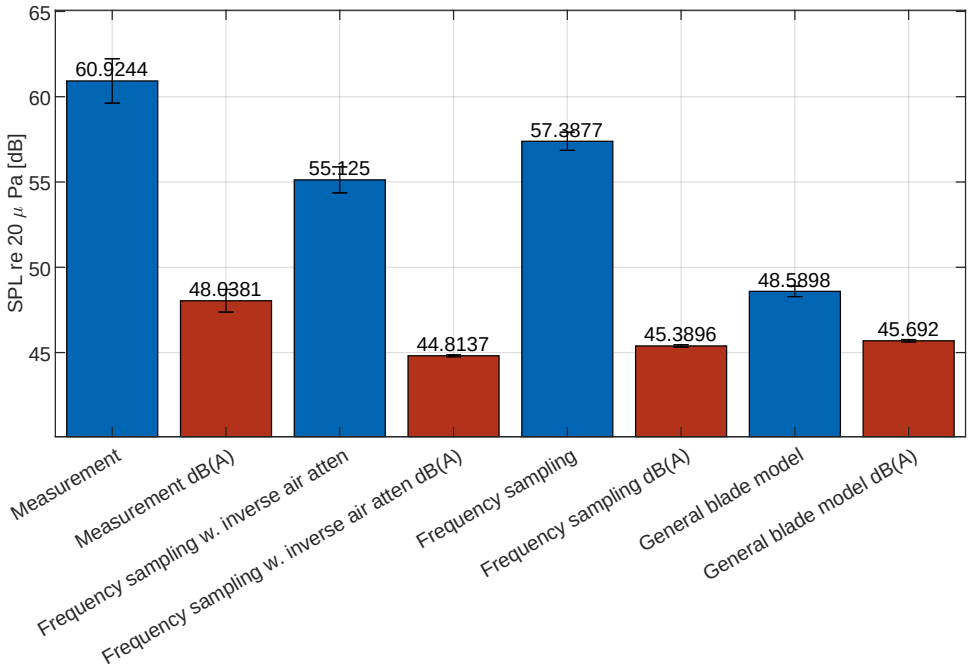

Figure 5.2: Sound pressure level for a measurement and simulations with different models at the position of the Long range measurement [200, 0, 0].

The results at 200 m show that the simulated spl deviates more from the recording than at 62 m. For the A-weighted levels, the calculated sound pressure level differs by up to approximately 3.5 dB. The non A-weighted levels deviate by a larger margin because the energy in the models is placed differently in the frequency spectrum.

With the results for the overall SPL presented, a 1/3-octave band analysis of the simulations compared with the measurement at the nearfield position with a dist is made to show how the models deviate. In fig 5.3 the frequency sampling method with inverse air attenuation is illustrated.

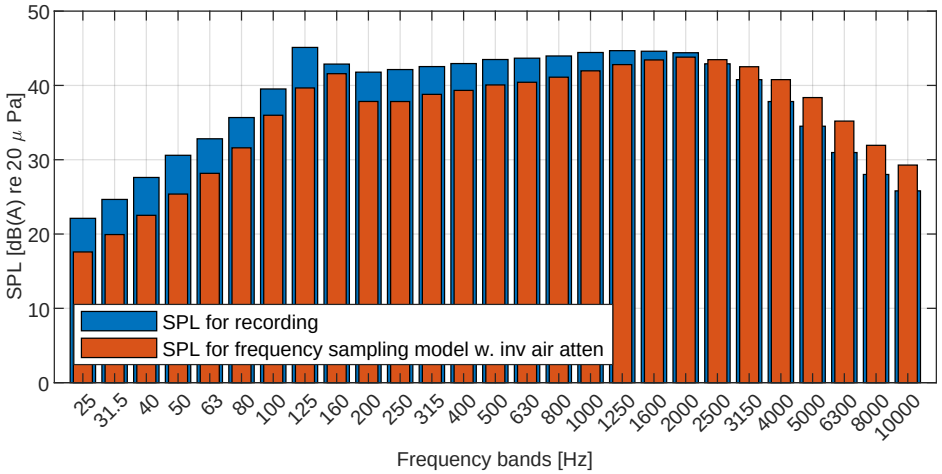

Figure 5.3: 1/3-octave band analysis of measurement and simulation at the near field measurement position

The A-weighted 1/3-octave analysis shows that the simulations contain more energy than the measurement in the frequency range above 2 kHz band and have less energy in the frequency below 2 kHz band. Furthermore, the tonal component of the wind turbine at the 125 Hz band, earlier shown in sec 4.1, is not represented in the simulation with higher energy than the adjacent bands. For the other model based on the frequency sampling method a 1/3-octave band analysis is shown in fig. 5.4.

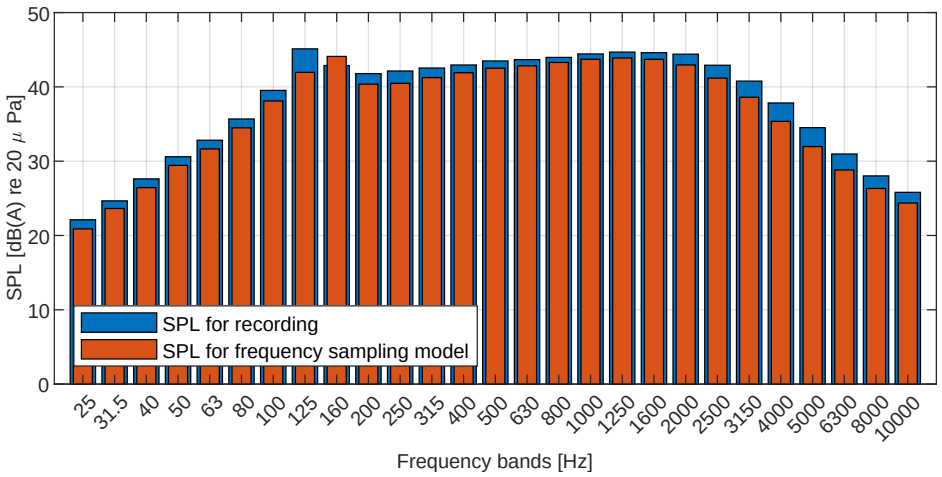

Figure 5.4: 1/3-octave band analysis of measurement and simulation at the near field measurement position

The shape of the simulation using this model fits the measurement better, compared to when inverse air attenuation is included in the model. The simulation is

consistently in the range of 1 dB to 4 dB below the measurement at every band except at the 160 Hz band. Here the simulations produce a slightly higher SPL. For the general blade model, which only simulates the trailing edge noise the result is plotted in fig 5.5.

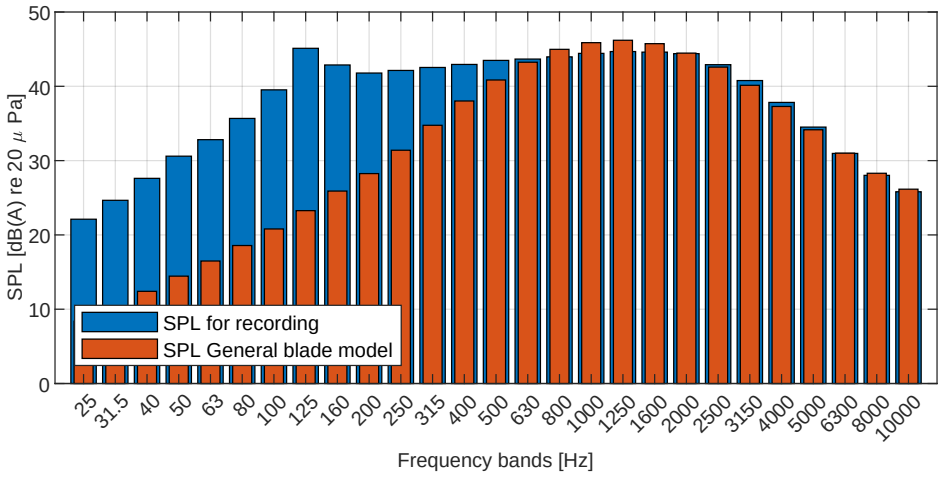

Figure 5.5: 1/3-octave band analysis of measurement and simulation at the near field measurement position

The general blade model deviates by large margins in the low frequency range below the 1 kHz band. In the frequency range above 1 kHz the results only have small deviations from the measurement.

These results provide information on how the simulator computes the energy in the different 1/3-octave bands with a given input. All of the plots are based on a 10 s period of the turbine/simulator. To give an insight into how the results change over time a spectrogram for the different models is also shown. The spectrogram for the measurement at the nearfield position is illustrated in fig. 5.6.

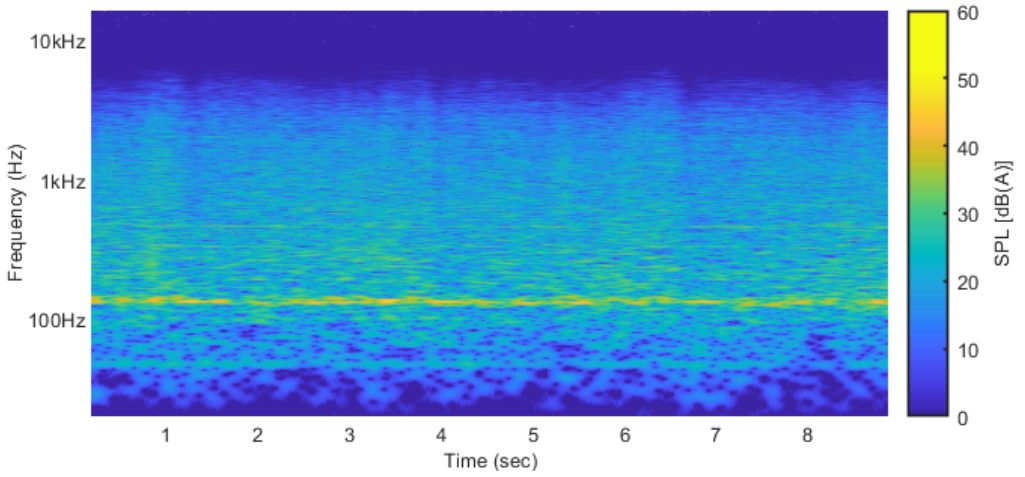

Figure 5.6: Spectrogram of measurement at the near field measurement position plotted in SPL dB(A).

The spectrogram shows the tonal components e.g. at 140 Hz from the recording and the tower interaction as dips in the energy, which is most clear in the high-frequency area e.g. at 1.5 s and 6.8 s. The spectrogram for the frequency sampling model with inv. air attenuation is shown in fig 5.7. The simulations show how the sampled tonal component from the measurement change frequency over time as the tonal component is included as a part of the moving sources thereby changing in both frequency and strength over time.

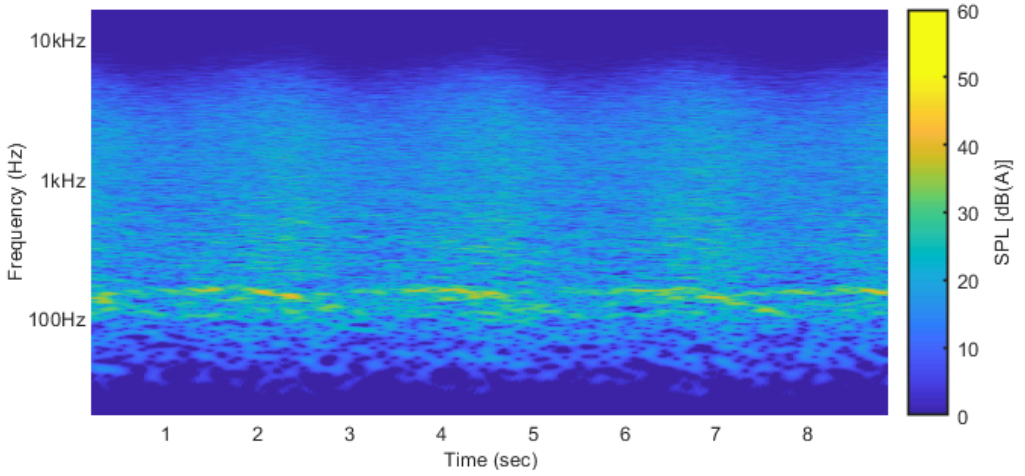

Figure 5.7: Spectrogram of simulation with the sound model with inv. air attenuation at the near field measurement position plotted in SPL dB(A).

Furthermore, the simulation shows a more periodic pattern in signal strength as

the three blades pass by, compared to the measurement where the overall level is more constant. The resulting spectrogram for the frequency sampled model is shown in fig. 5.8.

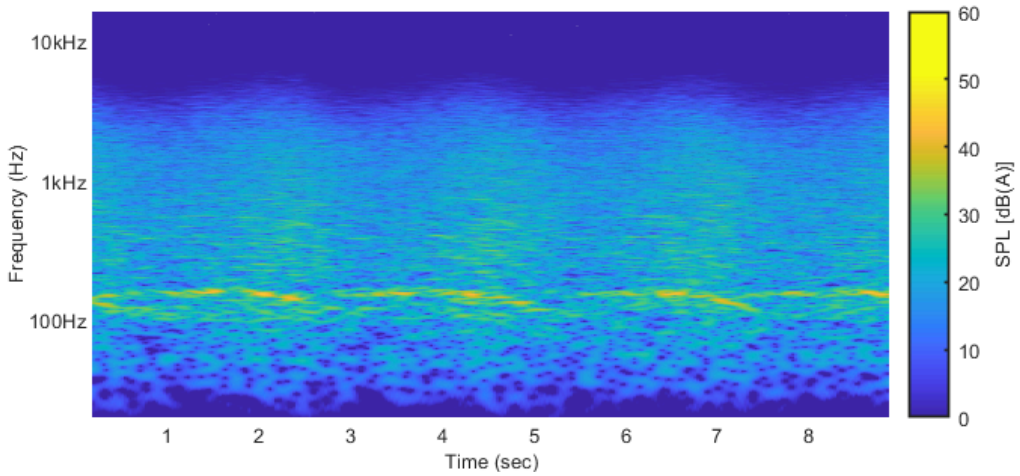

Figure 5.8: Spectrogram of simulation with the sound model based on frequency sampling at the near field measurement position plotted in SPL dB(A).

This result has many similarities with the spectrogram in fig 5.7 such as the varying tonal component and the periodic pattern. However, more energy is located in the low-frequency area and thereby making the tonal component stronger and the triangular shape of the energy move down in frequency.

The spectrogram for the general blade model is plotted in fig 5.9. In this model, the energy is centred around 1 kHz and the triangular pattern for the high-frequency content is now also present in the low-frequency area. No tonal components are present as this is not based on any recordings.

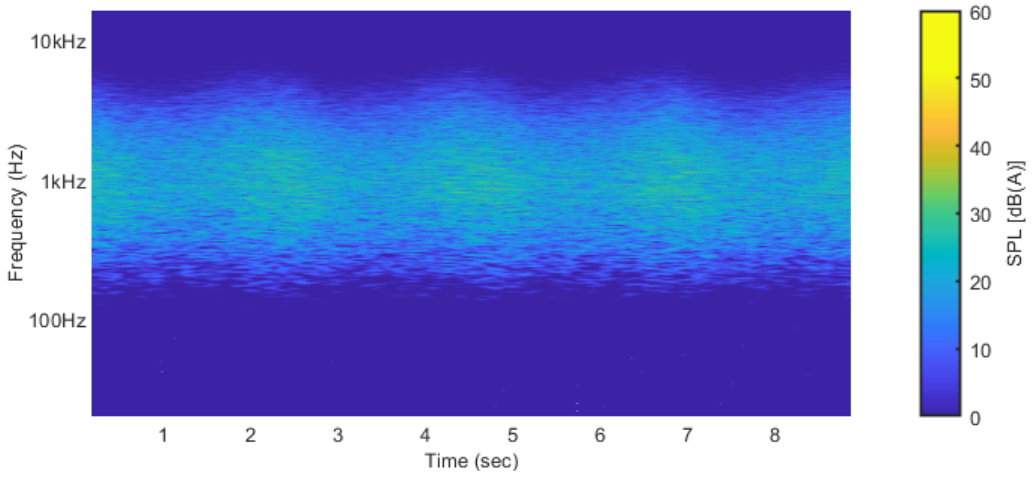

Figure 5.9: Spectrogram of simulation with the general blade model at the near field measurement position plotted in SPL dB(A).

All of these results are a part of verifying the propagation and sound models implemented in the simulator. However, the levels and spectrograms are only a part of the result. The actual sound produced by the simulator needs to be compared as well. For this, an informal listening test is conducted and the observations are presented.

5.1 Informal listening observations

This section seeks to describe to sound produced by the simulator compared to the recordings. This includes how the different parameters affect the sound and how the different sound models change the characteristics. The observations are made by the authors and are subjective opinions, devoid of statistical validity.

Sound models

The model based on frequency sampling has some of the characteristics, which the recording also has. However, the model generally sounds boomier (like there is more low frequency energy) than the corresponding recordings. This is irregardless of the position. Even though if the atmospheric attenuation is selected to be blade source, the sound becomes more realistic at short distances as added high frequency content compensates for the low frequency energy.

Listening to the model which is also based on the frequency sampling method but with inverse atmospheric attenuation included the sound experience becomes different. At longer distances the extra energy in the higher frequency area becomes too dominant compared to the recording. At the near field positions, this is slightly better and especially the comb-filter effects (with compacted field chosen) provide some similarities. The model sounds characteristically similar to the model without inverse atmospheric attenuation, but with generally more high-frequency content. When positioned close to the wind turbine ([44, -44, 0]) a characteristic high-frequency crackling follows close after the simulated blade is passing by.

The general blade model is far away from the actual measurements. The sound produced with this model is especially lacking energy in the low frequency areas, and sound very constant in its characteristic. It may be argued that it sound too perfect/ideal, i.e. there is a lack of imperfections that make it considerably less convincing. The narrow frequency area where the energy is located also makes the three blades sound more similar even though they are uncorrelated. This gives the overall sound a more predictable character clearly revealing that this is a simulation.

Atmospheric absorption

The atmospheric attenuation can cause big a big difference in the perceived sound. Without this parameter turned on the distance estimation becomes much more difficult. Close to the turbine, the blade source works well with the models that contain the lowest frequent energy, whereas combining it with another model can make the high frequencies too dominant.

Geometric attenuation

The geometric attenuation at long distances gives the same experience for the blade source or the hub source. Here the effects of the two converge towards each other. Standing close to the turbine the blade source makes the sound more realistic and gives the impression of the blades more clear than the hub source, where much of this effect disappears.

Reflection

At the heights from 0.1 m to 1.5 m, the effect of the reflection are very audible for hard surfaces, where a considerable sort-of tonal-shift can be heard in the simulation. This shift is very distinct from the frequency shift, which is assumed to be caused by the Doppler effect, when the blade is "moving past". Most of the complex reflection types sound quite similar. It can be difficult to distinguish between the more similar substrates (such as the difference between loose ground and compacted fields). The extremes such as water give a very different sound experience and the comb filter effects become more clear. But since there are no reference recordings for offshore turbines this is difficult to tell whether this is a good approximation.

Other observations

Regardless of the sound model or the combination of parameters, the simulator has a more periodic and predictable sound. Some elements such as birds in the background and the more unpredictable high-frequency content (maybe caused by turbulent airflow), stand out from the simulations. Whether this is the case for all turbines or a consequence of wear and tear on this particular wind turbine is not known at this time. For all models and when close to the turbine, the Doppler effect is highly audible, as the noise characteristics change, over time, from a more higher frequency characteristic to a lower one, when the source changes direction towards/away from the receiver.

Chapter 6

Discussion

The goal of the simulator has been to enable the auralization of a wind turbine and, while different turbines have different characteristic, a general assessment of the performance may be inferred by the comparison to the recorded wind turbine. Many different setups are available in the simulator and not all configurations have been documented or necessarily tested performance-wise. The addition of new effects contribute to additional modelling complexity and, while an increasingly complex model gives more possibilities of striking a configuration that performs well when compared against the actual wind turbine recording, the same configuration may not yield the same for another wind turbine.

The goal of including a general blade model has been to generalize the noise characteristic of a wind turbine, and while this consequently should represent the noise characteristics of a somewhat "standard wind turbine", the truth of the matter is that one would be hard pressed to standardize the design of wind turbines. Thus: it is not surprising to see the results favor the noise models based on the characteristic of the actual wind turbine. The design of present day wind turbines are company secrets, and the results of ongoing development. Therefore it may be necessary to perform new recordings of any new wind turbine, if a simulator of sufficient quality is necessary for investigation. This brings to attention the investigative aspect of the project: The desired quantification of "sufficient quality" is challenging. While one can look at the 1/3-octave bands of fig. 5.4, and conclude that this is quite close to the recorded, it does not necessarily reflect the audible similarity, i.e. how much one sounds like the other.

In the informal listening observations, it is noted how the recordings are distinct because of their imperfections. The cause of these seemingly random imperfections are hard to isolate and therefore also hard to model. For the simulation, the fluctuation of the signal over time is almost entirely congruent with the rotational frequency of the turbine (times 3); while the recording, at least audibly, seems to have fluctuations in-congruent with the rotational frequency. It could be argued that these

imperfections may be modelled by randomly introduced events or modulation, but without knowing how often or specifically why these appear it could quickly become based in presumption, and not necessarily an effect that is applicable for another wind turbine in other conditions. One hypothesis by the authors is that wind speeds fluctuations and vortices may be the cause, although to test this, it is necessary to include fluid dynamic modelling, which could defeat the purpose of a simulator where one can, computationally relatively fast (on a personal computer), adjust the position of the receiver and get an output for that position.

In the estimation of the ground effect, the presumption is that the reflected surface is a perfectly flat homogenous surface, however the surface of the recorded wind turbine had both: gravel, grassy area, ploughed fields and muddy ground near where these recordings were made, which complicates the classification of ground. The ground effect is furthermore based on a plane-wave assumption that, as stated in 4.5, may not be accurate when moving far away from the wind turbine. Spherical wave models would theoretically remedy this, but it is not known how much this would amount to in the simulator.

Furthermore investigating the effect of variable environmental parameters such as temperature, humidity and wind would be a step towards improving the simulator. How this would impact the sound of the simulator as well as the increase in computation is currently unknown but would be a natural step for further work.

Chapter 7

Conclusion

Through an analysis of different categories of wind turbine noise, it has been found that the most dominant noise source of large modern wind turbines is the trailing edge noise. This is a broadband noise and depends on the rotor size, rotor speed, blade angle etc. Furthermore, tonal noise, often generated by the generator, gearbox or other mechanical sources, is not considered an issue in modern wind turbines but can be present at shorter distances. The surrounding environment also has an impact on how the noise propagates. Parameters such as temperature, humidity, landscape, ground reflections, wind and obstacles can all affect the characteristics of the sound.

These parameters are simulated in different ways to make an auralisation of a wind turbine. A sound model of trailing edge noise based on a semi-empirical method is generated along with sound models based on recordings from an actual wind turbine. The recordings also act as a reference for the simulator at the recorded positions. With three different noise sources each located at tip of a blades the distance to a listener change over time which affects the sound and propagation. For this reason propagation parameters are implemented as filters and audio effects, with inspiration from standards like Nord 2000, Harmonise, ISO 9316 etc, to recreate an experience of the sound from a wind turbine. These parameters are geometrical attenuation, atmospheric attenuation, ground effect and a chorus simulating mooving sources.

The result is a simulation program in Matlab which enables a listener to choose a 3-dimensional position, different sound models and turn on/off or adjust environmental parameters to see/hear the effect of this. The sound is played back through a headset connected to the pc, and the visual effect of the parameters can bee seen on the spectrogrammes and frequency responses made by the simulator. From the author's perspective, a simulator producing an immitation of a spinning wind turbine has been produced. However, further work such as including varying turbulent wind conditions, temperature gradients and advanced fluid dynamics models would contribute to an even more plausible experience.

Acronyms

ADM acoustic distance model 53, 55–57, 60, 62

BEM boundary element method 29, 30, 32

FDTD finite-difference time-domain 29, 30, 32

FFT fast fourier transform 46

iFFT inverse fast Fourier transform 41, 42, 46, 65

IIR Infinite impulse response 69

IR impulse response 41, 42, 46, 64–66

ISM image-source Modelling 19, 20

LFO low frequency oscillator 52, 53

MaxSD maximum source distance 56

MinSD minimum source distance 56

SPL sound pressure level 11, 12, 14, 15, 44, 62, 85, 86, 92, 93, 95, 111, 113

Bibliography

[1] Wind Europe. "Wind Energy Today." Date of Access: 13-02/2023. (), [Online]. Available: https://windeurope.org/about-wind/wind-energy-today/.

[2] M. Ministeriet, *Vindmøllebekendtgørelsen - BEK nr 135 af 07/02/2019*, 2019. [Online]. Available: https://www.retsinformation.dk/eli/lta/2019/135.

[3] WindDenmark. "Der er klare regler for vindmølleplanlægning." Date of Access: 13-02/2023. (), [Online]. Available: https://winddenmark.dk/nyheder/nyhed/er-klare-regler-vindmolleplanlaegning.

[4] C. Chiu, S. C. Lung, and N. Chen, "Effects on low-frequency noise from wind turbines on heart rate variability in healty individuals," pp. 1–12, 2021.

[5] D. bowdler & Geoff leventhal, *Wind Turbine Noise*. Multi-Science Publishing Co. Ltd, 2011.

[6] K. A. T. V. Renterghem, *Predicting Outdoor Sound*, Second Edition. CRC Press, 2021.

[7] Danish Wind Industry Association. "Wind Turbines: Upwind or Downwind Machines?" Date of Access: 24-02/2023. (), [Online]. Available: http://xn--drmstrre-64ad.dk/wp-content/wind/miller/windpower\%20web/en/tour/design/updown.htm.

[8] T. Brooks, D. Pope, and M. Marcolini, "Airfoil self-noise and prediction," Aug. 1989.

[9] K. Kinzie, R. Drobietz, and B. Petitjean, "Concepts for wind turbine sound mitigation," May 2013.

[10] S. Oerlemans, P. Sijtsma, and B. M. López, "Location and quantification of noise sources on a wind turbine," *Journal of Sound and Vibration 299*, pp. 869–883, 2007.

[11] R. Makarewicz and R. Gołębiewski, "Amplitude modulation of wind turbine noise," *SF Journal of Aviation and Aeronautical Science*, 2018.

[12] S. Wagner, R. Bareiß, and G. Guidati, *Wind Turbine Noise*. Springer, 1996.

[13] Viden Om Vind. "Konkrete ulemper for vindmøllenaboen." Date of Access: 01-03/2023. (), [Online]. Available: https://videnomvind.dk/fordele-og-ulemper/konkrete-ulemper-for-vindmoellenaboen/.

[14] L. E. Kinsler, A. R. Frey, A. B. Coppens, and J. V. Sanders, *Fundamentals of Acoustics*, Fourth Edition. John Wiley & Sons, Inc., 2000.

[15] Danish Standards, *DS/EN ISO 9613-1*, 1993.

[16] American National Standards Institute, *ANSI/ASA S1.26-1995 (R2009) - Calculation Of The Absorption Of Sound By The Atmosphere*, 2009.

[17] B. Xie, *Head-Related Transfer Function and Virtual Auditory Display*, Second Edition. J. Ross, 2013.

[18] C. Hansen, C. Doolan, and K. Hansen, *Win dFarm Noise: Measurement, Assesment and Control*, First Edition. John Wiley & sons Ltd, 2017, ISBN: 978-1-118-82611-9.

[19] K. Attenborough, "Acoustical impedance models for outdoor ground surfaces," *Journal of Sound and Vibration (1985) W(4)*, pp. 521–544, 1984.

[20] C. M. Nyborg and W. Z. Shen, "New measurement technique for ground acoustic impedance in wind farm," 2020.

[21] J. Wu, J. Wang, Z. Sun, W. J. Zhu, and W. Z. Shen, "Determination of the parameters of ground acoustic-impedance in wind farms," 2020.

[22] E. Barlas, W. J. Zhu, W. Z. Shen, K. O. Dag, and P. Moriarty, "Consistent modelling of wind turbine noise propagation from source to receiver," 3297–3310, 2017.

[23] DELTA. "Proposal for Nordtest Method: Nord2000 - Prediction of Outdoor Sound Propagation." Date of Access: 15-02/2023. (), [Online]. Available: `https://forcetechnology.com/da/innovation/afsluttede-projekter/nord2000-stoejberegningsmetode-auralisering`.

[24] J. Reiss and A. McPherson, *Audio Effects Theory, Implementation and Application*. CRC Press, 2013.

[25] Bill Schweber, *The Doppler Effect: Now Widely Accepted and Easy to Use, Despite Its Initial Rejection*, 2021. [Online]. Available: `https://www.digikey.dk/da/blog/the-doppler-effect-now-widely-accepted-and-easy-to-use`.

[26] Danish Standards, *DS/EN ISO 9613-2*, 1997.

[27] J. R. Kuttler, "Differences Between the Narrow-Angle and Wide-Angle Propagators in the Split-Step Fourier Solution of the Parabolic Wave Equation," *IEEE TRANSACTIONS ON ANTENNAS AND PROPAGATION, VOL. 47, NO. 7, JULY*, pp. 1131–1140, 1999.

[28] E. M. Salomons, *Computational Atmospheric Acoustics*, First Edition. Kluwer Academic Publishers, 2001.

[29] S. Kirkup, "The Boundary Element Method in Acoustics: A Survey," 1–50, 2019.

[30] S. Preuss, C. Gurbuz, C. Jelich, S. K. Baydoun, and S. Marburg, "Recent Advances in Acoustic Boundary Element Methods," *Journal of Theoretical and Computational Acoustics Vol. 30, No. 3 2240002*, 1–40, 2022.

[31] P. Thorsson, K. Persson, M. Ögren, M. Smith, E. Pedersen, and J. forssén, "Creating sound immision mimicking real-life characteristics from a single wind turbine," *Elsevier Applied Acoustics 143*, 2018.

[32] L. Hannah, "Wind and temperature effects on sound propagation," 2006.

[33] A. A. Ammar, M. K. Julboub, and A. A. Elmghairbi, "Digital filter design (fir) using frequency sampling method," *University Bulletin, No. 15, Vol 3*, 2013.

[34] S. M. Kuo, B. H. Lee, and W. Tian, *Real-Time Digital Signal Processing: Fundamentals, Implementations and Applications*, Third. John Wiley & Sons, 2013, ISBN: 978-1-118-41432-3.

[35] V. Nukala and S. Maddula, "Influence on rotor solidity on trailing edge noise from wind turbine blades," 2018.

[36] Tomasz Woźniak, *Air absorption of sound as a digital filter – Part 1: Theory*, 2014. [Online]. Available: `https://codeandsound.wordpress.com/2014/08/21/absorption-of-sound-by-air-and-its-implementation-as-a-filter-part-1-theory/`.

[37] U. Zölzer, *DAFX: Digital Audio Effects*, Second Edition. John Wiley & sons Ltd, 2011.

[38] D. A. Bies and C. H. Hansen, *Engineering Noise Control - Theory and practice*, Fourth. Spon Press, 2009, ISBN: 0-203-87240-1.

[39] International Organization for Standardization, *DS/ISO 226 - Acoustics Normal equal-loudness-level contours*, 2003.

Appendix A

Appendix

A.1 Weighting curves for regulation and sound models

In order to explain the foundation on which many noise directives are based (explained in sec. 2.2), it is important to understand the human perception of SPL and why not all tonal contributions are weighted equally. A popular way to analyse sounds is the separation of a signal into its tonal or frequency components by means of the Fourier transformation.

The amplitude of the sinusoidal frequency component, measured in Pascal, denotes the difference in pressure exerted in the medium. While a doubling of amplitude may mean twice as high a sound pressure, it does not usually equate to a doubling of the perceived loudness. The current models of loudness are based on empirical evidence and the physiological understanding of the cochlea [14]. One such model, is the equal-loudness-level contours, that seeks to describe the relative perceived loudness of one frequency relative to another.

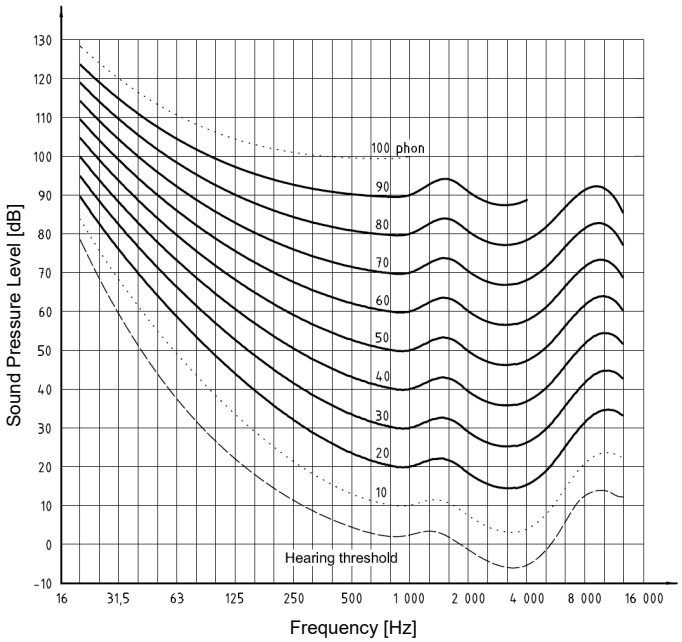

Figure A.1.1: Equal-loudness-level contours for pure tones under free-field listening conditions, according to the ISO 226 standard [39]. Dotted line indicating lack of experimental data and dashed line indicating the hearing threshold,

As is seen in fig. A.1.1, the curves of equal perceived loudness-level (measured in 'phon') can be seen; illustrating the relative differences needed for different pure-tones to be perceived as the same loudness. Phon is a logarithmic unit of the subjective measure of loudness (The linear counterpart being 'sone'). Many of the noise directives today, such as vindmøllebekendtgørelsen and IEC-61400-11 for wind turbines, make use of the so called A-weighting to determine the auditory impact [14]. This weighting curve is based on the shape of the equal loudness level contours at 40 phon, purposedly estimating the inverse. The A-weighting curve can be seen on fig. A.1.2.

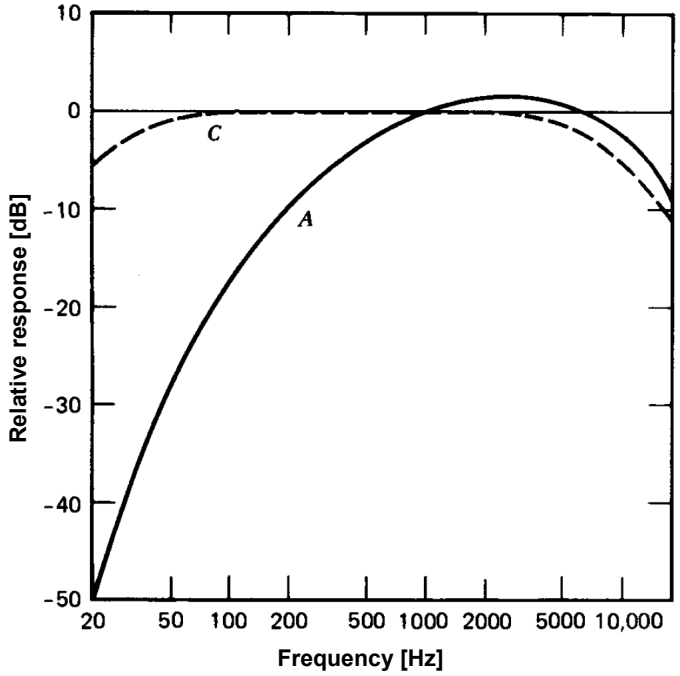

Figure A.1.2: Illustration of the A-weighting and C-weighting curve [14].

Figure A.1.2 shows the relative weighting curves for respectively A- and C-weighting, where intended application are the perceptually based de-emphasis of frequency components that otherwise would be overemphasised.

While A-weighting is generally applicable for most scenarios, where the levels are relatively normal, as it is based on the 40 phon curve on fig A.1.1; C-weighting may be considered more accurate for louder scenarios, as it is based on the 90 phon curve [14].

The flaws of A-weighting, reveal themselves as the levels rise. This is especially visible in fig. A.1.1 for near infra-sound frequencies: For high SPL, e.g. 100 dB at 20 Hz, a 20 dB increase in SPL equates to a much larger rise in phon, than the same 20 SPLincrease at 1 kHz 60 to 80 phon.

A.2 Normalized complex density & compressibility of ground

The normalized complex density & compressibility of ground is calculated in accordance with [18] (for a select frequency f and flow resistivity R_1), by use of the following equations.

Normalized Complex Density

The normalized complex density of ground (ρ_m) is calculated as:

$$\rho_m(f) = (1 + \sigma(f))^{-1} \tag{A.1}$$

The parameter σ is calculated as:

$$\sigma(f) = a(X(f)) + jb(X(f)) \tag{A.2}$$

$$\tag{A.3}$$

Functions 'a' and 'b' are presented further down. The parameter $X(f)$ is calculated as:

$$X(f) = \rho f / R_1 \tag{A.4}$$

$$\tag{A.5}$$

Where:

f	is the frequency of interest	$[s^{-1}]$
ρ	is the density of air (=1.21 @20 °C)	$[\mathrm{kg/m^3}]$
R_1	is the flow resistivity of the ground	$[kPa \cdot s/m^2]$

The functions 'a' and 'b' are defined as:

$$a(X) = \frac{T_3(T_1 - T_3)T_2^2 - T_4^2 T_1^2}{T_3^2 T_2^2 + T_4^2 T_1^2} \tag{A.6}$$

$$b(X) = \frac{T_1^2 T_2 T_4}{T_3^2 T_2^2 + T_4^2 T_1^2} \tag{A.7}$$

$$\tag{A.8}$$

where:

$$T_1 = 1 + 9.66X \tag{A.9}$$

$$T_2 = X(1 + 0.0966X) \tag{A.10}$$

$$T_3 = 2.537 + 9.66X \tag{A.11}$$

$$T_4 = 0.159(1 + 0.7024X) \tag{A.12}$$

$$\tag{A.13}$$

Normalized Complex Compressibility

The normalized complex compressibility of ground (κ) is calculated as:

$$\kappa(f) = (1 + (1 - \gamma) \cdot \tau(f))^{-1} \tag{A.14}$$

Where:

f	is the frequency of interest	$[s^{-1}]$
γ	is the ratio of specific heats (=1.402 @20 °C)	[-]
R_1	is the flow resistivity of the ground	$[kPa \cdot s/m^2]$

The parameter τ is calculated as:

$$\tau(f) = 0.592 \cdot a(X_1(f)) + jb(X_1(f)) \tag{A.15}$$

The parameter X_1 is calculated as:

$$X_1(f) = 0.856 \cdot X(f) \tag{A.16}$$

(A.17)

A.3 Ground Reflection Coefficient

This section presents the calculated reflection coefficients for ground at 30, 45 and 60 degrees angle of incidence, using the formula for plane-wave, i.e. eq. 4.28 found on page 73. This Reflection coefficient is calculated for 6 ground types, based on their corresponding flow resistivities:

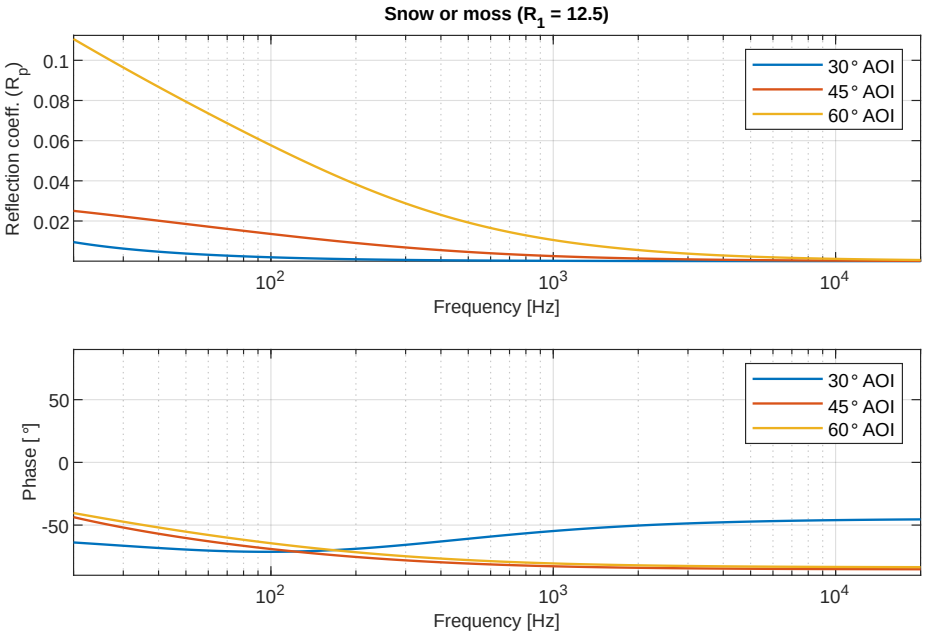

Figure A.3.1: Reflection coefficient for snow or moss, from 20 Hz to 20 kHz.

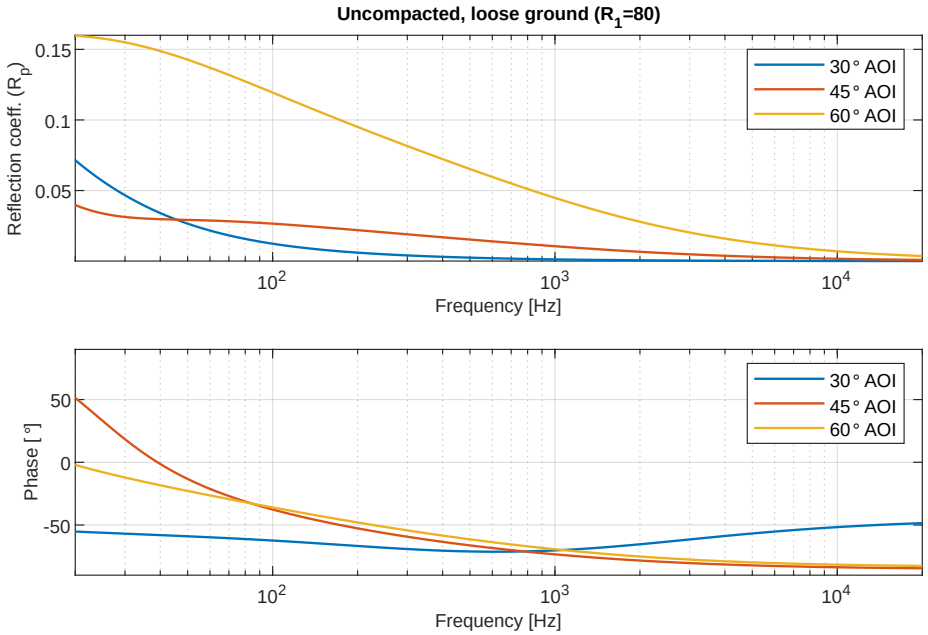

Figure A.3.2: Reflection coefficient for uncompacted or loose ground, from 20 Hz to 20 kHz.

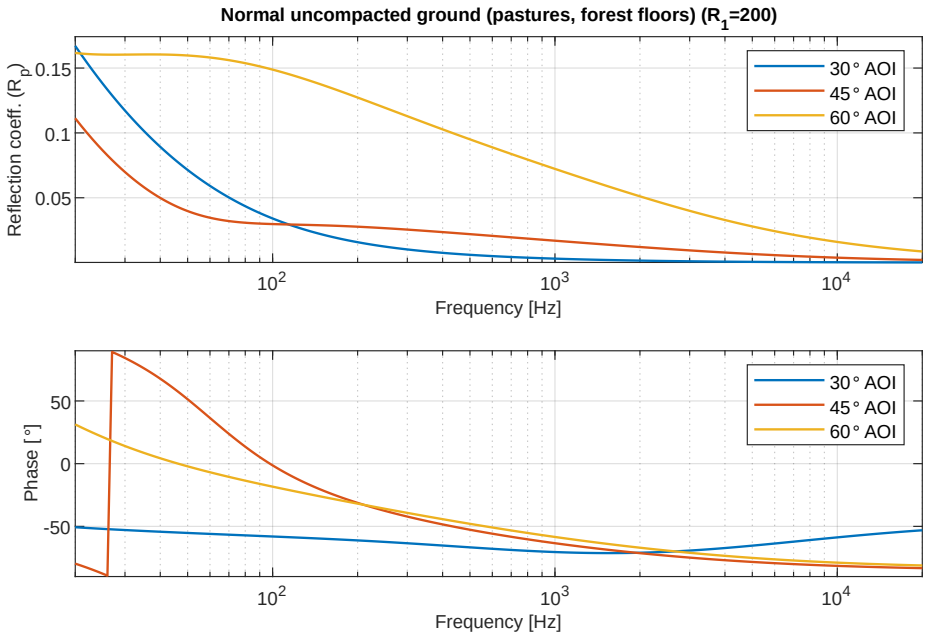

Figure A.3.3: Reflection coefficient for pastures or forest floors, from 20 Hz to 20 kHz.

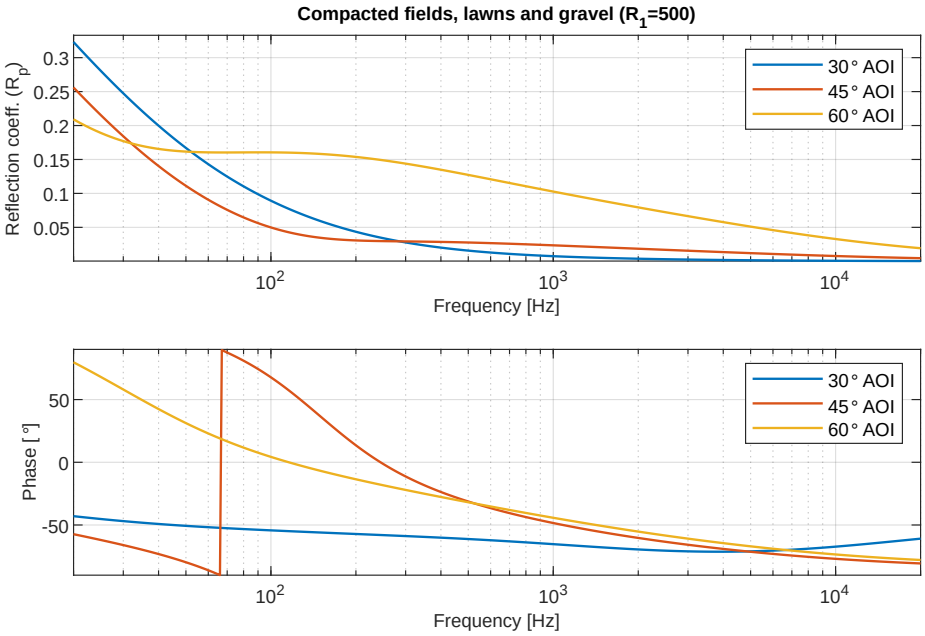

Figure A.3.4: Reflection coefficient for compacted fields, lawns or gravel, from 20 Hz to 20 kHz.

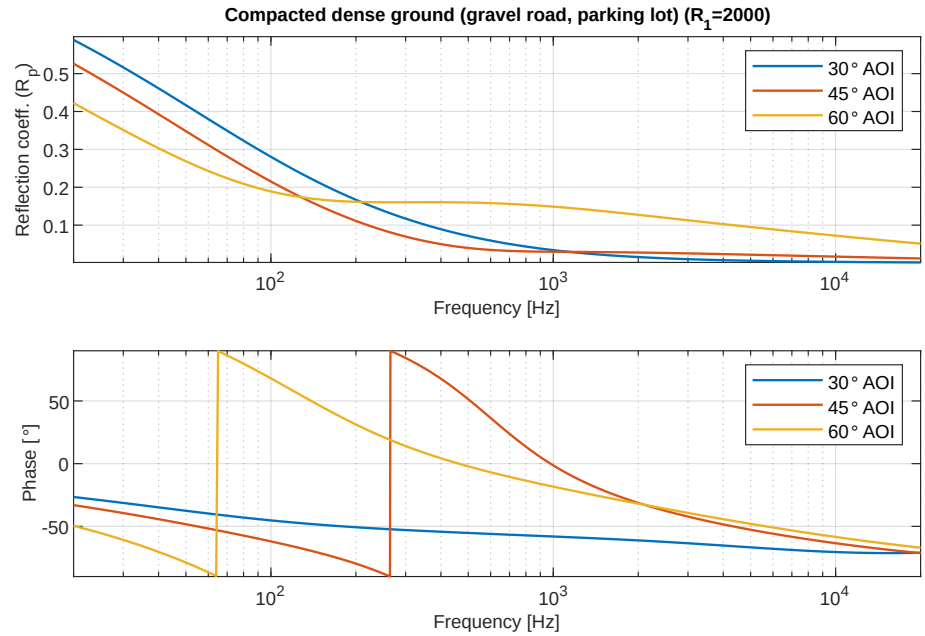

Figure A.3.5: Reflection coefficient for gravel road or parking lot, from 20 Hz to 20 kHz.

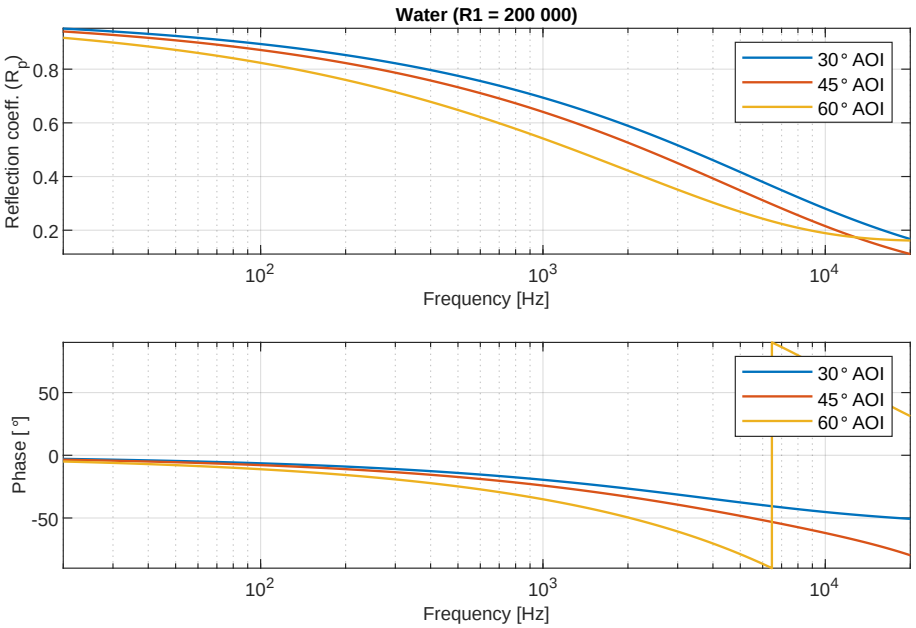

Figure A.3.6: Reflection coefficient for water, from 20 Hz to 20 kHz.

A.4 Measurements of Wind Turbine Noise

This measurement journal covers the acoustic measurement of wind turbine noise at multiple locations wrt. the wind turbine. The measurements were conducted in cooperation with Jesper Lumbye Andersen from Siemens Gamesa.

In accordance with Siemens, the location and identity of the wind turbine is redacted in this report. Furthermore, the results (the recorded data) are not released with the report.

Date	07/04/2023
Location	Denmark
Address	REDACTED
Participants	Jesper Lumbye Andersen & Jacob A. Rasmussen

Table A.4.1: Measurement journal details.

Purpose

The purpose is to measure the noise of a wind turbine at different distances and angles wrt. the wind turbine.

List of Equipment

The relevant equipment used for the measurement are listed in the following table:

Model	Brand	Function
Type 3050-A-060	B&K	Input Module
Type 4189	B&K	Free-field Microphone
Type 2669	B&K	Pre-amp
Type 4231	B&K	Sound Calibrator
IEC 61400 compliant acoustic plate	-	Microphone surface
200m Cables	-	Connection
Laser Coolshot Pro II	Nikon	Range finder
Steam Deck	Valve	Computer

Table A.4.2: List of hardware.

Setup

Measurements of three setups are conducted, with two of these presented in figure A.4.1:

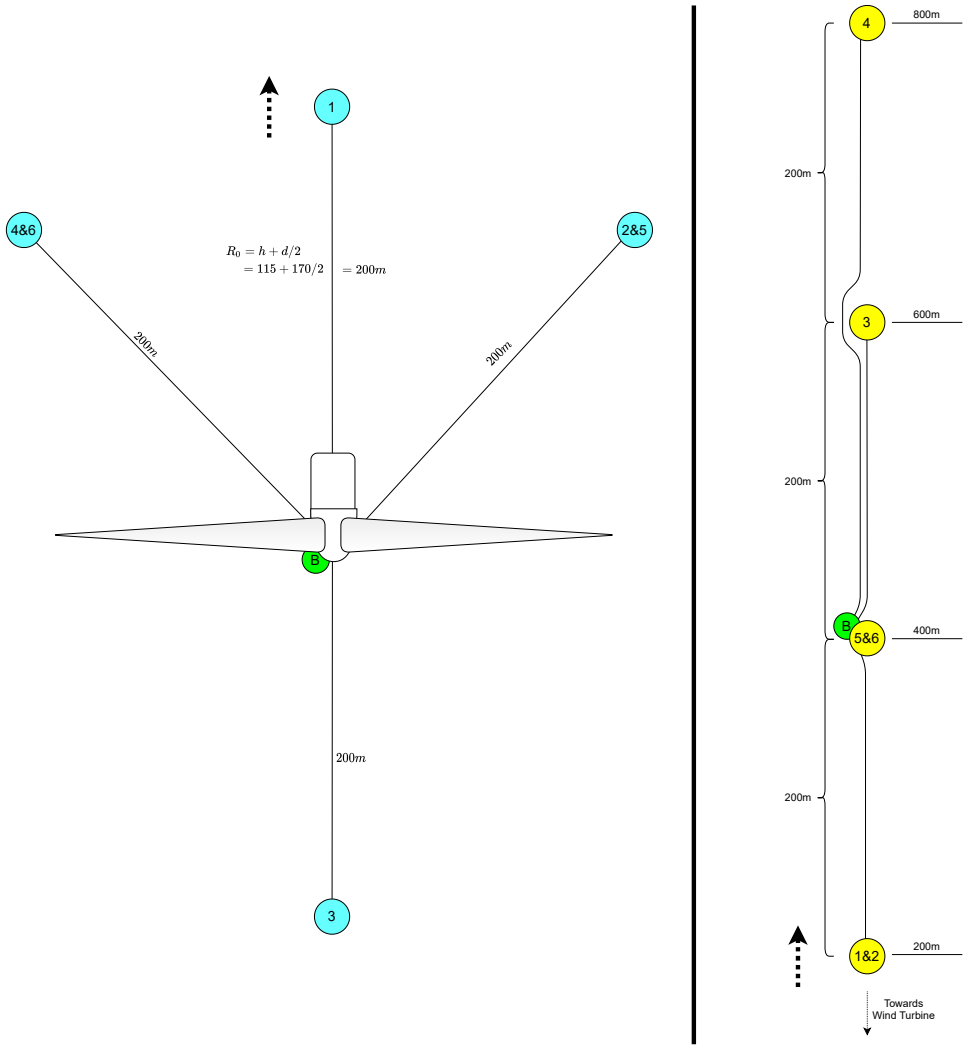

Figure A.4.1: Two different measurement microphone setup.

Figure A.4.1 show the two first noise measurement setups, where the long-range setup is illustrated on the right, with 6 microphones indicated by yellow position markers at distance 200, 400, 600, and 800 meter behind the wind turbine. The basestation (Input Module), where all microphones are connected, is placed at the 400m range, approximately 10m from mic 5 & 6. Microphone 2 & 6 are placed in a height of 1.5 m, with the rest being at 0 m. The basestation setup at 400 m is visible in figure A.4.2 and A.4.3.

Figure A.4.2: Microphone setup at 400 m.

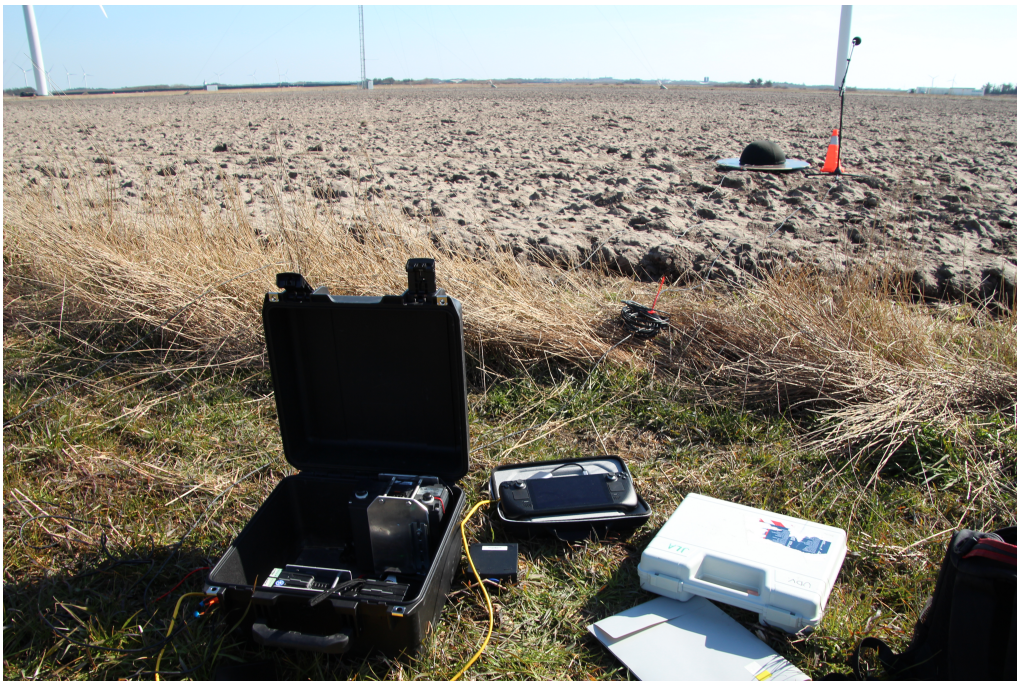

Figure A.4.3: Basestation near the 400 m mark.

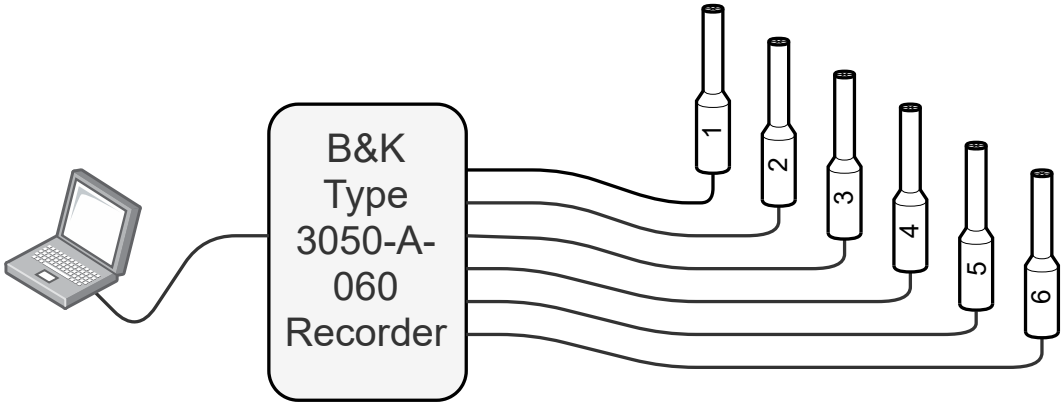

Figure A.4.4: Illustration of the connection setup near the base-station. In actuality, the microphones being considerably further away than visualised on the figure.

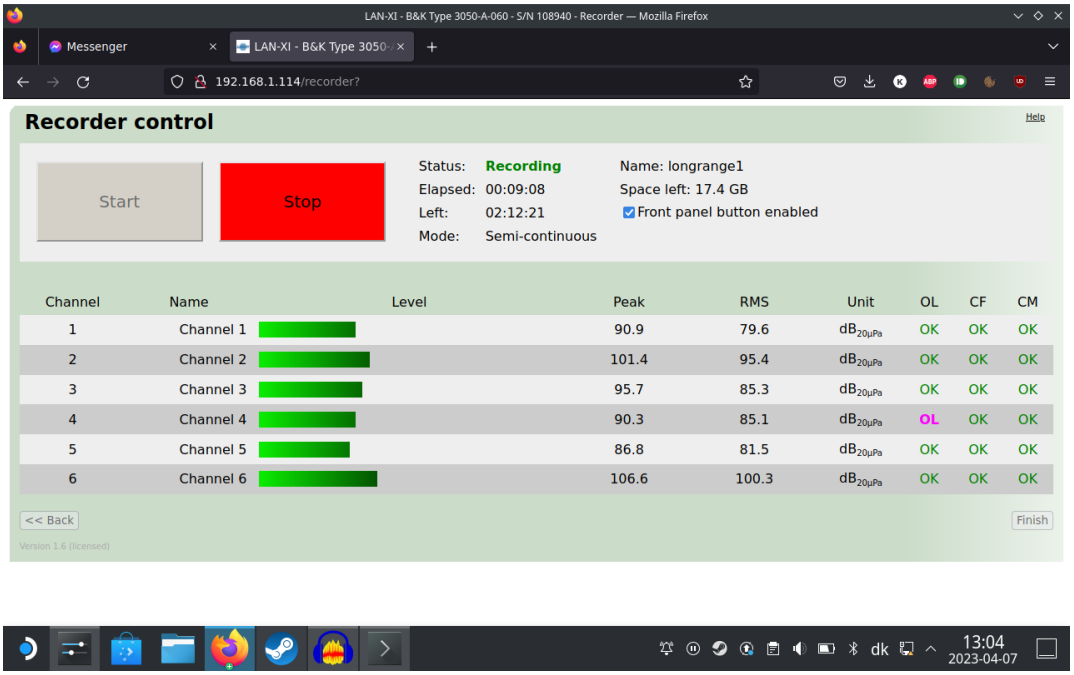

Figure A.4.5: Screenshot of the web interface accessed from the computer (Steam Deck) via browser.

The secondary microphone setup is illustrated on the left side of fig. A.4.1, with 6 microphones 200 m from the wind turbine. These are connected to the base station located underneath the wind turbine. Microphone 1 & 3 are placed respectively directly behind and in front of the wind turbine. Microphone 4 & 6, and 2 & 5 are placed at approximately 45 degrees askew of the median plane behind the turbine, as is also visible from fig. A.4.1. The median plane is, in this regard, defined as a vertical plane, extending forward and backward with respect to the nacelle direction of the wind turbine.

In this setup, microphone 5 & 6 are placed in a height of 1.5 m, and the rest at 0 m. One of these positions (Position 3) is shown in figure A.4.6:

Figure A.4.6: Microphone 200 m in front of the wind turbine (Cyan mic position '3', on fig. A.4.1).

The third measurement setup takes place close to the wind turbine. The placement is illustrated on fig. A.4.7:

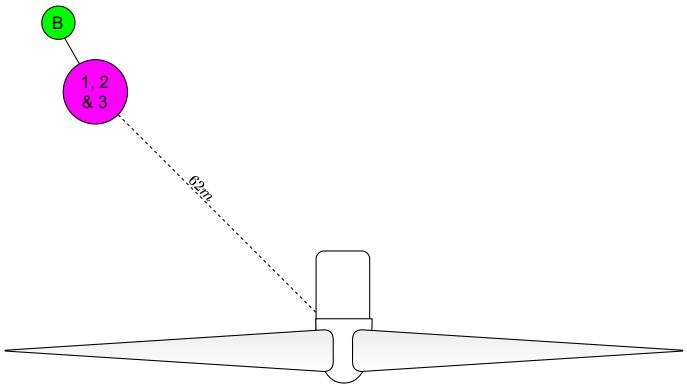

Figure A.4.7: Illustration of the third microphone setup

In the setup illustrated in fig. A.4.7, three microphones are setup at 62 m from the base of the wind turbine, at an angle of approximately 45° degrees from the median plane. The setup is shown in figure A.4.7:

Figure A.4.8: Third microphone setup, with 3 microphones (without secondary windshield).

Figure A.4.8 shows the 3-microphone setup used in the third setup. Mic 1 on the ground (shown without the secondary hemispherical windshield), mic 2 at a height of 1.1 m and mic 3 at a height of 1.5 m.

Method/Procedure

The following 3 procedures are followed:

Long range measurements:

1. The microphone positions are established according to the right-side illustrations of fig. A.4.1 (page 121), where the appropriate ranges are estimated by rangefinder. As the wind turbine may, over time, change direction in accordance with changing wind vectors, the first position (at 200 m) dictate the reference line upon which consecutive microphone positions are placed.

2. Microphone/preamp 1, 5, 3 and 4 are placed respectively at the 200, 400, 600 and 800 m marks. The microphones are placed in the middle of, and duct-taped to, the acoustic plates; then fitted with the two hemispherical wind screens.

3. Microphone/preamp 6 and 2 are placed at the 200 and 400 m marks respectively, in a height of 1.5 m from the ground, facing towards the wind turbine. The microphone is then fitted with a spherical windscreen.

4. The B&K Type 3050-A-060 input module is connected to the microphones by cable to, aswell as an external computer, as is illustrated in fig. A.4.4.

5. The measurements are commenced by the LAN-XI web interface from the external computer (via. browser), as is shown in fig. A.4.5.

6. The calibrator is coupled to each microphones for a minimum of 10 seconds.

7. The measurements are recorded for a minimum of 10 minutes while the wind turbine is operating in normal operational state.

8. The mode of the wind turbine is cycled to an 'off' state and measurements are recorded for a minimum of 10 minutes.

9. The mode of the wind turbine is cycled to a 'low noise' state and measurements are recorded for a minimum of 10 minutes.

Short range measurements:

1. The microphone positions are established according to the left-side illustrations of fig. A.4.1 (page 121), where ranges are estimated by rangefinder, and angle with respect to the facing direction of the turbine is estimated by eyesight, and geo-positionally recorded with a phone.

2. The Microphone/preamp are placed respectively at the positions recorded in step '1', with microphones 1, 2, 3, and 4, being placed in the middle of, and duct-taped to, the acoustic plates and then fitted with the two hemispherical wind screens.

3. Microphone/preamp 5 and 6 are placed in a height of 1.5 m from the ground, facing towards the wind turbine. The microphone is then fitted with a spherical windscreen.

4. The B&K Type 3050-A-060 input module is connected to the microphones by cable, aswell as to an external computer, as is illustrated in fig. A.4.4.

5. The measurements are commenced by the LAN-XI web interface from the external computer (via. browser), as is shown in fig. A.4.5.

6. The calibrator is coupled to each microphones for a minimum of 10 seconds.

7. The measurements are recorded for a minimum of 10 minutes while the wind turbine is operating in 'low noise' operational state.

8. The mode of the wind turbine is cycled to an 'off' state and measurements are recorded for a minimum of 10 minutes.

9. The mode of the wind turbine is cycled to a 'Normal' state and measurements are recorded for a minimum of 10 minutes.

Near-field measurements:

1. The microphone positions are established according to fig. A.4.7 (page 125), where ranges are estimated by rangefinder and the position is and geo-positionally recorded with a phone.

2. The Microphone/preamp 1, 2 and 3 are placed in the same location, however at differing heights, as is also shown in fig. A.4.8. Microphone 1 at ground level, 2 at 1.1 m from the ground, and 3 at 1.5 m from the ground.

3. Microphone 2 and 3 are fitted with spherical windscreens and faced towards the wind turbine. Microphone 1 is fitted with inner and outer hemispherical windscreens.

4. The B&K Type 3050-A-060 input module is connected to the microphones by cable, as well as to an external computer, as is illustrated in fig. A.4.4, however with only microphone 1,2 and 3 connected.

5. The measurements are commenced by the LAN-XI web interface from the external computer (via. browser), as is shown in fig. A.4.5.

6. The calibrator is coupled to each microphones for a minimum of 10 seconds.

7. The measurements are recorded for a minimum of 10 minutes while the wind turbine is operating in normal operational state.

Results

As per agreement with Siemens Gamesa, the recorded measurements results are not made public in neither the measurement journal nor the report. The results, however, are presented in 1/3rd octave format and spectrograms, for the sake of comparison. An extensive amount of results have been recorded, and for the sake of brevity a limited set will be presented here.

Long range results:

Results for 2 positions in the long range setup are presented in 1/3-octave bands.

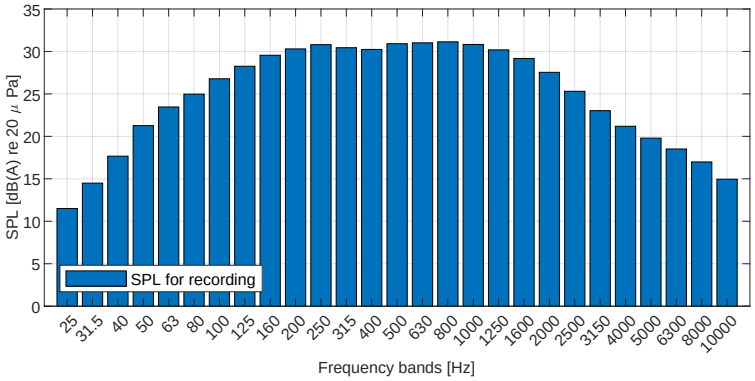

Figure A.4.9: 1/3-octve band for long range position 3.

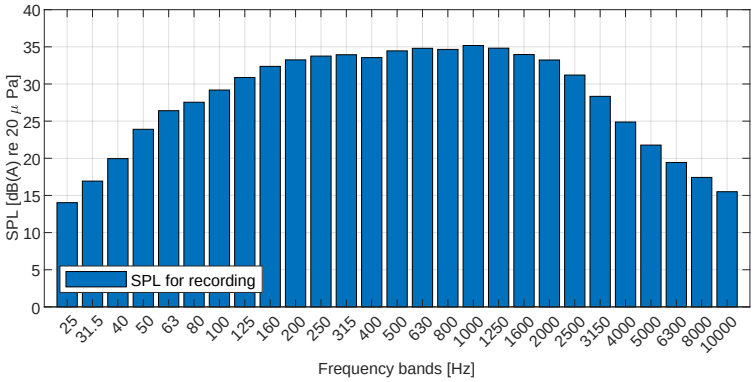

Figure A.4.10: 1/3-octve band for long range position 5.

Spectrograms for all long range positions are found below.

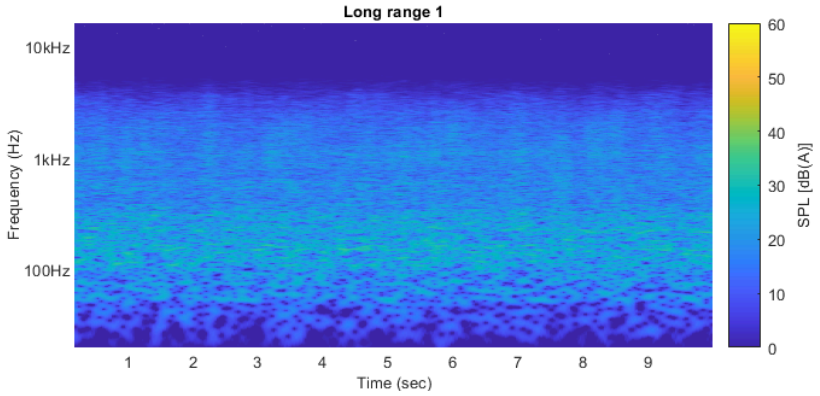

Figure A.4.11: Spectrogram of Long range position 1.

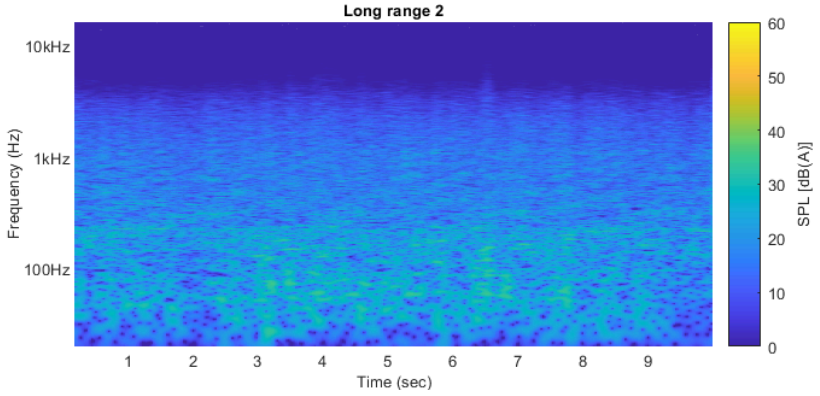

Figure A.4.12: Spectrogram of Long range position 2.

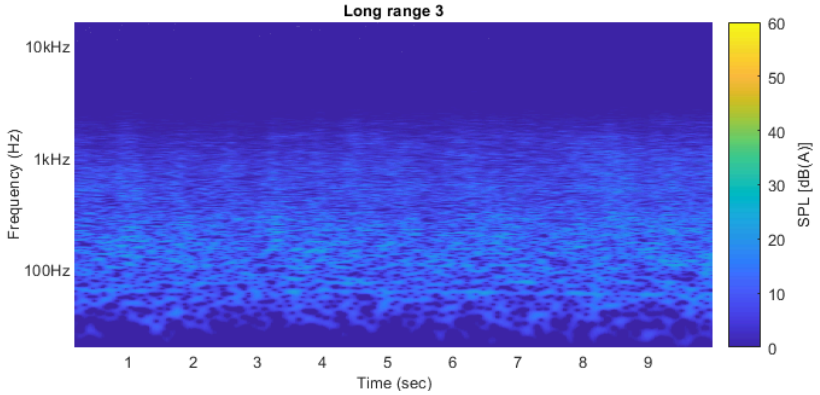

Figure A.4.13: Spectrogram of Long range position 3.

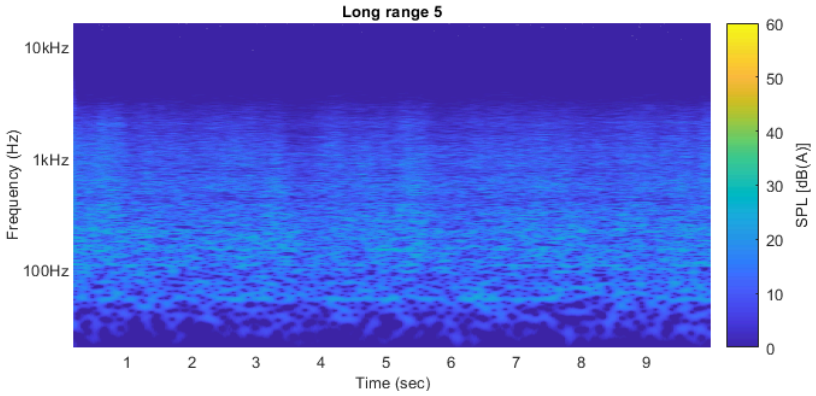

Figure A.4.14: Spectrogram of Long range position 5.

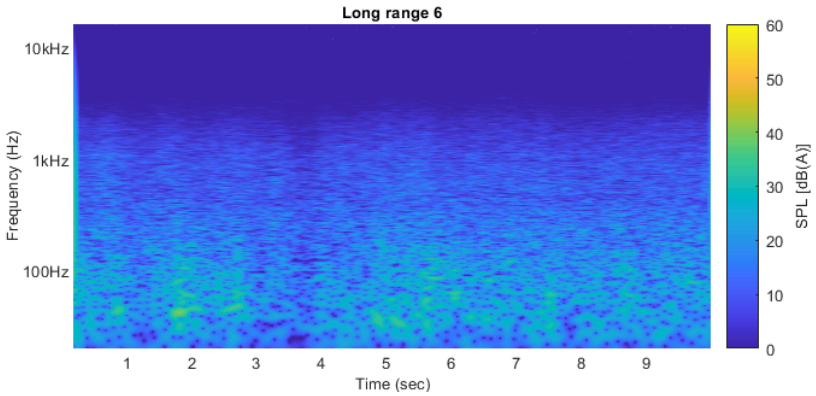

Figure A.4.15: Spectrogram of Long range position 6.

Short range results:

Results for 2 positions in the short range setup are presented in 1/3-octave bands.

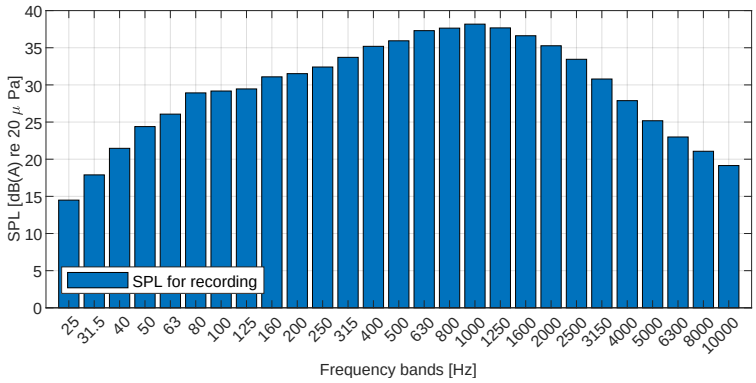

Figure A.4.16: 1/3-octve band for short range position 1.

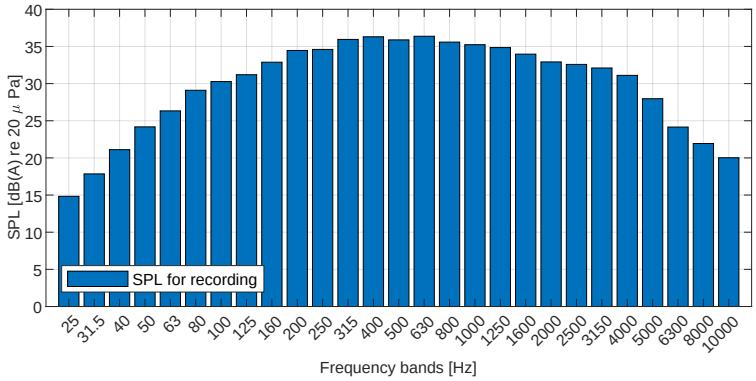

Figure A.4.17: 1/3-octve band for short range position 3.

Spectrograms for all short range positions are found below, for the turbine operating in low noise mode.

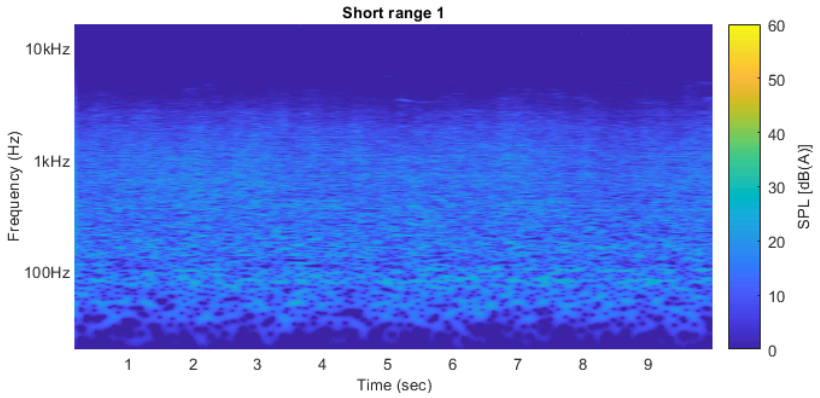

Figure A.4.18: Spectrogram of short range position 1.

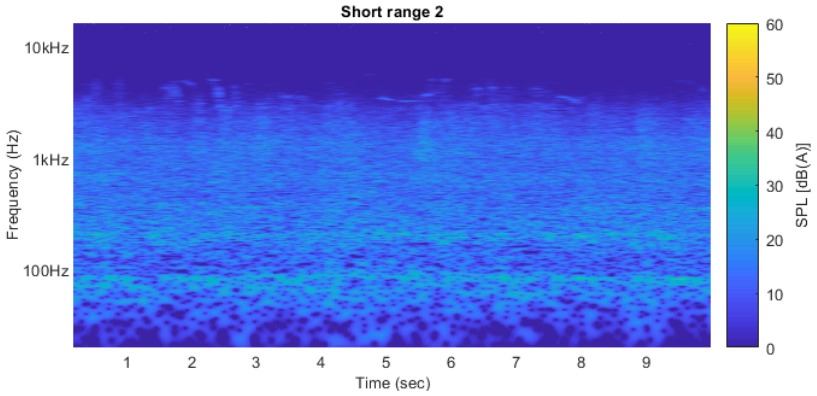

Figure A.4.19: Spectrogram of short range position 2.

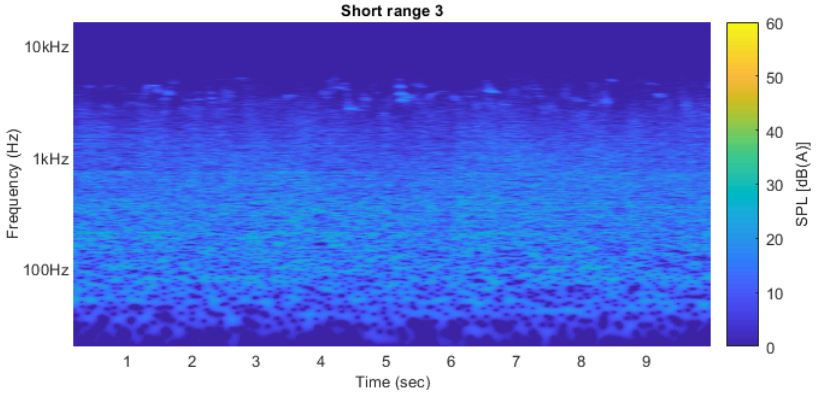

Figure A.4.20: Spectrogram of short range position 3.

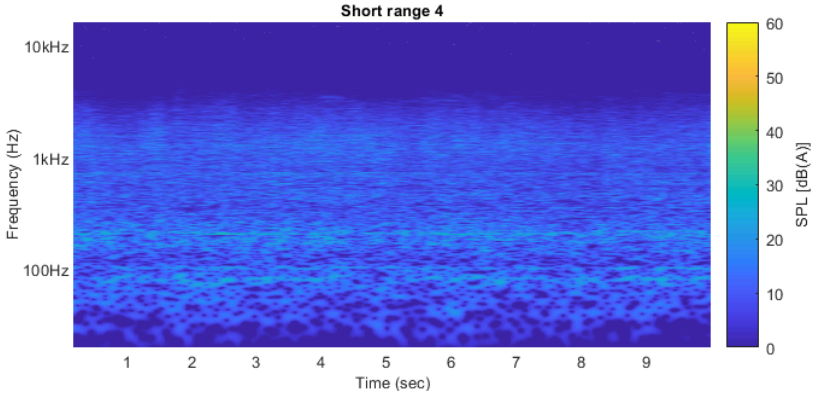

Figure A.4.21: Spectrogram of short range position 4.

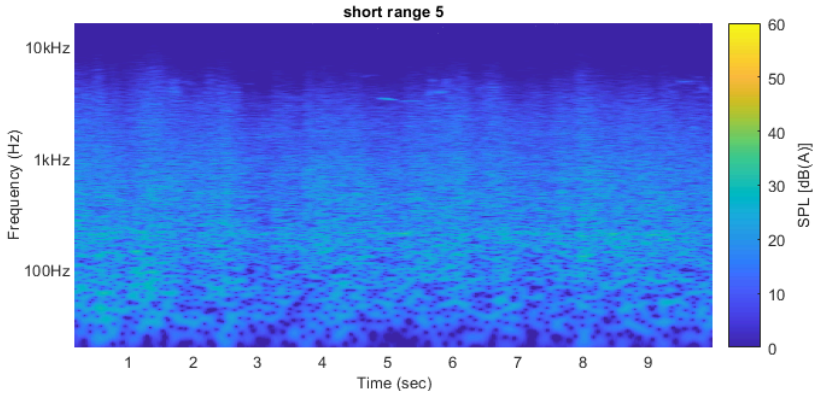

Figure A.4.22: Spectrogram of short range position 5.

Near field results:

Results for 1 position in the short range setup are presented in 1/3-octave bands.

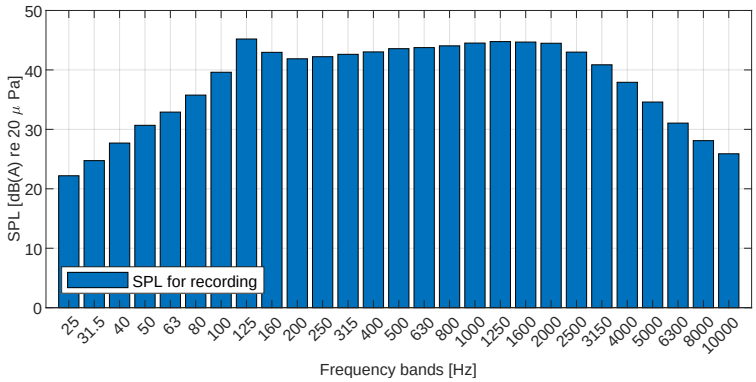

Figure A.4.23: 1/3-octve band for near field position 1.

Spectrograms for all short range positions are found below.

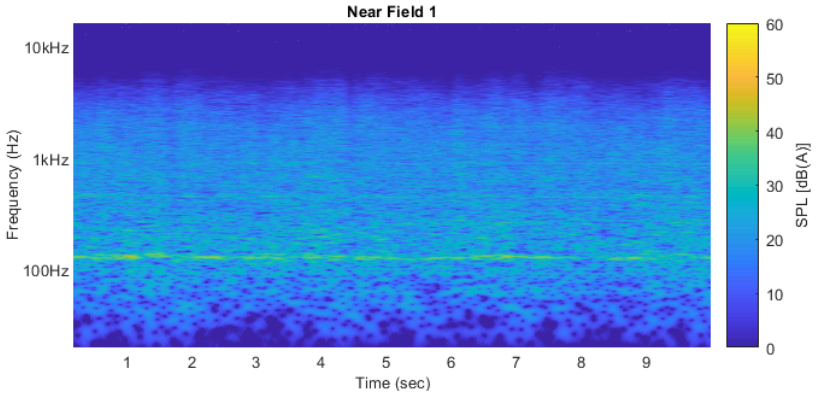

Figure A.4.24: Spectrogram of near field position 1.

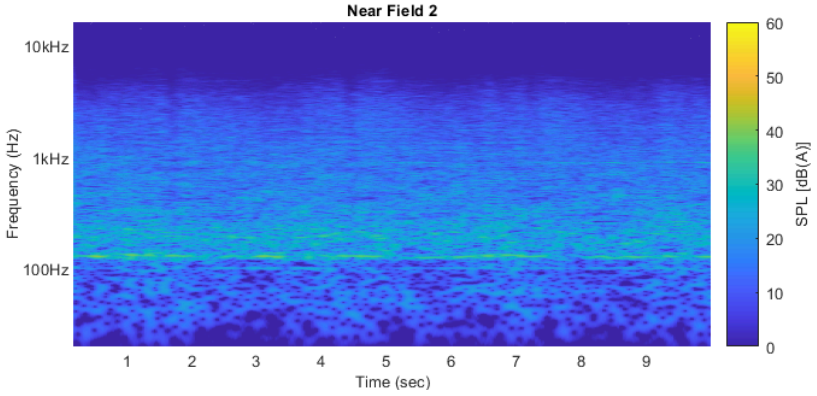

Figure A.4.25: Spectrogram of near field position 2.

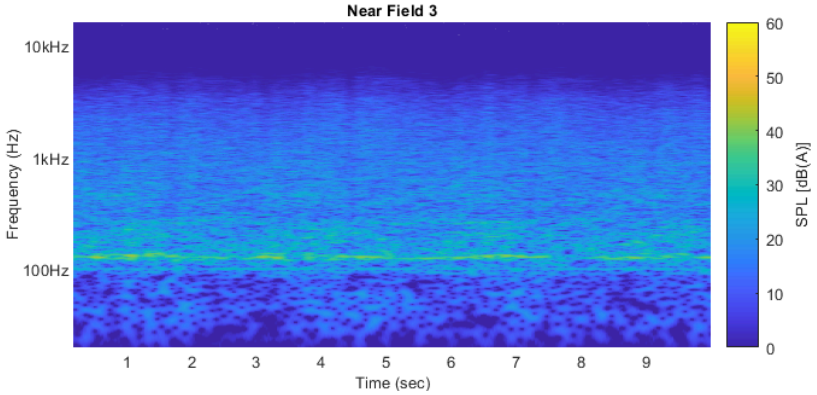

Figure A.4.26: Spectrogram of near field position 3.

Sources of Error

- **Equipment failure**: During setup of the long-range microphone positions, the connector broke in the attempt to connect position 4 (at 800 m) to the input module. For this reason, only 5 200 m cables where available and measurements from position 4 were discarded. This also resulted in abandoning position 6 in the short range setup.
- **Positional complications**: During the short-range setup, the position 200 m behind the wind turbine (Cyan position '1' in fig. A.4.1) would place the microphone in a ditch. Therefore the position was moved 5 m towards the windmill, and the position is therefore approximately at 195 m.
- **Birds**: During long-range setup, bird song was observed at the 400 m range and beyond, potentially contaminating parts of the recordings .

Sources of Uncertainty

- **Microphone range**: The microphones are placed at the selected distance, found by range finder, involving tolerances of the range finder as well as uncertainties from manual handheld point estimation.
- **Wind induced noise**: The measurements are affected by wind induced noise, remedied partially by windscreens.
- **Uneven terrain**: For some measurement positions, it proved difficult to estimate precise height with regard to the ground level, as the ground level itself was not exactly flat.
- **Atmospheric variations**: Many atmospheric elements changes over the course of a day, such as wind speed, direction and temperature. A clear example of this is the measurement point 200 m behind the wind turbine for both the short- and long-range setup, which means to serve at a reference between these 2 setups. In theory this position should be the same; in practice, however, the time between setting up the two arrangements produced a change in wind direction, and therefore the facing direction of the wind turbine.

A.5 Measurements and calibration of headphone output

This measurement journal covers the procedure of calibrating the output of a specific sound card and headphones to deliver a desired sound pressure level, for a specific numerical input.

Purpose

The purpose is to estimate the settings on an external sound card that will allow for a desired maximum sound pressure output level. By inference of linearity, this can be used to numerically designate the sound pressure level output resulting from the the playback program, i.e. Matlab.

List of Equipment

The relevant equipment and software used for the measurement are listed in the following tables:

Model	Brand	Function	AAU Nr.
Type 4134	B&K	Microphone	08129
Type 4231	B&K	Sound Calibrator	07631
Type 4153	B&K	Artificial Ear	07631
26AK	GRAS	Pre-amplifier	52665
12AQ	GRAS	Power Module	12362
Fireface UFX+	RME	Sound Card	108275
HD650	Sennheiser	Open back headphones	-
G501jw	ASUS	Computer	-

Table A.5.1: List of hardware.

Name	Brand	Function	Version
Fireface USB Settings	RME	Configuration	-
TotalMix FX	RME	Mixing/routing	1.75
MATLAB	MathWorks	Programming	R2022a
Audio Toolbox	MathWorks	Audio processing	3.2
calibrate.m	-	calibration file	-

Table A.5.2: List of software.

Setup

Two setups are used in conjunction in the calibration procedure. These setups are presented in figure A.5.1 and A.5.2:

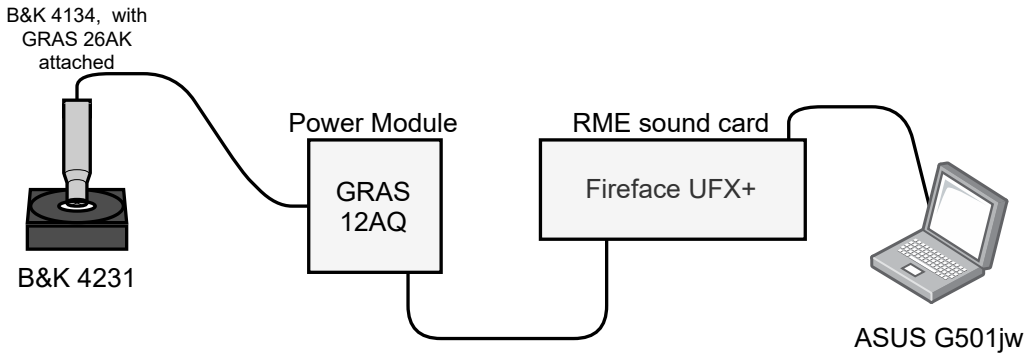

Figure A.5.1: Setup for measuring a known sound pressure level.

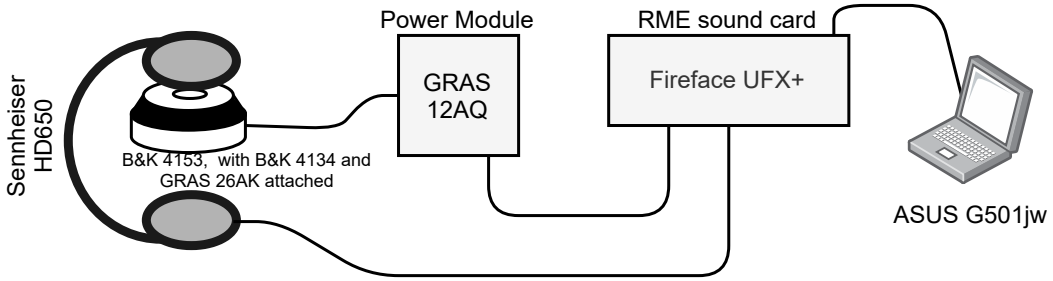

Figure A.5.2: Setup for measuring the sound pressure level output of a pair of headphones.

Method/Procedure

At first, the measurement of a known level is measured in Matlab. The setup is established according to fig. A.5.1, whereafter the software interface for the sound card (TotalMix) is opened. The attached microphone interface is adjusted to a gain of +30 in TotalMix. The GRAS Power Module is adjusted to 10 dB. The output level of the computer is set to max, and the Matlab script "calibrate.m" opened (file attached with the provided external software of the project).

In the script, the sound pressure level goal (`SPL_goal`) is adjusted to the desired output level (104.1 dB), and the corresponding desired numerical output from matlab (`numericalRMS_Goal`) is set to 0.178 ($\sim$15 dB headroom).
The parameter '`PlaybackLevelAdjustment`' is also set to -20.

The microphone should be attached to the sound calibrator, and the calibrator turned on. The script is paused until a key (e.g. enter) is struck, whereafter the signal is recorded for 10 seconds, during which the recording environment must be quiet. The calibration offset obtained from this can be saved, and the calibration procedure commented out, for eliminating the need of doing the first setup again.

This, however, has to be repeated, if using another microphone.

The setup is then arranged according to the illustration depicted in fig. A.5.2. TotalMix is opened again, and the output level of the headphone out is adjusted to $-10\,\mathrm{dB}$. The microphone and preamp is attached to the artificial ear, and the headphones are placed on this ear (e.g. by the edge of a table). The script is paused until a key (e.g. enter) is struck, whereafter a 1 kHz sine is played back for 12 seconds through the headset, recording is started immediately after, and records for 10 seconds. During this the recording environment must be quiet.

After this, the script may ask for one of three things:

1. The output SPL is below the goal, and the output of the amplifier must be turned up (gain increased). After this, the measurement must be run again.

2. The output SPL is above the goal, and the script gives a nummerical attenuation correction factor that must be put into the script (`SPL_CorrectionFactor`), whereafter the measurement must be run again.

3. The output SPL is within $\pm 0.5\,\mathrm{dB}$ of the goal, and the script gives a scaling factor that can be used in other scripts to know the output for a specific numerical input.

It should always be ensured that the microphone input does not clip. If it does, the microphone gain must be decreased, and the procedure redone from the beginning. Furthermore, if a desired SPL goal is set too high, the drivers/headphones may be driven beyond their linear capabilities, and care should be taken when setting this high. The script also has an adjustment factor (`PlaybackLevelAdjustment`) for this where the output level of the headphones may be decreased but the final scaling factor for the other program is lastly adjusted up again. This, of course, assumes, but may not result in linearity.

Results

With a '`numericalRMS_Goal`' of 0.178, and a '`SPL_Goal`' of $104.1\,\mathrm{dB}$ (along with a '`PlaybackLevelAdjustment`' of $-20\,\mathrm{dB}$), a Scaling Factor of 0.5780 is obtained from the script.

Sources of Error

- **Noise**: Any noise in the environment may result in the contamination of both recordings, potentially leading to incorrect estimated SPL levels

- **Headphone characteristics**: The headphone outputs a $1\,\mathrm{kHz}$ sine output, which may not represent how the levels may be for other frequencies.

Sources of Uncertainty

- **Headphone placement**: minor deviations in the headphone placement unto the artificial may lead to inconsistencies in the resulting scaling factors.
- **Environmental variations**: For example temperature, humidity and/or pressure changes of the surroundings.
- **Equipment variations**: For example temperature changes of equipment when in use, including both fluctuations and steady-state.
- **Equipment tolerances**: Combined tolerances of all equipment as stated in the individual data sheets.